4-15-2020 10:00 AM

Earthquake site characterization of rock sites in Eastern Canada and stiff ground sites in Vancouver, British Columbia

Sameer Ladak, *The University of Western Ontario*

Supervisor: Molnar, Sheri E., *The University of Western Ontario*
A thesis submitted in partial fulfillment of the requirements for the Master of Science degree in Geophysics
© Sameer Ladak 2020

Follow this and additional works at: https://ir.lib.uwo.ca/etd

Part of the Geophysics and Seismology Commons

Recommended Citation
Ladak, Sameer, "Earthquake site characterization of rock sites in Eastern Canada and stiff ground sites in Vancouver, British Columbia" (2020). *Electronic Thesis and Dissertation Repository*. 6972.
https://ir.lib.uwo.ca/etd/6972

This Dissertation/Thesis is brought to you for free and open access by Scholarship@Western. It has been accepted for inclusion in Electronic Thesis and Dissertation Repository by an authorized administrator of Scholarship@Western. For more information, please contact wlswadmin@uwo.ca.

Earthquake site characterization of rock sites in Eastern Canada and stiff ground sites in Vancouver, British Columbia

Abstract

Site characterization is a crucial component in assessing seismic hazard, typically involving *in situ* shear-wave velocity (V_S) depth profiling, and measurement of site amplification including site period. These methods are ideal for soil sites and less reliable in more complex geologic settings including rock sites. A multi-method approach to earthquake site characterization is tested at 25 seismograph stations across Eastern Canada. It is typically assumed these stations are installed on hard rock. We seek to identify which site characterization methods are most suitable at rock sites as well as to confirm the hard rock assumption. Active-source refraction and surface wave array techniques consistently provide velocity measurements at rock sites; passive-source array testing is less consistent but most suitable to constraining the rock Vs. Bayesian inversion of surface wave dispersion curves provides Vs probability distributions and importantly includes uncertainty in the rock Vs. We succeed in estimating rock Vs at 16 stations, among those we measure rock Vs at only 7 stations. The majority of sites are classified as hard rock but span hard-to-soft rock classification due to variance in Vs. A multi-method site characterization approach is also tested at stiff glaciated upland sites across Vancouver, British Columbia. From the 10 sites investigated, we determine an average Vs of 438 m/s for the glaciated sediments beneath Vancouver which vary in thickness from 20 m to over 100 m from north to south.

Keywords

Earthquakes, hard rock, earthquake site classification, surface wave dispersion, microzonation, V_{S30}, seismic hazard, microtremors, shear wave velocity, site effects

Summary for Lay Audience

There is earthquake hazard present in both Eastern and Western Canada. Eastern Canada is not near a plate boundary but has had historical large events that are possible in future. Western Canada is nearby an active plate boundary with lots of earthquakes, and southwestern British Columbia has the highest seismic hazard in Canada. Earthquakes cannot be predicted, but we can estimate the resulting ground shaking. The geology of the near surface impacts the amount of shaking that occurs in the event of an earthquake. Stiffer materials (e.g. rock) have a higher stiffness (velocity) than material that is softer (e.g. sand) and typically have lower intensity shaking than soft soil sites.

In Canada, networks of earthquake recording instruments (seismometers) are deployed in areas susceptible to earthquakes and near high consequence infrastructure (e.g. nuclear power plants) to monitor events. The earthquake recordings are used to develop models to predict expected shaking at the surface. Seismometers of the Canadian National Seismograph Network are installed on rock surfaces, assumed as hard rock. No testing is done at the seismometer location to verify this hard rock assumption. If the assumed stiffness of the rock is incorrect, then the model we develop to predict earthquake shaking will be incorrect. We perform non-invasive seismic testing at 25 seismic stations across Eastern Canada to verify this hard rock assumption. We also test a variety of non-invasive seismic methods to determine which method is most useful in confirming the rock's stiffness. These non-invasive seismic methods are best suited to soft ground, so we also test their applicability to measure stiffness at 10 stiff glaciated sites in Vancouver.

Co-Authorship Statement

This thesis is prepared in integrated article format. Sameer is the first author and performed the majority of the data analyses in the thesis. Field data collection for the Eastern Canada seismograph stations was performed by Samantha Palmer (PhD Candidate, University of Western Ontario) and Melanie Postman (NSERC, USRA Student). Preliminary refraction data analysis was performed by Frederick Jackson, former M.Sc. student.

Chapter 2 is published as: Ladak, S., Molnar, S., Palmer, S., & Atkinson, G. M. (2019). Application of active and passive seismic methods for determining the shear wave velocity profile at hard rock sites in Eastern Canada. Proceedings of the 12th Canadian Conference on Earthquake Engineering (12CCEE), Quebec City, Quebec, June 17-20, 2019, Paper 192-bN89-149.

Chapter 3 is prepared for publication in the Bulletin of the Seismological Society of America.

Chapter 4 is published as: S. Ladak and S. Molnar (2020). Site Characterization at Stiff Ground Sites in Vancouver, Metro Vancouver Seismic Zonation Mapping Project, Univ. Western Ontario with ICLR and EMBC, Report 20-01, 15 pg.

The thesis work and publications were completed under the supervision of Dr. Sheri Molnar.

Acknowledgements

I would like to express my deepest appreciation to my supervisor Dr. Sheri Molnar for the opportunity to work alongside her. I am deeply grateful for all of her help, guidance, and the opportunities given to me over the past two years. The final results of this work took a lot of interpretation and understanding and I thank her for all her time put in for the duration of this project.

I would like to thank all the friends I have made at Western and London during these two years for all their support. I would also like to thank the "fun fund" and everybody in the Good Vibrations and Excitations group for their support and necessary "tea breaks" in getting past this time period. I would also thank my family for all their love and support and it would not have been possible without their constant love and encouragement.

Table of Contents

List of Tables

List of Figures

List of Abbreviations and Symbols

AVA   Ambient Vibration Array

EHVSR   Earthquake Horizontal-to-Vertical Spectral Ratio

f_0   Fundamental frequency (Hz)

f_{peak}   Peak frequency (Hz)

GMM   Ground Motion Model

(HR) F-K   (High Resolution) Frequency - Wavenumber

HVSR   Horizontal-to-Vertical Spectral Ratio

MASW   Multi-channel Analysis of Surface Waves

MHVSR   Microtremor Horizontal-to-Vertical Spectral Ratio

MM   Multi-method

(M)SPAC   (Modified) Spatial Auto Correlation

NBCC   National Building Code of Canada

NEHRP   National Earthquake Hazards Reduction Program

PSWP   Probabilistic Shear-wave Velocity Profiling

V_p   Compression (P) -wave velocity (m/s)

V_R   Rayleigh-wave velocity (m/s)

V_s   Shear (S)-wave velocity (m/s)

V_{s30}   Time averaged Vs of the upper 30 meters (m/s)

Chapter 1 Introduction and Literature Review

This chapter provides the necessary prior information to understand the rationale for the thesis work. This chapter first presents the seismic hazard from earthquake occurrence in Eastern Canada and in Southwest British Columbia. Seismic hazard can be quantified through earthquake site characterization where local geology plays an important role in seismic hazard assessment. Local site conditions affect the frequency and amplitude content of seismic waves travelling from source to site, termed as an earthquake site effect. Earthquake site characterization involves the use of *in situ* seismic methods to determine properties of the subsurface ground conditions at a site of interest to predict earthquake site effects. Methods of earthquake site characterization can be grouped into non-invasive and invasive methods. Invasive methods are typically costly and intrude the subsurface. The focus of this thesis is on non-invasive methods due to their cost-effectiveness and ease in operation in not disturbing the subsurface. Non-invasive methods for site characterization have had success at soil sites whereas at non-soil sites (i.e. rock) they have had limited application. Results of earthquake site characterization can be simplified into earthquake site classification outlined by Canadian seismic design guidelines. This thesis focuses on the advancement of non-invasive site characterization techniques at stiff ground and rock sites in Eastern Canada and Vancouver, British Columbia respectively. Earthquake site characterization is important because earthquake recordings are used to develop ground motion models which use a seismic station's local site conditions and emphasizes them to be known and classified accurately. Classifying sites is important in creating microzonation maps to display seismic hazard (amplification, site class, displacement, etc.) due to local site effects.

1.1 Seismicity in Eastern Canada

About 450 earthquakes occur each year in Eastern Canada above magnitude (M) 2.5 with an average of 4 exceeding M 4 (Natural Resources Canada, 2018). The seismic hazard in Eastern Canada is high in some areas, e.g. Charlevoix, Quebec (Lamontagne and Ranalli, 1996), which have been historically known to produce large magnitude (M > 5) events. Seismicity in Eastern Canada occurs in clusters dominated by northeast to east regional compressive stress fields

(Adams and Basham, 1989). Most large earthquakes in Eastern Canada have occurred near Paleozoic or younger rifts or along rifted margins in areas where the continent has been weakened. The cause of these earthquakes has been thought to be the reactivation of crustal faults in areas of weakness (e.g. Adams, 1989 and Natural Resources Canada, 2018). Therefore, earthquakes typically occur in the shallow 30 km of the crust in Eastern Canada (Natural Resources Canada, 2018). There is seismic hazard present in Eastern Canada with some regions having larger hazard than others. The seismic risk is high in dense, highly populated areas which have been subject to seismicity in the past (i.e. Montreal, Ottawa, Quebec City, etc.).

A study reported by the Insurance Bureau of Canada (IBC) (AIR Worldwide, 2013) estimates that a moment magnitude (**M**) 7.1 earthquake in Charlevoix would cause $49 billion in direct damages (e.g. shaking, liquefaction, and fires caused) with an additional $11 billion in indirect damage (e.g. supply chain and network interruptions and other problems with connectivity between economic sectors) with most of the damage occurring in Quebec City. Seismic risk results from the hazard in factoring the vulnerability and exposure to a population and their economic loss (e.g. Ploeger et al., 2013). The 1944 **M** 5.8 Cornwall-Massena Earthquake caused an estimated 2 million dollars in damage at the time in mainly housing and infrastructure in Cornwall, Ontario and Massena, New York (Bent, 1996) and would cost approximately 30 million dollars (CAD) in 2019 (Bank of Canada, 2019). It is assumed by the public that there is little earthquake hazard in Eastern Canada due to not being near major plate boundaries but other components related to historic plate tectonics can trigger earthquakes. Figure 1 shows historical seismic events as well as measured earthquake locations until 2018 in Eastern Canada with sub-regions of interest outlined by Natural Resources Canada. Sub-regions of interest to this thesis are: Western Quebec (WQU), Northern Appalachians (NAP), Lower St. Lawrence (BSL), and Charlevoix (CHV).
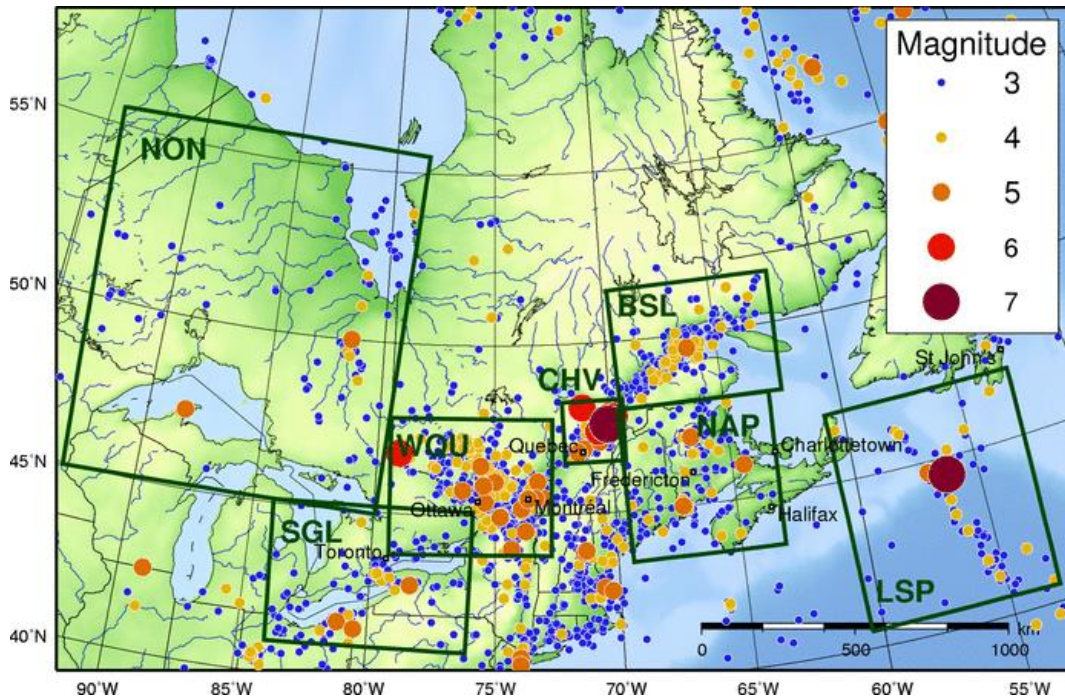
Figure 1.1: Seismicity in Eastern Canada (locations and magnitude shown by coloured circle) with sub-regions of interest outlined by solid lines (Natural Resources Canada, 2018).

The WQU encompasses the Ottawa valley from Montreal to Temiscaming which shows two patterns of seismicity (Figure 1.2). A concentrated region of seismicity occurs from Lake Timiskaming to Ottawa. This seismicity is associated with rift faults formed in the late Proterozoic and were active into the Paleozoic along the Ottawa River which is part of a larger rift fault structure which form the Ottawa Graben (Adams and Basham, 1989; Forsyth, 1981). A second region of concentrated seismicity occurs from Montreal to the Baskatong reservoir (North-West of Mont Laurier). This seismicity is likely related to crustal weakening from the Mesozoic track of the Great Meteor Hotspot (Ma and Eaton, 2007). Historical seismicity in the WQU includes 3 large (**M** > 5.5) earthquakes including the1732 **M** 5.8 (near Montreal), 1935 **M** 6.1 (near Timiskaming), and 1944 **M** 5.8 (near Cornwall) causing damage in areas such as Montreal.
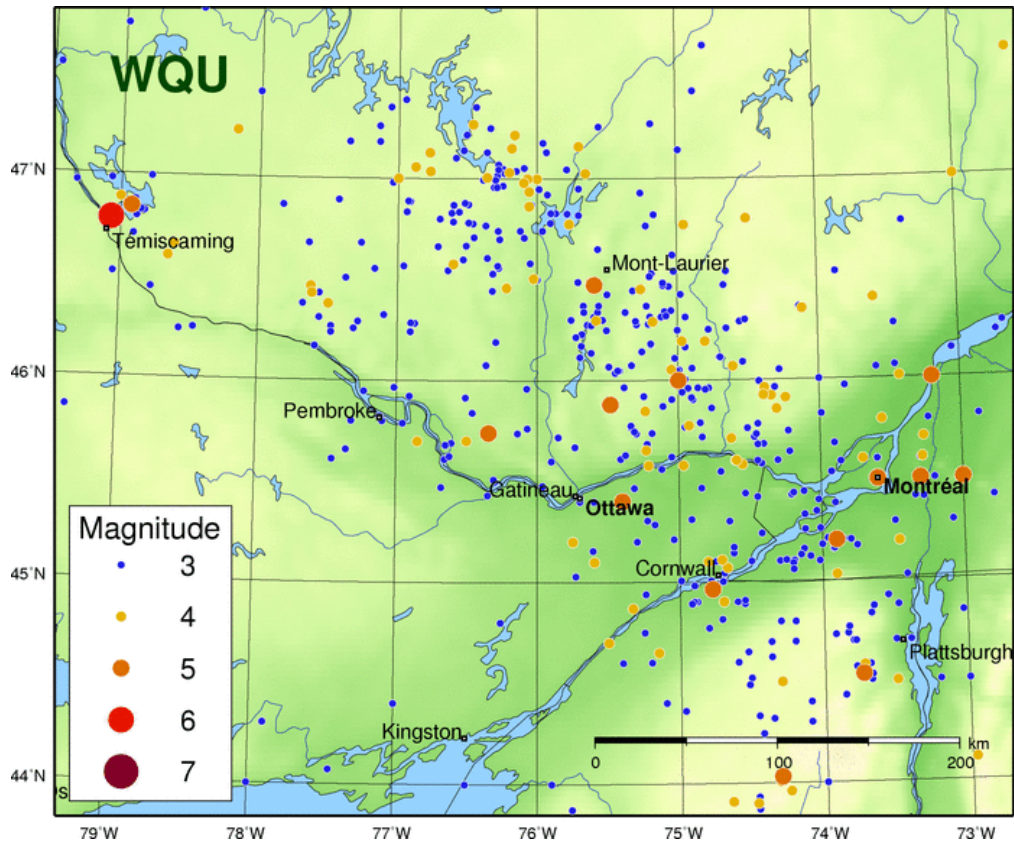
Figure 1.2: Sub-region WQU showing the seismicity of Western Quebec which encompasses Eastern Ontario (Natural Resources Canada, 2018).

Further northeast, CHV comprises Quebec City and is the most seismically active region in Eastern Canada with an estimated five **M** > 6 events (Figure 1.3). WQU, CHV, and BSL all lie among the same rift system. In CHV it gets a bit more complicated in containing part of a Devonian meteorite crater impact with a diameter of ~ 54 km consisting of a multi-ringed basin with central uplift (Adams, 1989; Ma, 2009). It has been proposed that meteor impacts weakened the rift faults and introduced its own fractures (Lamontagne, 1987). Typically, meteor impacts do not leave seismic signatures but Lamontagne (1987) exemplified that the Charlevoix impact crater may present a different case due to the weakening of paleorift faults. This sub-region contains the only loss of life directly due to an earthquake in Canada from the 1870 **M** 6.5 earthquake where the death of two children occurred in Les Èboulements (Lamontagne, 2008).
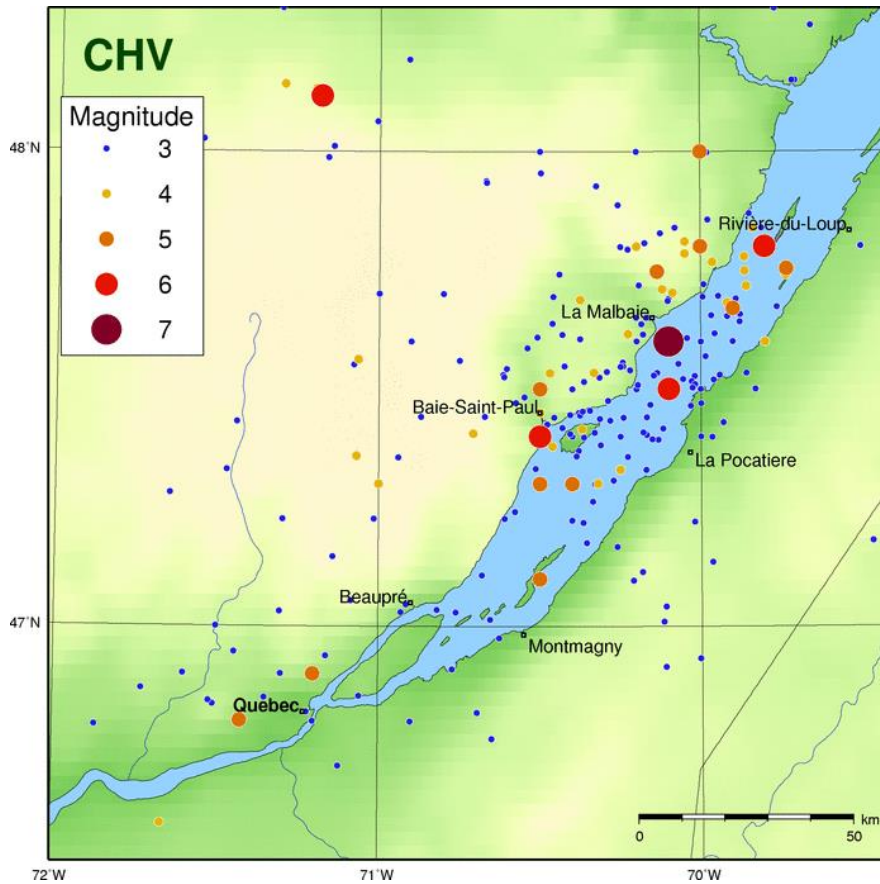
Figure 1.3: CHV seismic sub-region encompasses Quebec City and the St. Lawrence River and is the most seismically active area in Eastern Canada (Natural Resources Canada, 2018).

Continuing northeastward, the concentrated or clustered seismicity in CHV trends along the St. Lawrence in the BSL sub-region between Baie-Comeau and Sept-Iles (Figure 1.4). This region contains old rift faults similar to other areas on the St. Lawrence. Through studying focal mechanisms, it is suggested that Paleozoic rift faults are weak zones susceptible to seismicity related to glacial isostatic rebound (Adams, 1989). Magnitude three and four earthquakes occur at similar rate to CHV in its close proximity.
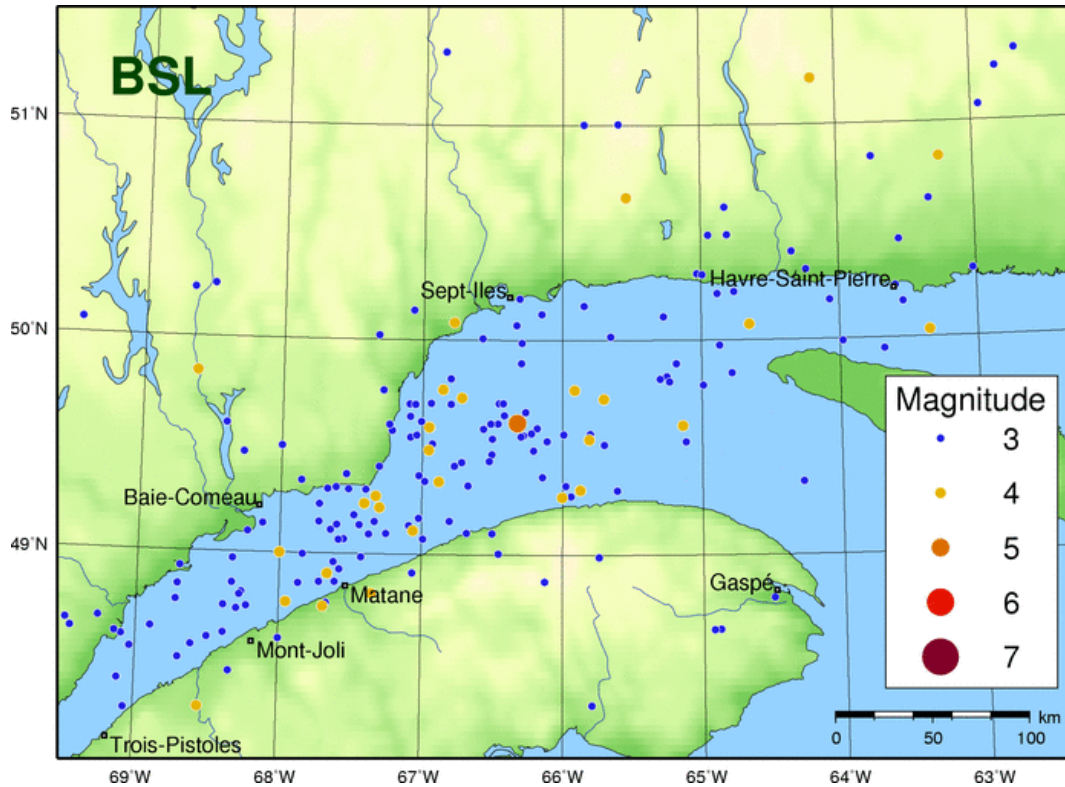
Figure 1.4: BSL seismic sub-region which is the Lower. St. Lawrence (Natural Resources Canada, 2018).

Southeast of CHV, the NAP sub-region includes most of New Brunswick (Figure 1.5). New Brunswick has a concentration of earthquakes in the Miramichi Highlands and near Passamaquoddy Bay (West of Saint John). There have been 3 **M** > 4.5 earthquakes near the New Brunswick and Maine border in 1817, 1869 and 1904 with an 1855 earthquake near Moncton. Geological and geophysical investigations have exemplified that all the earthquakes have occurred within a single granodiorite pluton (Adams, 1989).
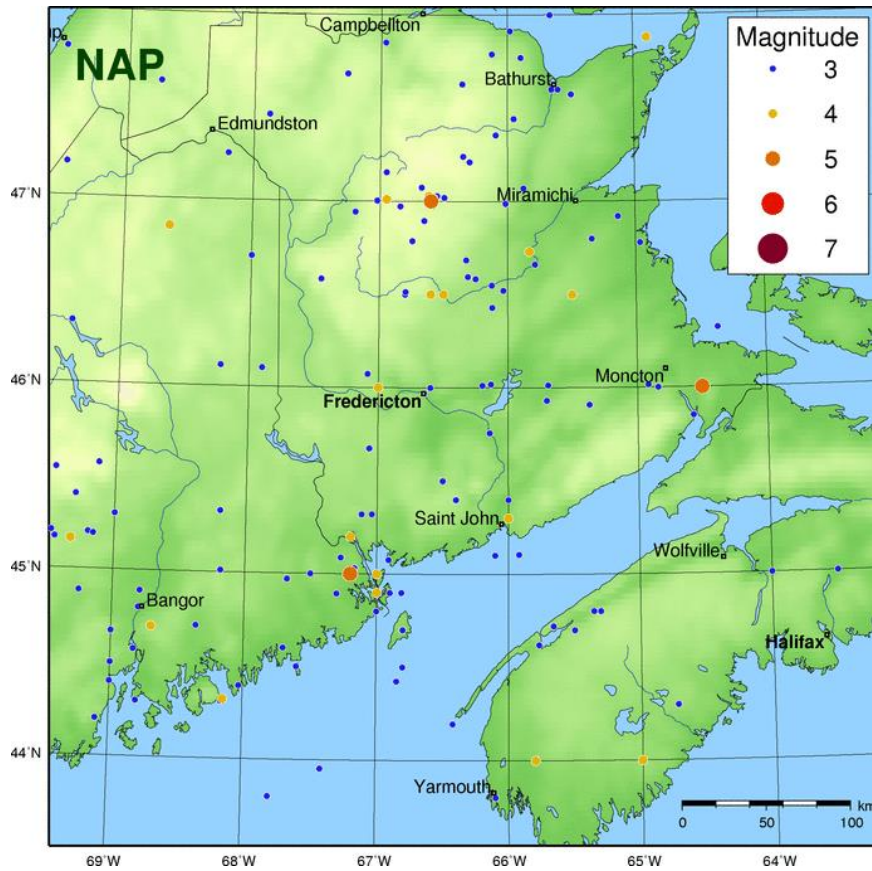
Figure 1.5: NAP seismic sub-region which contains some M > 4.5 events throughout New Brunswick (Natural Resources Canada, 2018).

1.2   Seismicity in Greater Vancouver

In contrast to Eastern Canada, the driving force of earthquakes in Southwest Canada is plate tectonics. The Pacific Coast is the most earthquake-prone area of Canada (Earthquakes Canada, 2019). The southwest coast of Canada is a unique area where three types of earthquakes can occur which contribute to its high hazard. These include shallow crustal, deeper inslab, and subduction zone interface earthquakes (Figure 1.6). Crustal earthquakes are shallow (< 30 km) and occur in the continental North American crust (e.g. 1946 **M** 7.3 Vancouver Island). The main source of crustal earthquakes in Greater Vancouver is the North American plate overriding the subducting Juan De Fuca plate. Crustal earthquakes are considered hazardous and damaging in the region due to their proximity to the surface. Inslab earthquakes are deeper (~40-60 km) and are generated in the subducting Juan De Fuca plate. Inslab events are concentrated along Georgia Strait, British Colombia to south of Puget Sound, Washington. The inslab 2001 **M** 6.8 Nisqually earthquake strongly shook the Seattle area and it was felt in Victoria and Vancouver

(Earthquakes Canada, 2011). The largest magnitude earthquakes occur along the interface boundary between the subducting Juan De Fuca plate and the overriding North American plate, known as the Cascadia subduction zone (CSZ). Paleoseismicity and historical records confirm a **M** 9 (e.g. Atwater et al., 1995; Satake et al., 1996) earthquake last occurred along the Cascadia Subduction Zone in 1700. Interface earthquakes have the potential to cause tsunamis which compounds the regional seismic hazard.
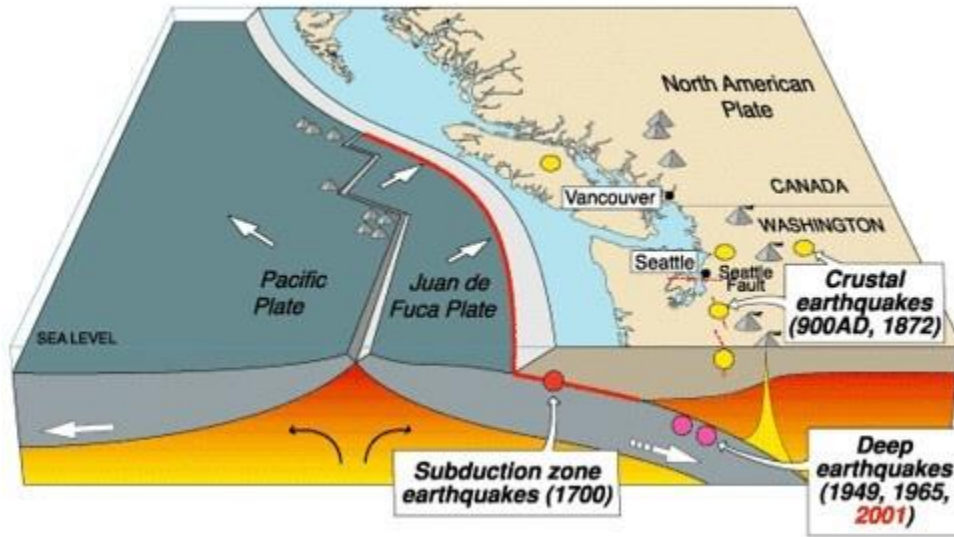
Figure 1.6: Earthquake source types occurring in southwest Canada and northwest United States (Modified from Pacific Northwest Seismic Network, 2011).

Southwestern British Columbia has the highest seismic risk in Canada due to its high seismic activity and exposure of its large population and critical infrastructure (e.g. Onur et al., 2005). The population of greater Vancouver is approximately 2.5 million people with important infrastructure connecting Canadians to the rest of the world (e.g. international airport, shipping and port facilities, etc.). Onur et al. (2005) performed risk assessments for a **M** 6.5 inslab event in the Strait of Georgia and estimated that the economic loss for only the municipality of Vancouver is around $3.5 billion. The IBC estimated that a **M** 9 CSZ interface event (AIR Worldwide, 2013) would cause $62 billion in direct loss and $12.7 billion in indirect losses. Site effects looked at in both studies assumed a standard site class C (discussed in 1.3 and 1.4). In reality, there is not one standard site class to describe earthquake shaking across greater Vancouver. Seismic microzonation mapping to capture variations in expected earthquake shaking due to site effects is underway for Metro Vancouver (e.g. Molnar et al., 2020).

1.3   Earthquake site effects

It is known through events such as the 2001 **M** 6.8 Nisqually, Washington earthquake that seismic waves propagating through soft sediments are amplified relative to stiffer ground (Shearer and Orcutt, 1987). In this event, artificial fill and soft soil sites were the most severely damaged areas as well as triggering other hazards (i.e. liquefaction) causing more damage (Frankel et al., 2008). Sites situated on hard rock had significantly less damage due to less amplification occurring at the surface. Greater damage typically occurred when the natural period of the buildings and the site closely matched. These observations suggest that a correct quantification of site effects is necessary for a complete assessment of seismic hazard. Earthquake site characterization involves the use of *in situ* methods to measure properties of subsurface ground materials that are important for predicting earthquake site effects. The contrast in softer and stiffer site conditions highlights the importance of earthquake site characterization due to the link between ground motion amplification and shear-wave velocity (Vs) of subsurface strata and bedrock (Kramer, 1996). Characteristics of ground motion at the surface (amplitude, frequency, and duration) is strongly controlled by subsurface earth materials where seismic waves travel through, especially in the upper 100 m (or less) of sediment (Hunter and Atukorala, 2015).

Earthquake site amplification is observed from shear waves which have travelled through the crust and reflect back and forth between a free surface of the ground and a significant impedance boundary at the soil-bedrock interface. Shear wave energy can be trapped in the soil layer causing a ringing at the fundamental resonance frequency (f_0) (Equation 1); site period is the inverse of f_0. For a one-dimensional soil column model with a single soil layer over rigid bedrock and the upward propagation of horizontally polarized shear (SH) waves, the resonance frequencies are dependent on the soil layer's average Vs (Vs_{AVG}) and thickness (h) where

$$f_n = (2n + 1)\left(\frac{Vs_{AVG}}{4h}\right) \; for \; n = 0, 1, 2, 3 \dots. \tag{1}$$

f_n is the resonance frequency at every mode (*n*), where n = 0 is the fundamental mode (Haskell, 1960). The SH-wave transfer function is defined by one dimensional (1D) site amplification; a transfer function is physically defined as the ratio between the output and input of a system in the

frequency domain. The resonance amplification depends on the seismic impedance (Z) (density (ρ) * Vs) contrast between soil and underlying rock,

$$A_{res} \sim \frac{\rho_{rock} Vs_{rock}}{\rho_{soil} Vs_{soil}} = \frac{Z_{rock}}{Z_{soil}}. \tag{2}$$

Broadband amplification occurs from shortening of shear wave wavelengths and an increase of shear wave amplitudes over a broad frequency bandwidth due to conservation of energy as waves travel from rock into soil. The predicted broadband amplification is

$$A_{broad} \sim \sqrt{\frac{\rho_{rock} Vs_{rock}}{\rho_{soil} Vs_{soil}}}. \tag{3}$$

For predicting 1D site amplification, the most important measure is a site's subsurface Vs depth profile. Hence, the significant efforts to develop Vs-based metrics to categorize sites (described in section 1.4) and *in situ* Vs depth profiling methods (described in section 1.5).

Lateral and vertical variability in subsurface materials leads to two- and three-dimensional earthquake site effects caused by sedimentary basins and/or topography. This thesis is focused on only 1D site amplification. Site effects can be expressed regionally by microzonation mapping. Microzonation maps have been produced for cities in Canada including Vancouver (Taylor et al. 2006), Victoria (Monahan et al., 2000), Ottawa (Motazedian et al. 2011), Quebec City (Perret and Lamarche, 2013), and Montreal (Rosset et al., 2015). There is a current project underway to generate microzonation maps for Greater Vancouver, including earthquake site effects and liquefaction and landslide susceptibility, discussed in Chapter 4.

1.4   Earthquake site classification

A relatively simple and quantitative measure to differentiate (categorize or group) sites based on their earthquake site response was sought for ground motion prediction and seismic design guidelines. The most ubiquitous earthquake site classification metric is the time-averaged Vs of the upper 30 m, known as Vs_{30}. Vs_{30} was first introduced by Borcherdt (1994) as most boreholes in California were drilled to a maximum of 30 m (100 feet), the maximum depth attainable in one day with available drilling equipment.

In Canada, the use of Vs_{30} for earthquake site classification was adopted in the National Building Code of Canada (NBCC) and Canadian Highway and Bridge Design Code (CHBDC) in 2005 and 2015, respectively (Table 1.1). There are six earthquake site classes, termed A to F. For

soils, the average standard penetration resistance (N_{60}) and undrained shear strength (S_u) of the upper 30 m can also be used for site classification. As this thesis is focused on stiff sediment and rock sites, these other average soil properties are not discussed further. Vs is considered the most practical site classification metric with its ability to classify any site class (including rock). Vs_{30} is calculated by taking into account the time the shear waves propagate in each subsurface layer (n), where $Vs_{30} = \frac{30}{\Sigma \frac{h_n}{Vs_n}}$.

1D broadband amplification is then predicted for other site classes based on a reference site class; in Canada, site class C (Vs_{30} of 450 m/s, Finn & Wightman 2003) was selected as the reference site class in NBCC 2005 to 2015. Period dependent factors were used to adjust hazard to different site classes. In NBCC 2020 (Adams et al., 2019; Kolaj et al., 2019) 450 m/s is no longer used as the reference condition and instead a direct calculation of hazard is performed using Vs_{30} directly.

Table 1.1: Seismic site classification defined by the NBCC 2015 for average properties in the top 30 m (National Research Council, 2015).

Site Class	Description	Average Shear Wave Velocity, $\overline{Vs}$ (m/s)	Average Standard Penetration Resistance $\overline{N_{60}}$	Soil Undrained Shear Strength, S_u (kPa)
A	Hard rock	$\overline{Vs} > 1500$	N/A	N/A
B	Rock	$760 < \overline{Vs} \leq 1500$	N/A	N/A
C	Very dense soil and soft rock	$360 < \overline{Vs} < 760$	$\overline{N_{60}} > 50$	$S_u > 100$
D	Stiff soil	$180 < \overline{Vs} < 360$	$15 \leq \overline{N_{60}} \leq 50$	$50 < S_u \leq 100$
E	Soft soil	$\overline{Vs} < 180$	$\overline{N_{60}} < 15$	$S_u < 50$
F	Other soil	Site-specific evaluation is required		

Proxy-based methods which use readily available remote sensing datasets to estimate Vs_{30} are desirable especially for large-scale seismic hazard assessment or when/where *in situ* measurements are not accomplished for various reasons (difficult location access, expense, etc.). Proxy Vs_{30} methods include the use of topographic slope (Allan and Wald, 2009; Lemoine et al., 2012), surficial geology including lithological units and age (Tinsley and Fumal, 1985; Wills et al., 2000), and combining both surficial geology and topography (Wills et al., 2015; Parker et al., 2017). Proxy based methods are very useful for regional mapping purposes but lead to greater error in Vs_{30} compared to direct Vs_{30} measurements. Yong (2016) demonstrated proxy methods underpredict Vs_{30} at lower velocities (site classes D and E) and overpredicts at higher velocities (site classes B and C) at several sites in California. It is possible to use proxy methods for Vs_{30}

estimation, but the end-user must remember that uncertainty in Vs_{30} is greater and the only way to reduce this uncertainty is to perform proper *in situ* site characterization.

Vs_{30} is only appropriate for 1D broadband amplification and poorly captures resonance amplification (f_0 or site period) or 3D basin or topographic effects. Site period has been proposed as a site classification parameter (e.g. Di Alessandro et al., 2012 and Zhao et al., 2006) or as a Vs_{30} proxy (Hassani and Atkinson, 2016) in areas where direct Vs measurement cannot be performed. Hassani and Atkinson (2016) examined the applicability of using site period as a Vs_{30} proxy for sites in Central and Eastern North America but concluded it is limited compared to using topographic slope or surficial geology and suggests that it is best to use all three together.

There have been attempts to have a robust scheme in site classification scheme using the microtremor horizontal-to-vertical spectral ratio (MHVSR) method (introduced in 1.5). A classification scheme of the MHVSR method was first proposed by Zhao et al. (2006) and developed further by Fukushima et al. (2007) but most recently by Di Alessandro et al. (2012). Using a site classification scheme for HVSR measurements helps classify and characterize stations into groups which have a similar site response. Di Alessandro et al. (2012) developed the classification scheme from Italian earthquake records where earthquake HVSR's (EHVSR) were computed to then classify them into categories (Table 1.2). Most importantly, from previous authors Di Alessandro et al. (2012) introduced the flat HVSR category to incorporate low amplification rock sites. Even though velocity is not measured with this scheme, it provides a classification scheme especially in areas where velocity measurements cannot be computed. This method of classification can test flat or broadband responses which can be an indicative of weathered rock site conditions as well as resonant peaks indicating surficial layers.

Table 1.2: Site classification scheme based on predominant site period (Tg) (Di Alessandro et al., 2012).

Class	Criterion (Tg indicates natural site period measured in seconds)
CL-I	Tg < 0.2 s
CL-II	0.2 s ≤ Tg < 0.4 s
CL-III	0.4 s ≤ Tg < 0.6 s
CL-IV	0.6 s ≤ Tg
CL-V	Tg not identifiable (Flat H/V and amplification < 2)
CL-VI	Broadband amplification/multiple peaks at Tg < 0.2 s
CL-VII	Tg not identifiable with multiple peaks over the entire period range

1.5   Non-invasive seismic methods for site characterization

Non-invasive seismic methods offer an affordable alternative to Vs profiling by using body or surface wave techniques. There are two types of waves generated when an applied force is acted upon the subsurface. The first are body waves which propagate spherically in a homogeneous medium from its energy source and the second is surface waves which propagate cylindrically from its respective energy source (Socco and Strobia, 2004). Body waves can be described by two types of waves: compressional (P) and shear (S) waves. In P waves, the particle motion of the wave is in the same direction as wave propagation whereas S waves' particle motion is perpendicular to the direction of the propagating wave. Surface waves mainly consist of Rayleigh waves and Love waves. Rayleigh waves have an elliptical particle motion where their ground motion is mainly perpendicular to their wavefront. Love waves are horizontally polarized shear waves where their particle motion is primarily in the horizontal plane (Hunter and Crow, 2015). Compared to body waves, surface waves are slower and arrive to the surface at a time later than body waves.

In vertically heterogeneous media, surface waves are dispersive in nature meaning that different frequencies (and wavelengths) travel with different velocities. Waves of high frequency (shorter wavelength) travel in the lower-velocity near surface compared to low frequency (longer wavelength) waves that travel in higher-velocity material at depth in the subsurface. In measuring surface (Rayleigh or Love) waves of increasing wavelength on the ground surface using geophones or seismometers, a dispersion curve is generated. A dispersion curve consists of the phase (or group) velocities of the surface waves at particular frequencies. Generally, seismic velocities are observed to increase with depth, i.e. waves with longer wavelengths (lower frequency) propagate faster than waves with shorter wavelengths as indicated by: $\lambda(f) = V_R(f)/f$, where $\lambda(f)$ is the Rayleigh wave wavelength at frequency f and $V_R(f)$ is the phase velocity of Rayleigh wave components of frequency f. Hence, a dispersion curve is essentially the site's velocity profile with depth. Inversion of the dispersion curve is required to model the 1D layered profile (including Vs) that gives rise to the measured surface wave phase velocities (Socco and Strobia, 2004).

There are many non-invasive seismic methods developed for measuring subsurface material velocities important to site characterization. Hunter and Crow (2015) list 8 Vs profiling methods

which are sub-divided into active- and passive-source seismic array methods for the purpose for site characterization in Canada. Active source methods are where body and surface waves are generated from a source (e.g. sledgehammer, dynamite, etc.). Active body wave methods used for the purpose of this thesis include compression wave velocity (Vp) refraction; vertical source generation and vertical-component geophones are used. Based on Snell's Law, a wave will refract away from the normal when it encounters a boundary of higher seismic impedance. Figure 1.7 presents a simple two-layer case where the upper layer 1 has lower velocity than the bottom layer 2, i.e., $v_1 < v_2$ (Lowrie 2007). In this case, the refracted wave is generated at acritical angle (i_c) which travels horizontally along the higher velocity interface as the head wave and will emerge at the same critical angle towards the surface to be measured by an array of geophones. The arrival times of the first wave breaks on the recorded waveforms are picked and plotted according to distance from the seismic source point (travel-time vs. distance plot in Figure 1.7). Two slopes are readily apparent (the hyperbolic arrival times of reflected arrivals is ignored here). A steeper slope line denoting relatively long travel-time of direct wave arrivals with increasing geophone distance; direct waves travel at lower v_1 in the upper layer. And a shallower-sloped line denoting relatively fast travel-time of refracted wave arrivals with increasing geophone distance; refracted waves travel at faster v_2 in the second layer. The critical angle (i_c) is

$$\sin(i_c) = \frac{v_1}{v_2}. \tag{5}$$

Through analyzing the raypaths geometrically, the depth (d) to layer 2 (thickness of layer 1) is

$$d = \frac{(t_i * v_1)}{2 * \cos(i_c)}, \tag{6}$$

where t_i is the intercept time determined by extrapolating the travel time of the refracted waves to x=0. Active source refraction surveying thereby provides direct measurement of the velocities of, and depths to, subsurface 'layers' of differing seismic impedance.
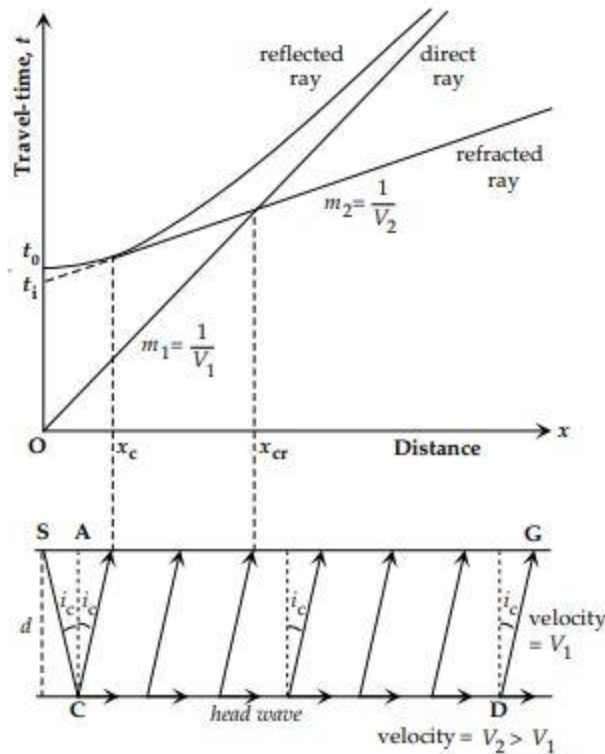
Figure 1.7: Travel time vs distance curves for the direct and refracted ray at a horizontal interface between two layers with a velocity of v_1 and v_2 separated at a depth d (Lowrie, 2007).

Active source surface wave techniques also involve source generation but instead focuses on measurement of later arriving, slower surface waves. The most popular version of this technique is known as multi-channel analysis of surface waves (MASW); (Park et al., 1999). MASW is an extension of the spectral analysis of surface waves (SASW) method (Nazarian and Stokoe, 1984) which takes advantage of multi-channel capabilities of seismographs (Phillips and Sol, 2015). MASW data is similarly acquired to seismic refraction surveying. The same equipment, layout of receivers, and shot locations are used with slightly different acquisition parameter settings. A line of 12 or more geophones are inserted at a particular spacing, connected to a seismic cable which is connected to the multi-channel seismograph. Increasing the number of geophones is beneficial to increase the array length (increases measurable wavelengths and therefore depth of investigation) as well as improve spatial sampling which aids in mode identification. A generally accepted axiom is that the source offset should be equal or greater than the desired depth of investigation. In this thesis, a vertical impact source and vertical-component geophones are used to measure Rayleigh wave velocities, whereas a shear-wave source and horizontal-component geophones would be required to measure Love waves.

MASW data are typically processed using a frequency-wavenumber (f-k) method. Phase velocities can be plotted versus frequency using energy maxima in the f-k domain (Gabriels et al., 1987). This is accomplished by a 2-D Fourier transform of the cross-correlation of recordings to calculate the 2-D amplitude spectrum (Molnar, 2015). The local energy maxima in the f-k domain is associated with the modes of propagation and from their location in the (f, k) plane, the surface wave phase velocity as a function of frequency (dispersion curve) can be resolved (Foti, 2000). Swept-sine filtering (Park et al., 1999) is another method that can be used to generate a dispersion curve but for this thesis, the f-k method was used. Using the f-k method for Vs profiling was first shown by Asten and Henstridge (1985) based on f-k methods of Capon (1969) and Lacoss et al. (1969). The phase velocity (c) of the dominant wave and its propagation direction (φ) is calculated by the wavenumber coordinates of the peak of the f-k spectrum (k_x, k_y) and is calculated for each frequency according to:

$$c = \frac{2\pi f}{\sqrt{k_x^2 + k_y^2}}.$$
(7)

The propagation direction of the dominant wave is calculated by

$$\varphi = \tan^{-1}\left(\frac{k_x}{k_y}\right).$$
(8)

Two-dimensional (2D) wavenumber coordinates are used in 2D array configurations, having both an "x and y" coordinate. 1D array configurations have 1D ("x or y") wavenumber as they are configured in one direction. 2D wavenumber coordinates (k_x and k_y) are simplified to only k in a 1D case in equations 7 and 8. The phase velocity and propagation direction of the dominant wave propagating across the array is defined by the vector of the peak in the wavenumber spectrum for a certain frequency (Molnar, 2015). Hence, the f-k method works best for surface waves of high energy with a limited azimuthal distribution (Molnar, 2015). A histogram of phase velocities is developed from time windows at certain frequencies. To improve the original f-k method, high resolution f-k (HRFK) was developed by Capon (1969) where weighting factors were added to each sensor's contribution in the array output to minimize uncorrelated noise. The HRFK method is theoretically able to distinguish between two waves travelling at close wavenumbers better than the f-k method (Wathelet, 2005).

Passive source methods do not require generating seismic waves but instead take advantage of the natural vibrations of the earth spanning low frequency (< 1 Hz) surface waves caused by

16

wind and lake/ocean waves as well as higher frequency (> 1 Hz) vibrations caused by human activity such as people walking or traffic. Seismic noise was traditionally sub-divided into lower frequency microseisms and higher frequency microtremors but is now simply referred to as 'microtremors' or 'ambient vibrations'. Surface waves become predominant at large distances due to their low geometric attenuation (Socco and Strobbia, 2004); hence, the basic assumption is the microtremor wavefield is typically dominated by surface waves.

Two main passive seismic methods are used for site characterization and are applied in this thesis. The first is the MHVSR method developed by Nogoshi and Igarashi (1971) in Japan which was then popularized by Nakamura (1989). To calculate the MHVSR, a single three-component (tri-axial) seismometer is needed. Basic workflow of the method includes measuring microtremors for an accustomed time (typically < 1 hour) for the site, calculating the mean Fourier spectrum over time for each component, and then calculating the ratio between the averaged horizontal and vertical spectra to produce the MHVSR. The maximum of the MHVSR generally occurs at the site fundamental frequency (Equation 1) due to shear-wave resonance when there is a significant impedance contrast at depth.

The MHVSR is a site amplification spectrum referenced to vertical component vibrations which are assumed to not be amplified by shear motions. Peaks in the MHVSR spectrum therefore relate to amplified shear motions, i.e., resonance amplification related to the soil's thickness and Vs (Equation 1). Hence, MHVSR is a useful technique at soil sites where f_0 is sensitive to the thickness and Vs of the soil layer whereas, rock sites theoretically display no site amplification (a "flat" MHVSR with amplification of one). In reality, at rock sites there can be some amplification over a wide frequency range (i.e., broadband) or at higher frequencies due to a weathered/fractured surface or the presence of surficial layers. The low cost of using this method and the simplicity in processing data is what makes it so popular in the use of earthquake site response studies.

The most appropriate measure of earthquake site amplification is the earthquake standard spectral ratio (SSR) introduced by Borcherdt (1970); the average horizontal Fourier spectrum at a soil recording site is divided by (referenced to) the average horizontal Fourier spectrum at a nearby rock site or downhole recording. The SSR is ideally averaged using recordings of

earthquakes of various magnitude, distance, and azimuths. In general, earthquake SSRs are relatively difficult to obtain, e.g., requires two seismometers, siting an appropriate nearby rock site, and for the instrumented rock site to have triggered or recorded, particularly in low seismicity regions. Field and Jacob (1993) applied MHVSR methodology but instead used earthquake motions. They demonstrated similarity of EHVSR with earthquake SSRs at soft lake basin sites in Mexico City. The SSR is the ideal (correct) method to obtain earthquake site amplification referenced to bedrock (soil column base); however, earthquake and microtremor HVSR methods are a "suitable approximation" to the SSR and only require one seismometer on soil. Suitable approximation means the site fundamental frequency is always obtained regardless of methodology (Molnar et al. 2018); however, the EHVSR and MHVSR amplification level often underestimates SSR amplification at the fundamental frequency (when impedance contrasts are lower than ~3) and consistently at higher frequencies. It is generally recommended that the MHVSR method will provide the site fundamental frequency but is not a direct measure of earthquake site amplification (e.g., Bard et al. 2005).

Through the MHVSR method, it is common application to estimate the depth to a major impedance boundary or to bedrock. It is possible to invert the MHVSR peak or the entire curve for layered earth models, i.e., Vs profiles. The forward problem is nonlinear and depends on several uncorrelated parameters which leads to non-uniqueness in that a single MHVSR is consistent with multiple Vs profiles (Piña-Flores et al., 2016). The inversion can be improved with joint inversion of dispersion (velocity) data and/or constraining model parameters based on external subsurface information (e.g. geotechnical testing). For rock sites with a flat MHVSR response, inversion cannot resolve model velocities, and additional information is needed. Whether there is broadband or high frequency peak amplification can be used as an indicator of the condition of the rock (i.e. soft/hard or fractured rock).

The second passive source method is the ambient vibration array (AVA) method where multiple sensors are used in 2D geometries (e.g., circles, triangles) to measure surface wave dispersion across the array. Spatial Autocorrelation (SPAC) is a technique developed by Aki (1957) to obtain dispersion estimates representative of the subsurface. Aki (1957) considered ambient noise as a temporal and stochastic process to evaluate the coherency between all sensors in the array (Okada, 2006; Claprood, 2015). The coherency spectra generated between all sensor pairs

are azimuthally averaged over interstation separations (Henstridge, 1979) to determine the average SPAC coefficient at each select frequency (SPAC curves) which have the shape of a zero-order Bessel function (Aki, 1957). Aki (1957) developed this method on the basis of the azimuthal average of the normalized spatial autocorrelation function ρ(r,f) at a distance (*r*) and frequency (*f*) can be shown as Equation 9:

$$\rho(r, f) = \frac{1}{2\pi\varphi(r = 0, f)} \int_0^{2\pi} \varphi(r, \theta, f) d\theta = J_0(\frac{2\pi rf}{c}), \tag{9}$$

where J_0 is the zero-order Bessel function, φ (r=0, f) is the average autocorrelation function at the centre of the array, φ (r, θ, f) is the cross correlation function for several stations located on a semi-circle in polar coordinates (*r, θ*) and the record at the origin with phase velocity (c) at frequency (f) (Chavez-Garcia et al., 2014).

A modified SPAC method (MSPAC) was developed by Bettig et al. (2001) to take into account asymmetrical array types for real-world applicability. The main difference between MSPAC and SPAC is that MSPAC does not calculate the average spatial autocorrelation through a constant radius but with rings instead (i.e., range in radius). MSPAC calculates the average spatial autocorrelation ($\overline{\rho_{r_1, r_2}}$) for ring radii r_1 and r_2 at angular frequency (ω). r and φ indicating the distance and azimuth of the direction between stations respectively, and θ being the azimuth of propagation shown as:

$$\overline{\rho_{r_1, r_2}}(\omega) = \frac{2}{\pi (r_2^2 - r_1^2)} \int_0^\pi \int_{r_1}^{r_2} \cos\left(\frac{\omega r}{c(\omega)} \cos(\theta - \varphi)\right) r \, dr \, d\varphi. \tag{10}$$

In using properties of the zeroth and first order Bessel functions, Equation 10 can be simplified to:

$$\overline{\rho_{r_1, r_2}}(\omega) = \frac{2}{r_2^2 - r_1^2} \int_{r_1}^{r_2} r J_0\left(\frac{\omega r}{c_R(\omega)}\right) dr = \frac{2}{r_2^2 - r_1^2} \frac{c(\omega)}{\omega} \left[r J_1\left(\frac{\omega}{c(\omega)} r\right)\right]_{r_1}^{r_2}. \tag{11}$$

An array can then be broken up into several symmetrical semicircular "sub-arrays" (k) defined by station pairings (i,j) that satisfy $r_{k1} < r_{ij} < r_{k2}$. For each "sub-array" the average spatial autocorrelation is calculated in:

$$\overline{\rho_k}(\omega) = \frac{2}{\pi(r_{k2}^2 - r_{k1}^2)} \sum_{r_{k1} < r_{ij} < r_{k2}} \rho\left(r_{ij}, \varphi_{ij}, \omega\right) \overline{rk} \Delta r_k \Delta \varphi_{ij}. \tag{12}$$

The determination of r_{k1} and r_{k2} results from a compromise between the number of stations per ring (azimuthal resolution) and the ratio Δr_k which should be as small as possible. The average of the spatial autocorrelation for each sub-array is calculated in Equation 12 and reduced in Equation 13 by: $\overline{r_k} = \frac{(r_{k2}+r_{k1})}{2}$, $\Delta r_k = r_{k2} - r_{k1}$, $\Delta\varphi_{ij} = \frac{(\varphi_{ij+1}-\varphi_{ij-1})}{2}$, and $\sum_{r_{k1} < r_{ij} < r_{k2}} \Delta\varphi_{ij} = \pi$:

$$\overline{\rho_k}(\omega) = \frac{1}{\pi} \sum_{r_{k1} < r_{ij} < r_{k2}} \rho(r_{ij}, \varphi_{ij}, \omega)\Delta\varphi_{ij}. \tag{13}$$

Once the average spatial autocorrelation $\overline{\rho_k}(\omega)$ is obtained from Equation 13, dispersion histogram plots are computed with phase velocity c(ω) against frequency. Phase velocities are acquired by non-linear inversion based on least squares adjustment (Tarantola and Valette, 1982) with the problem shown in Bettig et al. (2001). SPAC is preferable to other methods in that it requires fewer stations and smaller station separation to achieve similar dispersion characteristics than other methods (Okada, 2006). The f-k method mentioned above for MASW processing can also be applied in AVA to acquire dispersion histogram plots.

A dispersion curve is built through both active and passive methods where AVA obtains low frequency estimates and active MASW acquires high frequency estimates. The dispersion curve is later inverted in order to acquire a 1D Vs profile. The inversion of experimental surface wave data is a non-linear, non-unique, and a strongly mixed-determined process (Foti et al., 2017). Model parameters constrain the inversion through *a priori* information. Model parameters such as layer densities, thickness, Vp, and Vs is used. Dispersion curves can also be jointly inverted with MHVSRs to constrain the model further to reduce non-uniqueness. Local and global search methods are used to search for a suitable solution. Local search methods use an initial model which is iteratively updated with many possible models to solve for the misfit between the experimental and theoretical curves. The theoretical model is iteratively modified until the misfit becomes acceptably small. Global search methods are also used where many possible models defined in the parameter space to search for models with a small misfit. For the purpose of this thesis, two global-search methods are used and are described further in Chapter 2.5.

1.6 Site effects and characterization at rock sites

Chapter 2 and 3 of this thesis is the application of non-invasive techniques for the purpose of site characterization and classification at rock sites. Passive methods specifically have often been considered questionable at high velocity sites (Pileggi et al., 2011). This is due to the mechanics in surface wave generation where it is assumed that a sufficiently large velocity contrast is needed in order to develop surface waves with a detectable amplitude to be seen in the microtremor wavefield (Poggi et al., 2017). Active methods have had much more success in characterizing rock sites but common challenges still occur such as lateral variability and the generation of detectable surface waves.

Seismic hazard assessment involves the prediction of ground motions which rely on ground motion models (GMM). Ground motions are predicted via GMMs based on earthquake magnitude, source-to-site distance and site conditions, i.e., V_{s30}, but more frequently also f_0 (Hassani and Atkinson, 2018; Hassani and Atkinson, 2016). The largest uncertainties in ground motion prediction are typically due to site conditions. Measurement of V_{s30} at the site of interest is then accomplished to reduce uncertainty in the predicted ground motions, i.e., site-specific seismic hazard assessment. High-consequence facilities (e.g., nuclear power plants, hydro-electric dams) are typically located on rock and designed for long (10,000 year) return periods. The sole site classification measure for rock sites is V_{s30} (Table 1.1) whereas other methods such as undrained shear strength or standard penetration testing blowcounts can be used to classify soil sites. Hence, reduction in ground motion uncertainty for these high-consequence facilities relies significantly on V_{s30}. Another important seismic parameter for characterization of rock sites is seismic kappa (κ) which describes how spectral amplitudes decay as frequency increases (Atkinson, 1996; Anderson and Hough, 1984). Seismic κ is the measure of the slope of the amplitude decay at higher frequencies in the spectral domain (Palmer and Atkinson, 2018).

Rock sites have been explored scarcely for the purpose of site characterization due to the complexities they impose. Hard rock sites should exhibit no earthquake ground motion amplification but in reality, some amplification occurs at higher frequencies due to fractured and weathered layers near the surface (Tucker et al., 1984; Steidl et al., 1996; Boore and Joyner, 1997). With weathering and fracturing in the near surface, lateral variability is expected at rock sites. The presence of lateral variation complicates site characterization collected at seismic

stations as measurement locations are typically away from the station and may not be fully representative of the station's site conditions. Additional steps need to be taken to calibrate measurements to be representative of those taken at the station. With high velocity rock measurements being taken, slight variation in the wavenumber can lead to fluctuation in the measured velocity (Garofalo et al., 2016a). A variety of measures have been used to characterize rock sites including surficial geology, topography/morphology, V_{S30}, seismic κ, and f_0 (SERA, 2019).

Earthquake recording sites (seismograph stations) provide opportunity to validate site characterization methods compared to the observed site response. There is a growing effort in performing site characterization for seismic networks worldwide (e.g. SERA strong motion site characterization project). There have been notable attempts at evaluating site characterization methodologies at rock sites of the French (Hollender et al., 2018) and Swiss (Poggi et al., 2017) seismic networks. Surface wave methods to characterize hard-rock sites have had mixed success where some authors have been unsuccessful (e.g. Michel et al., 2014) but others have shown success (e.g. Garafalo et al., 2016b; Poggi et al., 2017; Hollender et al., 2018). Poggi et al. (2017) used both Love and Rayleigh wave AVA dispersion estimates in a joint inversion with their MHVSRs to determine Vs profiles. Other authors have had less success in the use of passive methods (e.g. Pileggi et al., 2011). Hollender et al. (2018) successfully used both Rayleigh-wave MASW (MAS_RW) and Love-wave MASW (MAS_LW) as well as AVA using both wave types to generate Rayleigh and Love dispersion curves which were jointly inverted with MHVSRs taken at the station. Overall, these studies have reinforced the use of a multi-method approach incorporating body waves (e.g. refraction) and taking into account Love waves (e.g. MAS_LW) to best characterize rock sites (Martin et al., 2017).

Rock velocities in Eastern Canada have been compiled as part of V_{S30} studies for urban seismic microzonation (e.g. Motazedian et al., 2011; Rosset et al., 2014; Molnar et al., 2020). Microzonation studies typically rely on a dense grid of geotechnical and geophysical measurements to outline hazardous areas prone to amplification. In Eastern Canada, Nastev et al. (2016) compiled geophysical and geotechnical data of the St. Lawrence Lowlands to develop a 3-D geologic model. Data collected consisted of seismic reflection and refraction surveys, downhole surveys, and Minivib high resolution seismic reflection profiling. Paleozoic and

Precambrian rock units were defined and measured at the base of 3-D modelling in the area. Regional differences in rock velocity between Ottawa and Montreal are related to variability in regional rock formations and by uneven weathering. The rock in Montreal (161 samples) has a mean Vs of 3059 m/s with a standard deviation of 745 m/s, whereas Ottawa rock (505 samples) has a mean Vs of 2700 m/s with a standard deviation of 680 m/s. This shows the variability of rock between the two areas and the changing rock velocities within the same city by the high standard deviation. Nastev et al. (2016) also compiled Vs_{30} based on the different rock ages in the St. Lawrence Lowlands and concluded that the Vs of Paleozoic rock is 1500 ± 500 m/s and Precambrian rock is 2500 ± 700 m/s (~700 samples).

Site characterization at rock sites has been accomplished at particular seismograph stations in Canada by researchers for various studies. Beresnev and Atkinson (1997) performed Vs refraction at 11 seismograph stations in Eastern Canada to compute the theoretical site response. 4 out of 11 stations were situated on rock and Vs profiles could be successfully built for all 11 stations. Rock Vs ranged from 1700-3100 m/s with an average of 2600 m/s for all 11 stations. One rock station in Alberta was analyzed by Farrugia et al. (2017) and Farrugia et al. (2018) using an *in situ* MHVSR and an EHVSR to build an amplification model and concluded that there is some amplification (~2) at higher frequencies but the average amplification is ~1. Siddiqqi and Atkinson (2002) looked at site amplification for a variety of "hard rock" stations in Eastern and Western Canada using EHVSRs and concluded that the average EHVSR for rock sites in Canada is 1.1 at 1 Hz and 1.2 at 10 Hz (0.1 standard deviation) with instances of regional variability. Braganza et al. (2016) also examined site amplification for 15 seismograph stations residing on rock in Eastern Canada using EHVSRs. It was concluded similar to Farrugia et al. (2018) that lower amplification was observed at lower frequencies and amplification increased at higher frequencies with some stations having amplification over 2 at frequencies above 10 Hz but the average amplification being less than 2. Atkinson and Cassidy (2000) looked at EHVSRs at 5 Tertiary bedrock stations and 3 "harder" batholithic stations (predating Tertiary bedrock) in Western Canada and created amplification estimates for different ground conditions. The rock had a similar response to studies done in Eastern Canada mentioned above with some stations exhibiting amplification greater than 2 at frequencies greater than 10 Hz.

Canadian National Seismograph Network (CNSN) stations are operated by the Geologic Survey Canada with over 100 high-gain instruments which are used to record small or large earthquakes at a variety of distances (Earthquakes Canada, 2019). CNSN stations are typically placed on outcropping rock in Eastern Canada for the purpose of earthquake location because: (1) recorded waveforms provide distinct first wave arrivals, and (2) all stations correspond to the same velocity model. It is generally assumed that seismograph stations placed on outcropping rock in Eastern Canada are located on "hard rock" meaning a $Vs_{30} \geq 1500$ m/s (e.g. Siddiqi, 2000); *in situ* field measurements are not performed prior to installation. Clusters of seismograph stations are placed in areas susceptible to earthquakes (e.g. Charlevoix, Québec) which are used to locate earthquakes. Earthquake recordings at these stations can be used to assess site response (e.g., EHVSRs) and high frequency ground motion attenuation (seismic κ). Site characterization has traditionally not been accomplished by NRCAN when installing CNSN or strong-motion stations. In contrast, in France the 'Réseau Accélérométrique Pemanent' (RAP) network consists of 150 stations where previous studies performed have proposed soil classes or Vs_{30} for some or all of the RAP stations (Hollender et al., 2018). Switzerland has also characterized many sites on their Swiss strong motion network (Michel et al., 2014) and their national cooperative for the disposal of radioactive waste network (Poggi et al., 2017). The Japanese KiK-net has their network fully characterized with available shear wave velocity profiles (e.g. Foti et al., 2011). Characterizing these stations and sites in general is important for damage mitigation and the generation of accurate GMM's appropriate to the ground conditions that stations are placed on.

1.7   Site effects and characterization at stiff ground sites

Chapter 4 of this thesis is the application of site characterization at stiff ground/rock sites in Vancouver, British Columbia. Stiff sites have been explored in site characterization studies globally and in Canada. There have been multiple examples worldwide but only a few examples are discussed in this section from Christchurch, New Zealand (Teague et al., 2018), Grenoble, France (Garofalo et al., 2016a), and in Chile (Molnar et al., 2015; Molnar et al., 2017).

Stiff gravel sites mixed with softer sediments have been investigated in Christchurch, New Zealand. AVA testing was applied using 10 sensors in large circular arrays (60, 200, and 400 m). Active MASW was also applied with both sledgehammer and vibroseis seismic sources with 2 and 10 m geophone spacing. 48 vertical geophones were used with the sledgehammer source and

15-24 geophones with the vibroseis. With the use of varied sources and geophone spacing, well-constrained Vs profiles were developed successfully for 14 sites in comparison to downhole Vs measurements. Velocity reversals were identified at some of these sites, identified by dispersion data plateaus or increases in phase velocity at higher frequencies. Teague et al. (2018) also attributes the increase in phase velocity at a higher frequency due to dispersion data transitioning from a higher Rayleigh wave mode back down to a lower mode. The transition of modes in dispersion data is attributed to an effective or superposed mode. The higher mode data results from the interbedding of stiff gravel with softer formations.

A stiff soil site in Grenoble, France was also investigated within the Interpacific project (Garofalo et al., 2016a). Active and passive surface wave methods were applied with multiple arrays and spacing. Active MASW was applied with 48 geophones for both 1 and 1.5 m spacing. AVA was also applied at 5-405 m circular spacing. Triangle and L-shape AVAs were performed with 18-300 m and 5-150 m spacing, respectively. 14 teams independently analyzed the survey datasets to determine Vs profiles. All 14 teams were able to develop a similar velocity profile of the top 100 m, with a low (< 0.04) coefficient of variation in the Vs_{30} values. This site specifically had very similar results between all teams highlighting the success of non-invasive methods at stiff soil sites.

In central and southern Chile 11 strong motion stations were characterized following the 2010 **M** 8.8 Maule earthquake using passive AVA. 3 Tromino sensors were placed in a triangle configuration equidistantly at 5 and 15 m. Dispersion estimates were obtained and inverted into Vs profiles for all 11 stations. 5 stations on stiff sediment were successfully classified as site class B or C with remaining 6 stations being on softer sediment. The subsurface beneath the stiff sediment stations was comprised of variable soils mixed with sand and gravel with soft sedimentary rock or volcanic tuff underlying. In Northern Chile, 17 stations were characterized using passive and active surface wave array testing. AVA was applied in a circular array with 6 sensors spaced between 5, 10, and 15 m. MASW was applied in Northern Chile with 12 sensors and spacing varying between 2 and 7 m. At 9 out of 17 stations, dispersion estimates could not be picked due to stations situated on rock and having flat MHVSRs.

In Canada, few published studies document site characterization on stiff soil. A few examples of site characterization performed in Vancouver are discussed here but a few more studies have been done in Canada (e.g., Molnar et al. 2012, Jackson 2017, and Assaf et al. 2018). Assaf et al. (2018) characterized stiff ground sites and stations in Vancouver as part of microzonation mapping in the region. Assaf et al. (2018) shows the successful classification of two stiff soil strong-motion stations in Vancouver where passive AVA was applied using a circular array of 7 sensors spaced from 5-30 m. MASW was also applied using a 24 geophone line with sensor spacing varying between 0.5-3 m. Vs profiles and therefore Vs_{30} was able to be acquired successfully in the characterization of these strong-motion stations. Jackson (2017) looked at 13 sites across southwest British Columbia. AVA was performed using 9 instruments in a circular-shaped array where sensor spacing varied from 5 to 25 m. Dispersion estimates were acquired at all sites and Vs_{30} could be calculated. In this study, site classes are updated from the current microzonation map (Taylor et al. 2006). The compiled mean Vs_{30} of stiff glaciated sites across southwestern British Columbia is 475 m/s ($\pm$ 78 m/s) (Monahan and Levson 2001). Similarly, the compiled mean Vs_{30} of stiff glaciated sites in the St. Lawrence Lowlands is 385 m/s ($\pm$ 152 m/s) (Nastev et al. 2016) and Ottawa 580 ($\pm$ 152 m/s) (Motazedian et al., 2011).

Through global and local studies, it is identified that non-invasive Vs profiling techniques applied at stiff ground sites do not poise as much of a challenge as at rock sites but are more complex than performing non-invasive testing at soft soil sites. Complexities can be imposed as seen in the Northern Chile study where lateral variability can still play a factor as well as having rock outcrops nearby these sites. Velocity reversals in the subsurface complicate dispersion mode interpretation, whether the fundamental mode is identified correctly or if multiple modes are mixing causing an "effective" mode. In the above studies, Vs profiles could be generated for all stiff ground sites past 30 m, therefore Vs_{30} could be calculated. Vs_{30} could be calculated for AVA surveys with spacing up to 15 m as well as active methods with multiple spacing to constrain the near surface. Larger arrays up to 30 m were performed to ensure that the 30 m resolution depth is acquired. Stiff soil sites have been characterized successfully and robustly through both active and passive surface wave methods, where a multi-method approach is also encouraged.

1.8 Thesis motivation

I aim to advance the use of non-invasive active- and passive-source seismic techniques at rock and stiff ground sites as few studies have demonstrated their effectiveness for site characterization of stiff-to-hard ground sites. I examine whether non-invasive methods provide robust Vs and site amplification estimates at hard rock sites at Eastern Canada seismograph stations and stiff ground sites in Metro Vancouver.

I aim to improve the site characterization of CNSN seismograph stations placed on rock in Eastern Canada in using a multi-method site characterization approach. Having *in situ* rock Vs measurements is crucial in generating accurate GMM's and for the safety of high consequence infrastructure (e.g. hydro-electric dams). I attempt to determine a Vs profile and Vs_{30} site class, site amplification function (MHVSRs and EHVSRs), and rock Vp through lab sample experiments and seismic refraction. A parallel study is also being performed in studying seismic kappa at the same CNSN seismograph stations (Palmer and Atkinson, 2020). Demonstrating the effectiveness of non-invasive seismic techniques for site characterization at stiff ground and rock sites is important to regional seismic microzonation mapping. I perform site characterization and classification at 10 stiff ground sites to summarize stiff ground in Vancouver and to add to the database of Vs measurements in the region and thereby improve future amplification or shake map products.

1.9 Organization of work

This thesis includes five chapters regarding non-invasive Vs profiling methods in attempts to classify supposed "hard rock" seismograph stations in Eastern Canada and stiff soil and rock sites in Vancouver.

The second chapter entails the multi-method approach in characterizing seismic stations in Eastern Canada to achieve Vs_{30} site classification at 25 CNSN stations assumed to be situated on "hard rock". Several non-invasive seismic techniques are applied including AVA, MASW, Vp refraction, Vp rock sample lab measurements, and MHVSR/EHVSR calculations. Not all methods were used at each station due to spatial and logistical constraints. Measurements were taken nearby the station in order for equipment to be placed in the ground. Dispersion estimates

were made at stations where methods were successful through MASW and AVA. Surface wave inversions are done through a Bayesian and a modified neighborhood algorithm. The Bayesian inversion approach was used in order to evaluate data error and model parameterization to produce the most probable velocity profile with quantitative uncertainty estimates in the final model. The modified neighborhood algorithm Vs profile is classified as the lowest misfit model in fitting the forward model best with also falling into the range of Vs profiles that the Bayesian inversion provides. Rock velocities are analyzed and presented in this chapter.

Chapter three applies measurements in chapter two in performing site classification at visited stations in Eastern Canada. Measurements were performed at a distance from the station where site conditions had to be calibrated to that of the conditions to which the seismograph station is residing on. A multi-method approach is applied in this chapter to give an assessment of the site conditions the station is placed on. Vs_{30} calculations are given in this section for both inversion methods. One Vs_{30} indicating the best fitting model's site class through the modified neighborhood algorithm and another Vs_{30} showing a range of possible Vs_{30} through the Bayesian inversion software. Vs_{30} extrapolation is also performed at stations where the resolution depth does not exceed 30 m from analyzing dispersion estimates.

The fourth chapter is compilation of additional work completed in improving the present microzonation map of Vancouver (e.g. Molnar et al., 2020) where stiff glaciated sediment sites are evaluated. These sites are looked at in addition to building a database of Vs measurements in a site classification map which will be used in the project. They are compared with the site classification from Taylor et al. (2006). These are included as additional work and velocity profiles that others can use for their respective purposes. Methods for Vs profiling include non-invasive active and passive surface wave methods (MASW and AVA) which are jointly inverted with MHVSRs to best-represent the site conditions. This is a small portion of work put towards the bigger project in a site amplification map of the region.

Chapter five presents and summarizes overall findings and conclusions in this thesis. Rock velocities found throughout Eastern Canada are summarized and compared with previous studies. Additional methods are suggested to add to the multi-method approach to improve site

characterization at both stiff soil and rock sites. The importance of having a dense grid of Vs measurements for microzonation projects is summarized, specifically for Vancouver.

1.10   References

Adams, J. (1989). Seismicity and Seismotectonics of Southeastern Canada. *Annals of the New York Academy of Sciences*, *558*(1), 40-53.

Adams, J., & Basham, P. W. (1989). Seismicity and seismotectonics of Canada's eastern margin and craton. In *Earthquakes at North-Atlantic passive margins: neotectonics and postglacial rebound* (pp. 355-370). Springer, Dordrecht.

Adams, J., Allen, T., Halchuk, S., & Kolaj, M. (2019). Canada's 6th Generation Seismic Hazard Model, as Prepared for the 2020 National Building Code of Canada. *12th Can. Conf. Earthquake Engineering*.

AIR Worldwide. (2013). Study of Impact and the Insurance and Economic Cost of a Major Earthquake in British Columbia and Ontario/Quebec. Boston, MA.

Aki, K. (1957). Space and time spectra of stationary stochastic waves, with special reference to microtremors. *Bulletin of the Earthquake Research Institute, University of Tokyo*, *35*(3), 415-456.

Allen, T. I., & Wald, D. J. (2009). On the use of high-resolution topographic data as a proxy for seismic site conditions (Vs_{30}). *Bulletin of the Seismological Society of America*, *99*(2A), 935-943.

Anderson, J. G., & Hough, S. E. (1984). A model for the shape of the Fourier amplitude spectrum of acceleration at high frequencies. *Bulletin of the Seismological Society of America*, *74*(5), 1969-1993.

Assaf, J., Molnar, S., Naggar, H., Sirohey, A. (2019). Site Characterization at Strong Motion Stations in Metro Vancouver. *Proceedings of the 12th CCEE (Canadian Conference on Earthquake Engineering) 2019*.

Asten, M. W., & Henstridge, J. D. (1984). Array estimators and the use of microseisms for reconnaissance of sedimentary basins. *Geophysics*, *49*(11), 1828-1837.

Atkinson, G. M. (1996). The high-frequency shape of the source spectrum for earthquakes in eastern and western Canada. *Bulletin of the Seismological Society of America*, *86*(1A), 106-112.

Atkinson, G. M., & Cassidy, J. F. (2000). Integrated use of seismograph and strong-motion data to determine soil amplification: response of the Fraser River Delta to the Duvall and Georgia Strait earthquakes. *Bulletin of the Seismological Society of America*, *90*(4), 1028-1040.

Atwater, B. F., Nelson, A. R., Clague, J. J., Carver, G. A., Yamaguchi, D. K., Bobrowsky, P. T., ... & Kelsey, H. M. (1995). Summary of coastal geologic evidence for past great earthquakes at the Cascadia subduction zone. *Earthquake spectra*, *11*(1), 1-18.

Bank of Canada. "Inflation Calculator." *Bank of Canada*, https://www.bankofcanada.ca/rates/related/inflation-calculator/. Last accessed April 1st, 2019

Bard, P., Jongmans, D., Ohrnberger, M., & Wathelet, M. (2005). *Site Effects Assessment Using Ambient Excitations (Sesame) - Recommendations for quality array measurements and processing*. European Commission - Research General Directorate.

Bent, A. L. (1996). Source parameters of the damaging Cornwall-Massena earthquake of 1944 from regional waveforms. *Bulletin of the Seismological Society of America*, *86*(2), 489-497.

Beresnev, I. A., & Atkinson, G. M. (1997). Shear-wave velocity survey of seismographic sites in eastern Canada: Calibration of empirical regression method of estimating site response. *Seismological Research Letters*, *68*(6), 981-987.

Bettig, B., Bard, P. Y., Scherbaum, F., Riepl, J., Cotton, F., Cornou, C., & Hatzfeld, D. (2001). Analysis of dense array noise measurements using the modified spatial auto-correlation method (SPAC): application to the Grenoble area. *Bollettino di Geofisica Teorica ed Applicata*, *42*(3-4), 281-304.

Boore, D. M., & Joyner, W. B. (1997). Site amplifications for generic rock sites. *Bulletin of the seismological society of America*, *87*(2), 327-341.

Borcherdt, R. D. (1970). Effects of local geology on ground motion near San Francisco Bay. *Bulletin of the Seismological Society of America*, *60*(1), 29-61.

Borcherdt, R. D. (1994). Estimates of site-dependent response spectra for design (methodology and justification). *Earthquake spectra*, *10*, 617-617.

Braganza, S., Atkinson, G. M., Ghofrani, H., Hassani, B., Chouinard, L., Rosset, P., ... & Hunter, J. (2016). Modeling site amplification in eastern Canada on a regional scale. *Seismological Research Letters*, *87*(4), 1008-1021.

Capon, J. (1969). High-resolution frequency-wavenumber spectrum analysis. *Proceedings of the IEEE*, *57*(8), 1408-1418.

Claprood, M., (2015). Spatially Averaged Coherency Spectrum (SPAC) Ambient Noise Array Method; in Shear Wave Velocity Measurement Guidelines for Canadian Seismic Site Characterization in Soil and Rock, (ed.) J.A. Hunter and H.L. Crow; Geological Survey of Canada, Earth Science Sector, General Information Product 110 e, p. 93-101.

Chávez-García, F. J., Manakou, M. V., & Raptakis, D. G. (2014). Subsoil structure and site effects: A comparison between results from SPAC and HVSR in sites of complex geology. *Soil Dynamics and Earthquake Engineering*, *57*, 133-142.

Di Alessandro, C., Bonilla, L. F., Boore, D. M., Rovelli, A., & Scotti, O. (2012). Predominant-period site classification for response spectra prediction equations in Italy. *Bulletin of the Seismological Society of America*, *102*(2), 680-695.

Farrugia, J. J., Molnar, S., & Atkinson, G. M. (2017). Noninvasive Techniques for Site Characterization of Alberta Seismic Stations Based on Shear-Wave. *Bulletin of the Seismological Society of America*, *107*(6), 2885-2902.

Farrugia, J. J., Atkinson, G. M., & Molnar, S. (2018). Validation of 1D Earthquake Site Characterization Methods with Observed Earthquake Site Amplification in Alberta. *Bulletin of the Seismological Society of America*, *108*(1), 291-308.

Field, E., & Jacob, K. (1993). The theoretical response of sedimentary layers to ambient seismic noise. *Geophysical research letters*, *20*(24), 2925-2928.

Finn, W. L., & Wightman, A. (2003). Ground motion amplification factors for the proposed 2005 edition of the National Building Code of Canada. *Canadian Journal of Civil Engineering*, *30*(2), 272-278.

Forsyth, D. A. (1981). Characteristics of the western Quebec seismic zone. *Canadian Journal of Earth Sciences*, *18*(1), 103-119.

Foti, S. (2000). *Multistation methods for geotechnical characterization using surface waves* (p. 229).

Foti, S., Parolai, S., Bergamo, P., Di Giulio, G., Maraschini, M., Milana, G., ... & Puglia, R. (2011). Surface wave surveys for seismic site characterization of accelerometric stations in ITACA. *Bulletin of Earthquake Engineering*, *9*(6), 1797-1820.

Foti, S., Hollender, F., Garofalo, F., Albarello, D., Asten, M., Bard, P. Y., ... & Forbriger, T. (2017). Guidelines for the good practice of surface wave analysis: A product of the InterPACIFIC project. *Bulletin of Earthquake Engineering*, *16*(6), 2367-2420.

Frankel, A. D., Carver, D. L., & Williams, R. A. (2002). Nonlinear and linear site response and basin effects in Seattle for the M 6.8 Nisqually, Washington, earthquake. *Bulletin of the Seismological Society of America*, *92*(6), 2090-2109.

Fukushima, Y., Bonilla, L. F., Scotti, O., & Douglas, J. (2007). Site classification using horizontal-to-vertical response spectral ratios and its impact when deriving empirical ground-motion prediction equations. *Journal of Earthquake Engineering*, *11*(5), 712-724.

Gabriels, P., Snieder, R., & Nolet, G. (1987). In situ measurements of shear-wave velocity in sediments with higher-mode Rayleigh waves. *Geophysical prospecting*, *35*(2), 187-196.

Garofalo, F., Foti, S., Hollender, F., Bard, P. Y., Cornou, C., Cox, B. R., ... & Forbriger, T. (2016a). InterPACIFIC project: Comparison of invasive and non-invasive methods for seismic site characterization. Part I: Intra-comparison of surface wave methods. *Soil Dynamics and Earthquake Engineering*, *82*, 222-240.

Garofalo, F., Foti, S., Hollender, F., Bard, P. Y., Cornou, C., Cox, B. R., ... & Teague, D. (2016b). InterPACIFIC project: Comparison of invasive and non-invasive methods for seismic site characterization. Part II: Inter-comparison between surface-wave and borehole methods. *Soil Dynamics and Earthquake Engineering*, *82*, 241-254

Haskell, N. A. (1960). Crustal reflection of plane SH waves. *Journal of Geophysical Research*, *65*(12), 4147-4150.

Hassani, B., & Atkinson, G. M. (2016). Applicability of the site fundamental frequency as a VS 30 proxy for central and eastern North America. *Bulletin of the Seismological Society of America*, *106*(2), 653-664.

Hassani, B., & Atkinson, G. M. (2018). Site-Effects Model for Central and Eastern North America Based on Peak Frequency and Average Shear-Wave VelocitySite-Effects Model for CENA Based on Peak Frequency and Average Shear-Wave Velocity. *Bulletin of the Seismological Society of America*, *108*(1), 338-350.

Henstridge, J. D. (1979). A signal processing method for circular arrays. *Geophysics*, *44*(2), 179-184.

Hollender, F., Cornou, C., Dechamp, A., Oghalaei, K., Renalier, F., Maufroy, E., ... & Boutin, V. (2018). Characterization of site conditions (soil class, Vs$_{30}$, velocity profiles) for 33 stations from the French permanent accelerometric network (RAP) using surface-wave methods. *Bulletin of Earthquake Engineering*, *16*(6), 2337-2365.

Hunter, J.A. and Atukorala, U. (2015). Chapter 1.0: Introduction; *in* Shear Wave Velocity Measurement Guidelines for Canadian Seismic Site Characterization in Soil and Rock, (ed.) J.A. Hunter and H.L. Crow; Geological Survey of Canada, Earth Science Sector, General Information Product 110 e (2015), p. 8-17.

Hunter, J. A. M., Crow, H. L., Arsenault, J. L., Atukorala, U., Best, M. E., Campos, D., ... & Dutrisac, H. (2015). *Shear wave velocity measurement guidelines for Canadian seismic site characterization in soil and rock*. Natural Resources Canada.

Jackson, Frederick Andrew. (2017). "Assessment of Earthquake Site Amplification and Application of Passive Seismic Methods for Improved Site Classification in the Greater Vancouver Region, British Columbia" *Electronic Thesis and Dissertation Repository*. 4938. https://ir.lib.uwo.ca/etd/

Kolaj, M., Allen, T., Mayfield, R., Adams, J., & Halchuk, S. (2019). Ground-motion models for the 6th Generation Seismic Hazard Model of Canada. In *12th Canadian Conference on Earthquake Engineering*.

Kramer, S. L. (1996). *Geotechnical Earthquake Engineering*. Upper Saddle River, New Jersey: Prentice Hall Inc.

Lacoss, R. T., Kelly, E. J., & Toksöz, M. N. (1969). Estimation of seismic noise structure using arrays. *Geophysics*, *34*(1), 21-38.

Lamontagne, M. (1987). Seismic activity and structural features in the Charlevoix region, Quebec. *Canadian Journal of Earth Sciences*, *24*(11), 2118-2129.

Lamontagne, M. (2008). Casualties directly caused by an earthquake in Canada: First contemporaneous written accounts from the M 6.5 Charlevoix, Quebec, earthquake of 20 October 1870. *Bulletin of the Seismological Society of America*, *98*(3), 1602-1606.

Lamontagne, M., & Ranalli, G. (1996). Thermal and rheological constraints on the earthquake depth distribution in the Charlevoix, Canada, intraplate seismic zone. *Tectonophysics*, *257*(1), 55-69.

Lemoine, A., Douglas, J., & Cotton, F. (2012). Testing the applicability of correlations between topographic slope and Vs_{30} for Europe. *Bulletin of the Seismological Society of America*, *102*(6), 2585-2599.

Lowrie, W. (2007). *Fundamentals of geophysics*. Cambridge: Cambridge University Press.

Ma, S., & Eaton, D. W. (2007). Western Quebec seismic zone (Canada): Clustered, midcrustal seismicity along a Mesozoic hot spot track. *Journal of Geophysical Research: Solid Earth*, *112*(B6).

Ma, S. (2009). Seismicity and Seismotectonics in Eastern Canada and Vicinity. *University of Western Ontario PHD Thesis*.

Michel, C., Edwards, B., Poggi, V., Burjánek, J., Roten, D., Cauzzi, C., & Fäh, D. (2014). Assessment of site effects in alpine regions through systematic site characterization of seismic stations. *Bulletin of the Seismological Society of America*, *104*(6), 2809-2826.

Molnar, S., (2015). Frequency-wavenumber (f-k) Ambient Noise Array Method; in Shear Wave Velocity Measurement Guidelines for Canadian Seismic Site Characterization in Soil and Rock, (ed.) J.A. Hunter and H.L. Crow; Geological Survey of Canada, Earth Science Sector, General Information Product 110 e, p. 102-119.

Molnar, S., Ventura, C. E., Boroschek, R., & Archila, M. (2015). Site characterization at Chilean strong-motion stations: Comparison of downhole and microtremor shear-wave velocity methods. *Soil Dynamics and Earthquake Engineering*, *79*, 22-35.

Molnar, S., Braganza, S., Farrugia, J., Atkinson, G., Boroschek, R., & Venture, C. (2017). Earthquake site class characterization of seismograph and strong-motion stations in Canada and Chile. In *Proc. from the 16th World Conf. on Earthquake Engineering*.

Molnar, S., Cassidy, J. F., Castellaro, S., Cornou, C., Crow, H., Hunter, J. A., ... & Yong, A. (2018). Application of microtremor horizontal-to-vertical spectral ratio (MHVSR) analysis for site characterization: State of the art. *Surveys in Geophysics*, *39*(4), 613-631.

Molnar, S., J. Assaf, A. Sirohey, S. Adhikari (2020). Overview of local site effects and seismic microzonation mapping in Metropolitan Vancouver, British Columbia, Canada. *Engineering Geology*, 270, 105568.

Monahan, P. A., Levson, V. M., McQuarrie, E. J., Bean, S. M., Henderson, P., & Sy, A. (2000). Relative Earthquake Hazard Map of Greater Victoria showing areas susceptible to amplification of ground motion, liquefaction and earthquake-induced slope instability. *British Columbia Geological Survey, Ministry of Energy and Mine*, 2000-1.

Monahan, P. A., & Levson, V. M. (2001). Development of a Shear Wave Velocity Model of the Near-Surface Deposits of Southwestern British Columbia, Canada.

Motazedian, D., Hunter, J. A., Pugin, A., & Crow, H. (2011). Development of a Vs_{30} (NEHRP) map for the city of Ottawa, Ontario, Canada. *Canadian Geotechnical Journal*, *48*(3), 458-472.

Nakamura, Y. (1989). A method for dynamic characteristics estimation of subsurface using microtremor on the ground surface. *Railway Technical Research Institute, Quarterly Reports*, *30*(1).

Nastev, M., Parent, M., Benoit, N., Ross, M., & Howlett, D. (2016). Regional Vs_{30} model for the St. Lawrence Lowlands, Eastern Canada. *Georisk: Assessment and Management of Risk for Engineered Systems and Geohazards*, *10*(3), 200-212.

National Research Council. (2015). *National Building Code of Canada* (Vol. 1). Ottawa, ON.

Natural Resources Canada, Earthquakes Canada. (2011). *Earthquakes in Southwestern British Columbia*. Retrieved September 11, 2019, from http://www.seismescanada.rncan.gc.ca/pprs-pprp/pubs/GF-GI/GEOFACT_earthquakes-SW-BC_e.pdf

Natural Resources Canada, Earthquakes Canada. (2018). Earthquake zones in Eastern Canada. Retrieved April 4, 2019, from http://www.seismescanada.rncan.gc.ca/zones/eastcan-en.php

Natural Resources Canada, Earthquakes Canada. (2019). Introduction to the Canadian National Seismograph Network. Retrieved from http://earthquakescanada.nrcan.gc.ca/stndon/CNSN-RNSC/index-en.php

Natural Resources Canada, Earthquakes Canada. (2019). Seismic zones in Western Canada. Retrieved from http://earthquakescanada.nrcan.gc.ca/zones/westcan-en.php

Nazarian S. and Stokoe II K.H. (1984). In situ shear wave velocity fromspectral analysis of surface waves. *Proceedings of the 8th Conference on Earthquake Engineering- San Francisco*, Vol. **3**, pp. 31–38. Prentice–Hall, Inc.

Nogoshi, M., & Igarashi, T. (1971). On the amplitude characteristics of microtremor—Part 2: Journal of the Seismological Society of Japan, 24, 26–40.

Okada, H. (2006). Theory of efficient array observations of microtremors with special reference to the SPAC method. *Exploration Geophysics*, *37*(1), 73-85.

Onur, T., Ventura, C. E., & Finn, W. L. (2005). Regional seismic risk in British Columbia—damage and loss distribution in Victoria and Vancouver. *Canadian journal of civil engineering*, *32*(2), 361-371.

Palmer, S.M., and Atkinson, G.M. (2018) Bedrock Site Conditions and Kappa in Charlevoix, Quebec. Seismological Research Letters: Volume 89 Number 2B, pp 750 and 821.

Palmer, S. M., & Atkinson, G. M. (2020). The High-Frequency Decay Slope of Spectra (Kappa) for $M \geq$ 3.5 Earthquakes on Rock Sites in Eastern and Western Canada. *Bulletin of the Seismological Society of America*, *110*(2), 471-488.

Park, C. B., Miller, R. D., & Xia, J. (1999). Multichannel analysis of surface waves. *Geophysics*, *64*(3), 800-808.

Parker, G. A., Harmon, J. A., Stewart, J. P., Hashash, Y. M., Kottke, A. R., Rathje, E. M., ... & Campbell, K. W. (2017). Proxy-based VS 30 estimation in central and eastern North America. *Bulletin of the Seismological Society of America*, *107*(1), 117-131.

Pacific Northwest Seismic Network (2011). Cascadia Subduction Zone. Retrieved from https://pnsn.org/outreach/earthquakesources/csz.

Perret, D., & Lamarche, L. (2013). Microzonage sismique des villes de Québec - Ancienne-Lorette et réserve indienne Wendake (période de vibration des terrains), Québec. *Natural Resources Canada*. doi: 10.4095/292641

Phillips, C. and Sol, S., (2015). Multichannel Analysis of Surface Waves (MASW) Technique for Hazard Studies; *in* Shear Wave Velocity Measurement Guidelines for Canadian Seismic Site Characterization in Soil and Rock, (ed.) J.A. Hunter and H.L. Crow; Geological Survey of Canada, Earth Science Sector, General Information Product 110 e, p. 61-65.

Pileggi, D., Rossi, D., Lunedei, E., & Albarello, D. (2011). Seismic characterization of rigid sites in the ITACA database by ambient vibration monitoring and geological surveys. *Bulletin of Earthquake Engineering*, *9*(6), 1839-1854.

Piña-Flores, J., Perton, M., García-Jerez, A., Carmona, E., Luzón, F., Molina-Villegas, J. C., & Sánchez-Sesma, F. J. (2016). The inversion of spectral ratio H/V in a layered system using the diffuse field assumption (DFA). *Geophysical Journal International*, ggw416.

Ploeger, S. (2013). Seismic Loss Estimation for the National Capital Region: A Discussion on Hazus. *3rd Annual CSCE Conference*.

Poggi, V., Burjanek, J., Michel, C., & Fäh, D. (2017). Seismic site-response characterization of high-velocity sites using advanced geophysical techniques: application to the NAGRA-Net. *Geophysical Journal International*, *210*(2), 645-659.

Rosset, P., Bour-Belvaux, M., & Chouinard, L. (2015). Microzonation models for Montreal with respect to Vs$_{30}$. *Bulletin of Earthquake Engineering*, *13*(8), 2225-2239.

Satake, K., Shimazaki, K., Tsuji, Y., & Ueda, K. (1996). Time and size of a giant earthquake in Cascadia inferred from Japanese tsunami records of January 1700. *Nature*, *379*(6562), 246-249.

SERA. (2019). Seismology and Earthquake Engineering Research Infrastructure Alliance of Europe. Retrieved October 1, 2019, from http://www.sera-eu.org/home.

Shearer, P. M., & Orcutt, J. A. (1987). Surface and near-surface effects on seismic waves—theory and borehole seismometer results. *Bulletin of the Seismological Society of America*, *77*(4), 1168-1196.

Siddiqi, J. A. (2000). *Horizontal-to-vertical component ratios for earthquake ground motions recorded on hard rock sites in Canada* (Doctoral dissertation, Carleton University).

Siddiqqi, J., & Atkinson, G. M. (2002). Ground-motion amplification at rock sites across Canada as determined from the horizontal-to-vertical component ratio. *Bulletin of the Seismological Society of America*, *92*(2), 877-884.

Socco, L. V., & Strobbia, C. (2004). Surface-wave method for near-surface characterization: a tutorial. *Near Surface Geophysics*, *2*(4), 165-185.

Steidl, J. H., Tumarkin, A. G., & Archuleta, R. J. (1996). What is a reference site?. *Bulletin of the Seismological Society of America*, *86*(6), 1733-1748.

Tarantola, A., (1987). Inverse Problem Theory: Methods for Data Fitting and Model Parameter Estimation, Elsevier, Amsterdam.

Tarantola, A., & Valette, B. (1982). Generalized nonlinear inverse problems solved using the least squares criterion. *Reviews of Geophysics*, *20*(2), 219-232.

Taylor, G. W., Monahan, P., White, T. W., & Ventura, C. E. (2006). British Columbia school seismic mitigation program. Dominant influence of soil type on life safety of greater Vancouver and lower mainland schools of British Columbia. 8th U. S. National Conference on Earthquake Engineering, San Francisco, California.

Teague, D., Cox, B., Bradley, B., & Wotherspoon, L. (2018). Development of Deep Shear Wave Velocity Profiles with Estimates of Uncertainty in the Complex Interbedded Geology of Christchurch, New Zealand. *Earthquake Spectra*, *34*(2), 639-672.

Tinsley, J. C., & Fumal, T. E. (1985). Mapping Quaternary sedimentary deposits for areal variations in shaking response. *Evaluating Earthquake Hazards in the Los Angeles Region—An Earth Science Perspective*, *1360*, 101-126.

Tucker, B. E., King, J. L., Hatzfeld, D., & Nersesov, I. L. (1984). Observations of hard-rock site effects. *Bulletin of the Seismological Society of America*, *74*(1), 121-136.

Wathelet, M. (2005). Array recordings of ambient vibrations: surface-wave inversion. *PhD Diss., Liége University*, *161*.

Wills, C. J., Petersen, M., Bryant, W. A., Reichle, M., Saucedo, G. J., Tan, S., ... & Treiman, J. (2000). A site-conditions map for California based on geology and shear-wave velocity. *Bulletin of the Seismological Society of America*, *90*(6B), S187-S208.

Wills, C. J., Gutierrez, C. I., Perez, F. G., & Branum, D. M. (2015). A Next Generation Vs_{30} Map for California Based on Geology and Topography. *Bulletin of the Seismological Society of America*, *105*(6), 3083-3091.

Yong, A. (2016). Comparison of measured and proxy-based VS 30 values in California. *Earthquake Spectra*, *32*(1), 171-192.

Zhao, J. X., Irikura, K., Zhang, J., Fukushima, Y., Somerville, P. G., Asano, A., ... & Ogawa, H. (2006). An empirical site-classification method for strong-motion stations in Japan using H/V response spectral ratio. *Bulletin of the Seismological Society of America*, *96*(3), 914-925.

Chapter 2 Multi-Method Non-Invasive Testing at "Hard Rock" Stations in Eastern Canada

2.1 Introduction

Seismograph stations in Eastern Canada are typically placed on outcropping rock in areas where earthquakes occur or around high consequence infrastructure (e.g. nuclear power plants and hydro-electric dams). Seismographs on rock provide clean first arrivals for earthquake detection and location purposes. Seismograph stations in Eastern Canada are assumed to be placed on "hard rock" ($Vs_{30} > 1500$ m/s) within site class A in accordance with the NBCC. *In situ* site characterization measurements are typically not accomplished prior to installation which highlights the importance in knowing the ground conditions the instruments are placed on. Knowing the ground conditions that stations are placed on is crucial for developing GMM's and understanding site response in the case of an earthquake. Rock sites pose a challenge in acquiring the proper site characterization in that drilling through rock with invasive methods is not ideal; a 30 m deep hole would cost approximately $6,000 ($200 per meter). Non-invasive methods are a less-expensive alternative but have their own challenges from needing sufficient space away from the station and in the measurement of velocities directly on the rock outcrop. 25 seismograph stations were visited in summer and fall 2017 (Figure 2.1) to perform *in situ* non-invasive site characterization measurements at these stations; a parallel study is determining seismic kappa (Palmer and Atkinson, 2020; Atkinson, 1996) at the same stations.
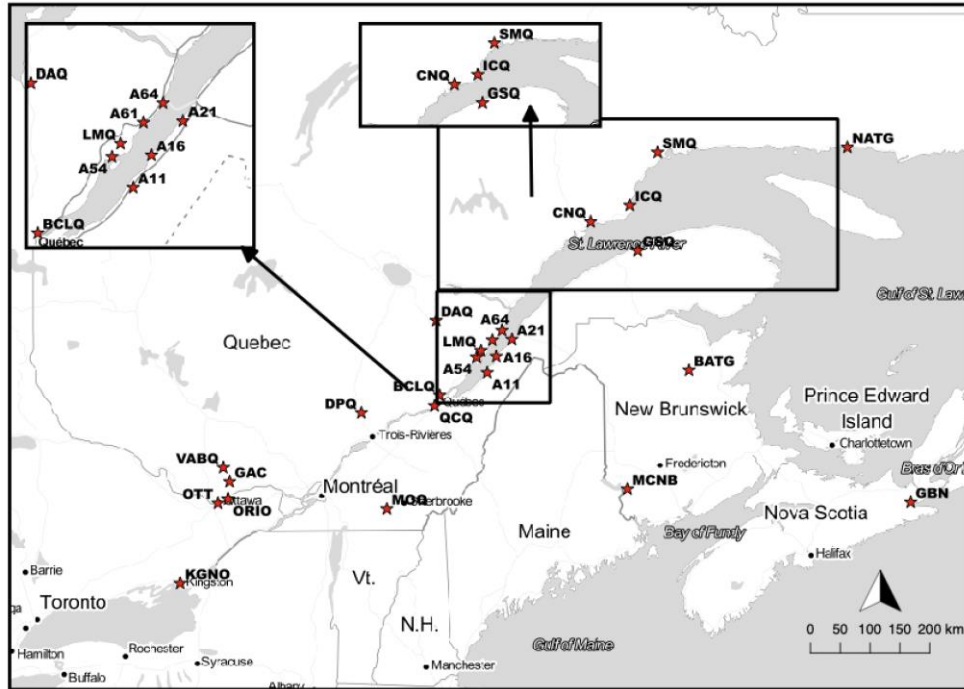
Figure 2.1: Locations of the 25 investigated seismograph stations in Eastern Canada are shown by stars, labels are the station code (Ladak et al., 2019).

A multi-method approach was used to characterize each station, including determining a Vs profile and additional site properties such as compression wave velocity (Vp) and Poisson's ratio. Surface wave array methods used include active-source multi-channel analysis of surface waves (MASW) and passive-source ambient vibration array (AVA). Surface wave dispersion data was inverted to develop a 1D Vs profile and provide estimates of the rock Vs. Vp refraction was used to acquire rock Vp to constrain dispersion inversions and to calculate the rock Poisson's ratio. Microtremor measurements were taken at each station and the microtremor horizontal to vertical spectral ratio (MHVSR) is then calculated. At three stations, rock samples were collected and brought back to perform laboratory Vp measurements for comparison. Earthquake data was acquired from the AutoDRM service from Natural Resources Canada to calculate earthquake HVSRs (EHVSR) by Samantha Palmer to compare with MHVSRs.

The list of stations and their bedrock and surficial geology from available maps is provided in Table 2.1. The rock age is identified for each station to compare with rock velocities from Nastev et al. (2016) as well as to anticipate the ground conditions around each station.

Table 2.1: Visited stations with their associated coordinates and elevation. Bedrock geology from Natural Resources Canada (2013). Surficial geology data is obtained from Fulton (1995).

Station, coordinates and elevation	Bedrock Geology map	Surficial Geology map	Station Installation
A11 Lat: 47.2431 ^{0}N, Long: 70.1969 ^{0}W Elevation: 55 m	Paleozoic (Cambrian) offshelf miogeoclinal sedimentary rocks	Glaciomarine littoral and nearshore sediments	Concrete, insulated vault
A16 Lat: 47.4680 ^{0}N, Long: 70.0096 ^{0}W Elevation: 13 m	Paleozoic (Cambrian) offshelf miogeoclinal sedimentary rocks	Glaciomarine offshore sediments	Concrete, insulated vault
A21 Lat: 47.7045 ^{0}N, Long: 69.6892 ^{0}W Elevation: 47 m	Paleozoic (Ordovician) sedimentary rocks	Glaciomarine offshore sediments	Concrete, insulated vault
A54 Lat: 47.4568 ^{0}N, Long: 70.4134 ^{0}W Elevation: 377 m	Paleozoic (Ordivician) Sedimentary rocks	Glacial sediments - Blanket	Concrete, insulated vault
A61 Lat: 47.6936 ^{0}N, Long: 70.0914 ^{0}W Elevation: 380 m	Precambrian (Mesoproterozoic) gneiss and metamorphic rocks	Glaciomarine offshore sediments	Concrete, insulated vault
A64 Lat: 47.8274 ^{0}N, Long: 69.8914 ^{0}W Elevation: 132 m	Paleozoic (Ordovician) sedimentary rocks	Glacial Sediments - Blanket	Concrete, insulated vault
BATG Lat: 47.2767 ^{0}N, Long: 66.0599 ^{0}W Elevation: 336 m	Paleozoic (Ordovician) bimodal volcanic rocks	Glacial Sediments - Blanket	Rock outcrop
BCLQ Lat: 46.9264 ^{0}N, Long: 71.1727 ^{0}W Elevation: 147 m	Paleozoic (Ordovician) sedimentary rocks	Glaciomarine offshore sediments	Rock outcrop
CNQ Lat: 49.3020 ^{0}N, Long: 68.0746 ^{0}W Elevation: 200 m	Precambrian (Mesoproterozoic) paragneiss and other metamorphic rocks	Glacial sediments - Veneer	Re-inforced concrete on bedrock
DAQ Lat: 47.9627 ^{0}N, Long: 71.2437 ^{0}W Elevation: 939 m	Precambrian (Mesoproterozoic) intrusive igneous rocks (e.g. charnockite)	Glacial sediments - Veneer	Re-inforced concrete on bedrock
DPQ Lat: 46.6803 ^{0}N, Long: 72.7771 ^{0}W Elevation: 179 m	Precambrian (Mesoproterozoic) gneiss	Glacial sediments - Veneer	Re-inforced concrete on bedrock

GAC Lat: 45.7032 ^{0}N, Long: 75.4776 ^{0}W Elevation: 167 m	Precambrian (Mesoproterozoic) intrusive granitoid rocks	Glaciomarine offshore sediments	Underground vault
GBN Lat: 45.4079 ^{0}N, Long: 61.5128 ^{0}W Elevation: 47 m	Paleozoic (Cambrian – Devonian) sedimentary rocks	Glacial Sediments - Blanket	Rock outcrop
GSQ Lat: 48.9142 ^{0}N, Long: 67.1106 ^{0}W Elevation: 398 m	Paleozoic (Cambrian-Ordovician) offshelf miogeoclinal sedimentary rocks	Bedrock	Re-inforced concrete on bedrock
ICQ Lat: 49.5223 ^{0}N, Long: 67.2715 ^{0}W Elevation: 58 m	Precambrian (Mesoproterozoic) gneiss and other metamorphic rocks	Glaciomarine littoral and nearshore sediments	Rock outcrop
KGNO Lat: 44.2272 ^{0}N, Long: 76.4934 ^{0}W Elevation: 89 m	Paleozoic (Ordivician) sedimentary rocks	Glacial Sediments - Blanket	Basement of building
LMQ Lat: 47.5485 ^{0}N, Long: 70.3258 ^{0}W Elevation: 455 m	Paleozoic (Ordovician) sedimentary rocks	Glacial Sediments - Blanket	Underground insulated vault
MCNB Lat: 45.5958 ^{0}N, Long: 67.3198 ^{0}W Elevation: 167 m	Paleozoic (Silurian) sedimentary rocks	Glaciofluvial ice contact sediments	Underground insulated vault, on concrete
MOQ Lat: 45.3115 ^{0}N, Long: 72.2409 ^{0}W Elevation: 845 m	Paleozoic (Cambrian – Ordivician) mafic volcanic rocks	Glacial sediments - Veneer	Re-inforced concrete on bedrock
NATG Lat: 50.2872 ^{0}N, Long: 62.8102 ^{0}W Elevation: -2 m	Precambrian (Mesoproterozoic) sedimentary rocks	Bedrock	Rock outcrop
ORIO Lat: 45.4515 ^{0}N, Long: 75.5110 ^{0}W Elevation: 74 m	Paleozoic (Ordovician) sedimentary rocks	Glaciomarine offshore sediments	Rock outcrop
OTT Lat: 45.3942 ^{0}N, Long: 75.7167 ^{0}W Elevation: 77 m	Paleozoic (Ordovician) sedimentary rocks	Glacial Sediments - Blanket	Underground insulated vault, on concrete
QCQ Lat: 46.7792 ^{0}N, Long: 71.2756 ^{0}W Elevation: 90 m	Paleozoic (Cambrian) Offshelf miogeoclinal sedimentary rocks	Glaciomarine offshore sediments	Basement of building

SMQ Lat: 50.2225 °N, Long: 66.7025 °W Elevation: 344 m	Precambrian (Mesoproterozoic) gneiss and other metamorphic rocks	Glacial sediments - Veneer	Re-inforced concrete on bedrock
VABQ Lat: 45.9047 °N, Long: 75.6079 °W Elevation: 210 m	Precambrian (Mesopreterozoic) Metamorphic rocks containing paragneiss	Glacial sediments - Veneer	Rock outcrop

2.2   Non-invasive seismic testing

Over the duration of summer and fall 2017, active and passive non-invasive seismic data was collected at 25 CNSN stations in Eastern Canada. The stations were located across multiple provinces in Eastern Canada including Ontario, Quebec, Nova Scotia, and New Brunswick with a focus on stations in Ottawa and the Charlevoix Seismic Zone. These stations were selected based on their suitability in determining seismic kappa (Palmer and Atkinson, 2018) which is being determined in a parallel study (Palmer and Atkinson, 2020). The stations were selected in having at least 10 $\mathbf{M} > 1.5$ earthquakes within 50 km of the station.

Our aim was to acquire reliable velocity measurements of the shallow rock beneath the station using multiple non-invasive active and passive seismic techniques. Most seismographs are installed on outcropping rock; some are installed on the rock surface in the basement of buildings or seismic vaults (Table 2.1). Seismic arrays for dispersion and refraction measurements require some space or an open area for testing. Hence, in most cases our survey locations could not coincide with the installed seismograph and were located 10's of meters away (100's of meters in few cases) in an open area representative of the rock below the seismograph. Only MHVSR measurements were suitable immediately at, on the same concrete pad, or beside the seismograph. Table 2.2 lists the tested site conditions and the largest achievable array spacing at each station; see Appendix A for location testing maps for each station. Site characterization information (velocity profiles, etc.) determined from each method and their applied success at rock sites in Eastern Canada is presented here in Chapter 2. Chapter 3 focuses on earthquake site characterization and classification of each station.

Table 2.2: List of seismograph stations and details of *in situ* non-invasive testing accomplished at each station. Notations are as follows: SS = single station MHVSR measurements, P = passive AVA, A = active MASW and Vp refraction measurements, and A_Tromino indicates MASW testing performed with Trominos.

Station	Measurements performed: Ground Conditions	Sensor Spacing	Distance from Station (m)
A11	SS: Rock	N/A	0
A16	SS: Thin soil over rock	N/A	0
	P: Soil/gravel	3, 6, 9, and 12 m	80
	A: Soil cover	0.5 m	15
A21	SS: Soil/rock mix	N/A	0
A54	SS: Soil cover	N/A	0
	P: Soil cover	3,6, and 9 m	10
	A: Soil cover	0.5 m	10
A61	SS: Soil cover	N/A	0
	P: Gravel	5, 10, and 15 m	45
	A: Soil/Gravel	1 and 3 m	5
A64	SS: Concrete pad	N/A	0
	P: Rock	3, 6, 9, and 12 m	160
	A: Thin soil layer over rock	0.5 m	25
BATG	SS: Soil cover	N/A	0
	P: Gravel/soil mix	3, 6, 9, 12, and 15 m	30
	A: Gravel	1 and 2 m	85
BCLQ	SS: Rock	N/A	0
	P: Soil	3, 6, 9, and 12 m	35
	A: Soil	1 m	55
CNQ	SS: Concrete	N/A	0
	P: Soil over rock	3, 6, 9, and 12 m	125
	A: Soil over rock	0.5 m	10
DAQ	SS: Rock	N/A	0
	P: Rock	2, 4, and 6 m	5
	P: Soil	4, 8, and 12 m	30
	A: Soil	1 m	20
DPQ	SS: Rock	N/A	0
	P: Thin soil over rock	3, 6, and 9 m	30
	A: Soil	0.5 and 1 m	5
GAC	SS: Soil cover	N/A	0
	A_Tromino: Soil	1 and 3 m	25
GBN	SS: Rock	N/A	0
	P: Stiff soil	3, 6, 9, and 12 m	20
	A: Mix of soil/gravel/sand	0.5 and 1 m	16
GSQ	SS: Soil/gravel cover	N/A	0
	P: Soil/gravel	3, 6, 9, and 12 m	210
	A: Soil	1 m	10
ICQ	SS: Rock	N/A	0
	P: Rock	2 and 4 m,	50
	P: Soil	5, 10, and 15 m	60
	A_Tromino: Sand/soil	1, 3, and 5 m	60

KGNO	P: Grass/soil	3, 6, and 12 m	170
	A: Soil	1 m	170
LMQ	SS: Concrete	N/A	0
	P: Gravel	3, 6, 9, and 12 m	20
	A: Mix of soil, and gravel	1 and 2 m	20
MCNB	P: Soil	5, 10, and 15 m	20
	A: Soil	1 and 1.5 m	5
MOQ	SS: Concrete	N/A	0
	P: Gravel	3, 6, and 9 m	30
	A: Soil	1 m	20
NATG	SS: Rock	N/A	0
	P: Rock	5, 10, and 15 m	300
	A: Soil	0.5 and 1 m	45
ORIO	SS: Soil cover	N/A	0
	P: Soil	3, 6, 9, and 12 m	5
	A: Soil	1 m	45
OTT	SS: Concrete pad	N/A	0
	P: Soil	5, 10, and 15 m	185
	A: Soil	1 and 3 m	210
QCQ	SS: Concrete pad	N/A	0
	P: Soil	10, 15, and 20 m	90
	A: Soil	1 and 3 m	140
SMQ	SS: Concrete pad	N/A	0
	P: Rock	3, 6, and 9 m	10
	$A_{Tromino}$: Gravel	1 and 3 m	45
VABQ	SS: Concrete pad	N/A	0
	P: Soil	5, 10, and 15 m	10
	A: Soil	1 m	60

AVA data was collected using 5 tri-axial MoHo Trominos®. The sensors measure velocity in three orthogonal directions over frequencies from 0.1 to 1028 Hz at a 128 Hz sampling rate. An internal or external GPS is used for accurate timing via satellite. Four sensors were located at the apex of a cross-shape geometry with a fifth central sensor. AVA spacing varied from a minimum of 2 m, up to 30 m maximum, depending on the space available at each station. The array radius is varied to measure dispersion at many frequencies or wavelengths; larger array spacing measure longer wavelengths which penetrate deeper into the subsurface. Microtremors were recorded for approximately 30 minutes for each array setup.

MASW and Vp refraction surveys were performed with the same equipment and survey design. A Geode seismograph at 500 Hz sampling was used with a linear array of 24 vertical 4.5-Hz geophones. For MASW testing, recordings were acquired continuously, whereas for Vp refraction testing, a 2 s recording is acquired via seismic triggering. An 8 lb sledgehammer was used as the seismic source which was struck vertically on an aluminum plate at each end. Source

offsets of 5 and 15 m on both ends of the geophone line were used. Geophone spacing varied from 0.5 up to 3 m depending on available space near the station. The spacing between geophones were increased to sample lower frequency bandwidths. MASW was also performed with 5 tri-axial Trominos at stations where geophones could not be inserted into the ground (noted as $A_{Tromino}$ in Table 2.2). Tromino spacing varied from 1, 3, and 5 m with the same source offset distances of 5 and 15 m at each end. Using Trominos for MASW measurements provided a higher sampling frequency of 1028 Hz to capture shallow rock velocities at some stations. Figure 2.2 shows an example of the array configuration and spacing for active MASW and passive AVA testing.

a)

b)

c)

d)
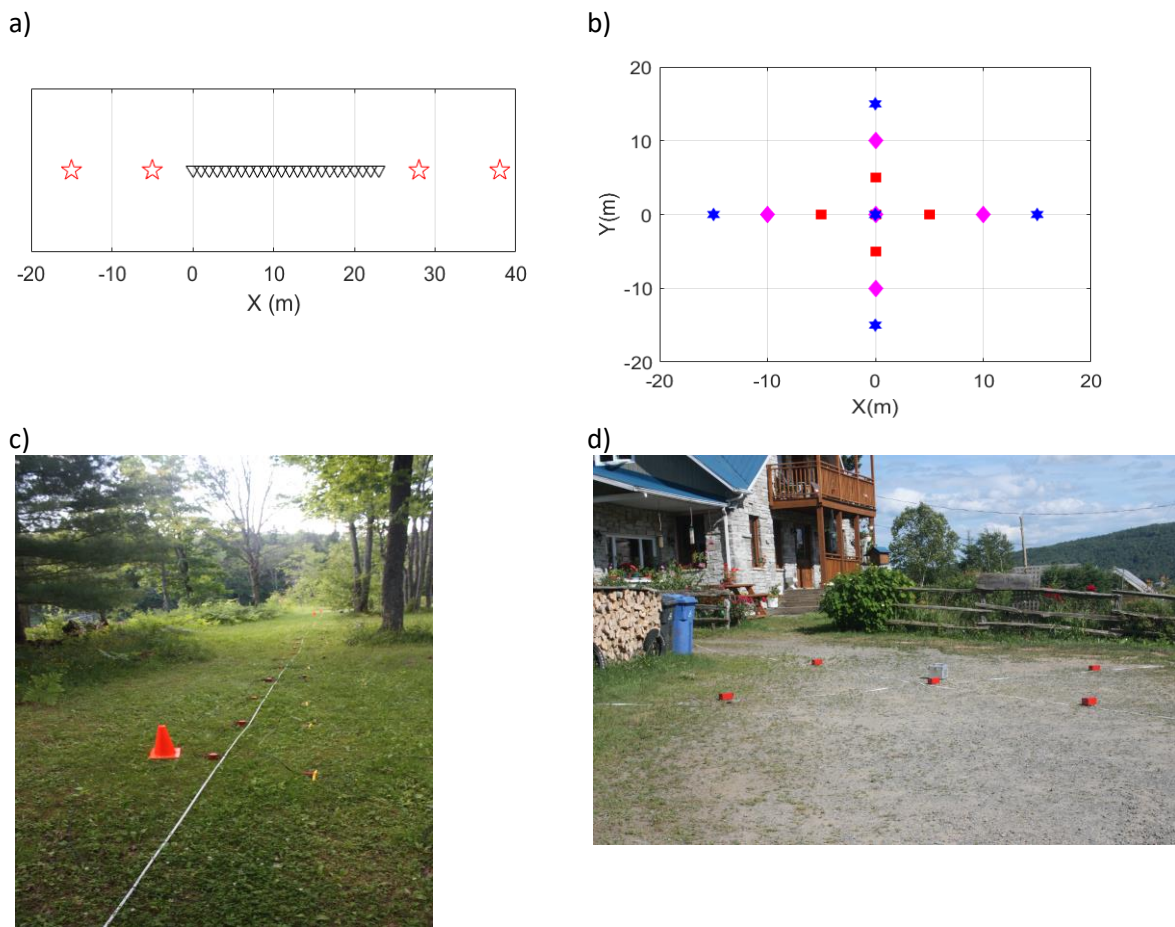
Figure 2.2: Example array configuration and spacing for a) active MASW and refraction testing (inverted triangles denote geophone locations, stars show shot locations), and b) passive AVA testing for 5, 10, and 15 m array radii (symbols denote Tromino locations and colours designate each array). Sample field photos of c) active MASW and refraction testing at station BCLQ and d) AVA measurements at station DPQ.

MHVSR measurements (noted as "SS" in Table 2.2) were accomplished *in situ* using a single Tromino sensor placed primarily on the residing rock beside the CNSN seismograph or on its

concrete pad (Figure 2.3). At a few stations (MCNB and KGNO), the CNSN seismograph was not accessed and MHVSR measurements were performed on rock or soil as nearby as possible. For comparison, EHVSRs were also calculated using the earthquake recordings of the CNSN seismograph. Array average MHVSRs were calculated from AVA measurements accomplished nearby the station as AVA measurements could not be taken directly on the rock outcrop.

a)

b)
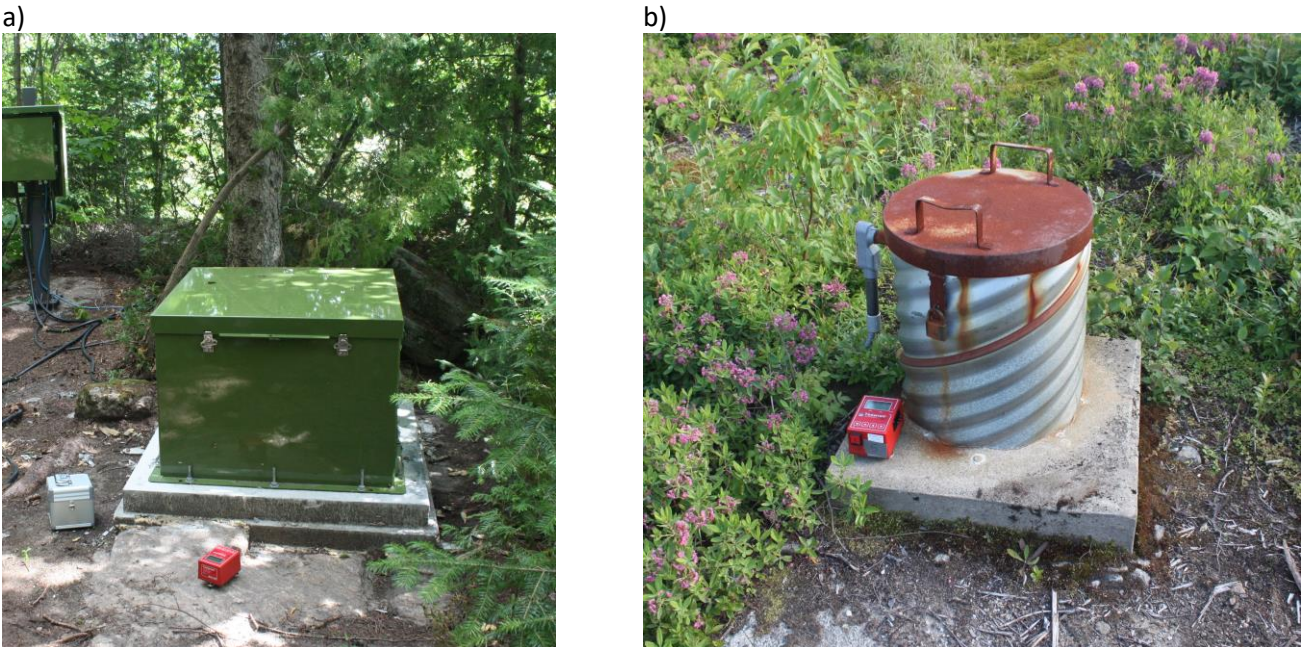
Figure 2.3: MHVSR measurements taken on the a) residing rock beside station DPQ and b) concrete pad at station CNQ.

A time-averaged MHVSR from each Tromino recording was calculated using 30 second time windows overlapped by 50% and smoothed using the Konno and Ohmachi (1995) filter. Bad time windows caused by man-made noise or other anomalous activity noted during the field notes were removed. If the Tromino recordings are from AVA testing, then a site average MHVSR was calculated using the edited time-averaged MHVSRs from each of the five sensors for all array apertures at a station. Figure 2.4 shows the differing conditions from the station and the measurement location through their generated MHVSRs where the estimated site response differs for example stations A64 and BCLQ. Examples in figure 2.4 show differing MHVSRs at the measurement and station locations; where at station A64 the ground conditions are similar in both station and array measurements containing a low amplification response with rock near the surface and station BCLQ where the ground conditions differ clearly with more sediment cover at the measurement location than at the station resulted in the sharp high frequency peak (remaining stations are in Appendix B).
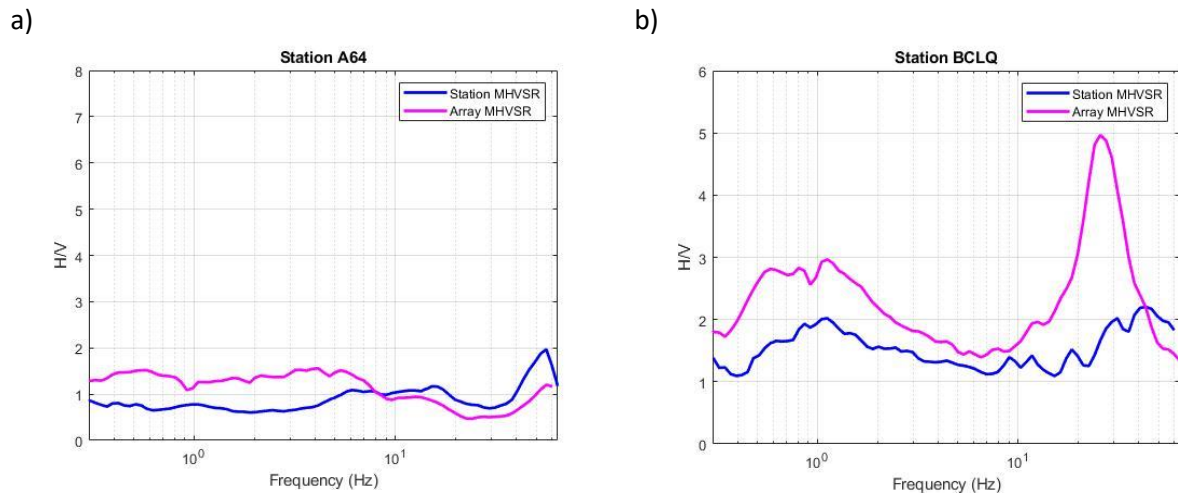
Figure 2.4: *In situ* **single station MHVSR calculated for the station (blue) and the site average MHVSR at 160 and 35 m distance from the station (purple) for stations a) A64 and b) BCLQ, respectively.**

AVA recordings were prepared for dispersion analysis by synchronizing using GPS timing (accomplished automatically by the Tromino's proprietary software Grilla) and converted to ASCII. AVA and MASW array recordings are converted to applicable file formats and imported to Geopsy (version 20170109; Wathelet, 2008), an online open-source software for time-series processing and dispersion analyses. MASW data recorded by the Geode system in SEGY format was converted to miniseed format using a Python routine. Once imported to Geopsy, shot gathers are created by cutting time windows of 1 or 2 seconds around each shot from the continuous recordings. Similarly, MASW data collected with Trominos were imported as ASCII files into Geopsy and pre-processed into 1 or 2 seconds shot gathers.

At three stations, representative surface outcrop rock samples were selected and brought back to Western University. These intact rock samples were cut and underwent laboratory Vp measurements to estimate the station's rock Vp and to compare with the *in situ* refraction Vp measurements. Rock sample Vp measurements were performed by myself and Samantha Palmer in the department's Experimental Petrology Sample Preparation Laboratory (Figure 2.5). Samples were first cut into 1-cm cylindrical shape samples. The sample is clamped and an ultrasonic pulse (P-wave) is generated into one end of the sample, travels through the sample, and is measured by a detector pad at the other end. The arrival time of the pulse is picked in the

45

source and receiver waveforms. This measured travel time provides the sample's Vp given the known sample length.

a)

b)

Figure 2.5: Photos of laboratory rock sample Vp measurements showing a) the whole apparatus and b) a clamped 1-cm cylindrical sample from station A16.

2.3   Station MHVSR and EHVSR comparison

The station MHVSR was calculated using *in situ* microtremor recordings accomplished at the CNSN seismograph, either on the same concrete pad or on the residing rock (Figure 2.3). The MHSVR method allows us to estimate site amplification in direct comparison to conditions to which the CNSN seismometer is installed. Table 2.3 summarizes MHVSR results for the Eastern Canada seismograph stations; the last column reports reliable dispersion bandwidths at the station and is discussed in section 2.4. Site amplification for rock sites is generally flat (as expected) and may display a peak frequency (f_{peak}). At stations KGNO and MCNB there was no direct access to the CNSN seismograph. MHVSRs for stations A11 and A21 were not representative of the site, contaminated due to external effects (e.g., wind) and are removed from the MHVSR database. In addition, MHVSRs for stations QCQ, LMQ, MOQ, and OTT are also removed due to contamination from human-made noise present at their station, e.g., fans or other

sustained noise is observed throughout their recordings and the vertical spectrum amplitude is increased.

Table 2.3: Summary of MHVSR and EHVSR results for the visited Eastern Canada seismograph stations. The frequency bandwidth from which reliable dispersion estimates are obtained by active MASW (labelled A) and passive AVA (labelled P) array testing is also provided. Amp = amplification.

Station	MHVSR	EHVSR	Reliable Dispersion Bandwidth (Hz)
A11	N/A – Wind effects; station on a hill	Flat, low Amp	Not Measured
A16	Flat, low Amp	Flat, low Amp	A: 22-48
A21	N/A – Wind effects; station on a hill	Flat, low Amp	Not Measured
A54	Flat, low Amp	Flat, low Amp	A: 20-120
A61	f_{peak} at 25 Hz, high Amp across all f	Flat, high Amp	A: 25-70
A64	Flat, low Amp	f_{peak} at 25 Hz	P: 25-35, A: 89-135
BATG	Amp at 0.7 and 25 Hz	Not provided	A: 15-100
BCLQ	Amp at 1.5 Hz and 45 Hz	Not provided	A: 30-75
CNQ	f_{peak} at 5 Hz	Not provided	Unsuccessful
DAQ	Flat, high Amp	Not provided	A: 12-80
DPQ	Flat, low Amp	Not provided	A: 15-85
GAC	Amp at 20-40 Hz	Not provided	A:170-480
GBN	f_{peak} at 50 Hz	Not provided	A: 20-125
GSQ	Flat, low Amp	Not provided	A: 10-115
ICQ	f_{peak} at 5 Hz	Not provided	P: 15-25, A: 60-215
KGNO	N/A – No Access	Not provided	P: 21-35, A: 50-100
LMQ	N/A – external noise	N/A – external noise	A: 10-90
MCNB	N/A – No access	Not provided	A: 45-125
MOQ	N/A – external noise	Not provided	Unsuccessful
NATG	f_{peak} at 7 Hz	Flat, low Amp	Unsuccessful
ORIO	f_{peak} at 55 Hz	Not provided	P: 10-30, A: 30-215
OTT	N/A – external noise	N/A - external noise	P: 5-20, A: 20-120
QCQ	N/A – external noise	Not provided	P: 10-25, A: 30-170
SMQ	f_{peak} at 5 Hz	Not provided	Unsuccessful
VABQ	Flat, low Amp	Not provided	Unsuccessful

Figure 2.6 shows the average MHVSR for each station. Figure 2.6a displays expected flat MHVSRs (amplification < 2) which indicate competent or hard rock conditions, i.e., low to no amplification. In Figure 2.6b, MHVSRs with amplification > 2 are shown. These MHVSRs are amplified at low frequencies, over nearly all frequencies (broadband amplification), or over a narrow range at high frequencies (resonant amplification). Softer rock towards surface from weathering, jointing, etc., would lead to broadband amplification (e.g. CNQ). The presence of

thin soil over stiff to hard rock would lead to high amplification (resonance) at high frequency (e.g. ORIO). Topographic (outcropping rock) effects would lead to amplification at the frequencies related to the topography's shape and height.

a)   b)
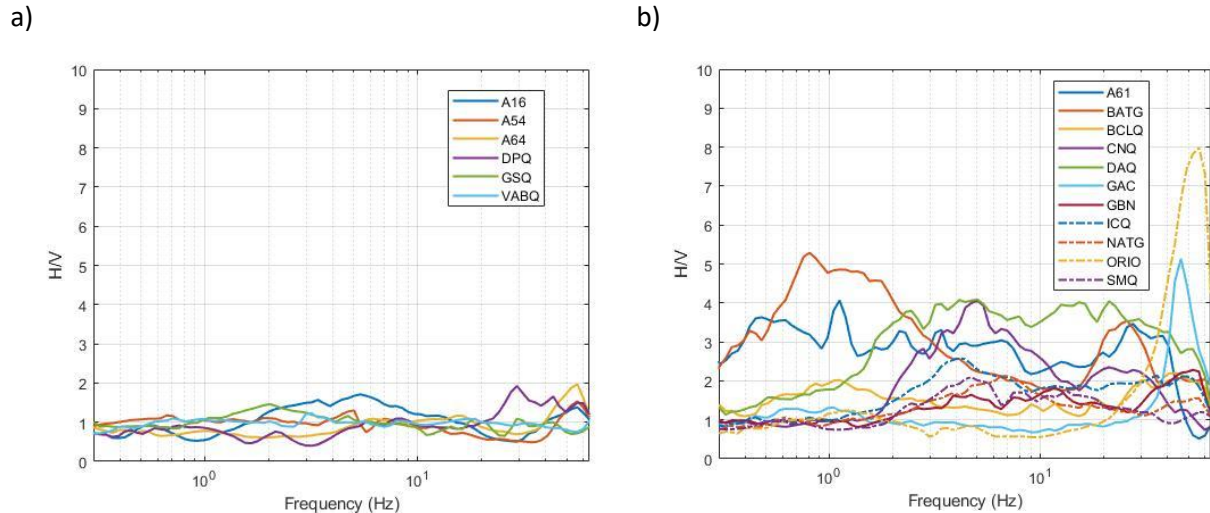
Figure 2.6: MHVSR measurements at seismograph stations with a) flat response and b) broadband or resonant amplification.

EHVSRs were generated by Samantha Palmer for 10 stations using earthquake recordings from **M** > 3.5 events within 150 km of the station. The station's average EHVSR is compared with the measured station's average MHVSR in Figure 2.7. Station LMQ and NATG only had one earthquake recording which fit the criteria therefore, the EHVSR standard deviation could not be calculated. For stations A11 and A21, the MHVSR is not available and only the EHVSR is shown. Overall, low amplification is observed and there is general agreement between the average EHVSR and MHVSR at each station. There is agreement in the station's MHVSR and EHVSR even when they deviate from the typical low amplification demonstrating consistent site effects. Station A61 has amplification occurring at multiple frequencies in both the EHVSR and MHVSR indicating potentially softer rock; the high amplification at low frequencies in the EHVSR is likely due to wind effects. Disagreement between the EHVSR and MHVSR is observed at station LMQ. The CNSN seismograph is located ~3 m below ground surface on the concrete floor of a seismic vault. The MHVSR measurement is at the ground surface. Stations LMQ and OTT had suspected man-made noise in their calculated MHVSRs which is also seen similarly in their EHVSR.
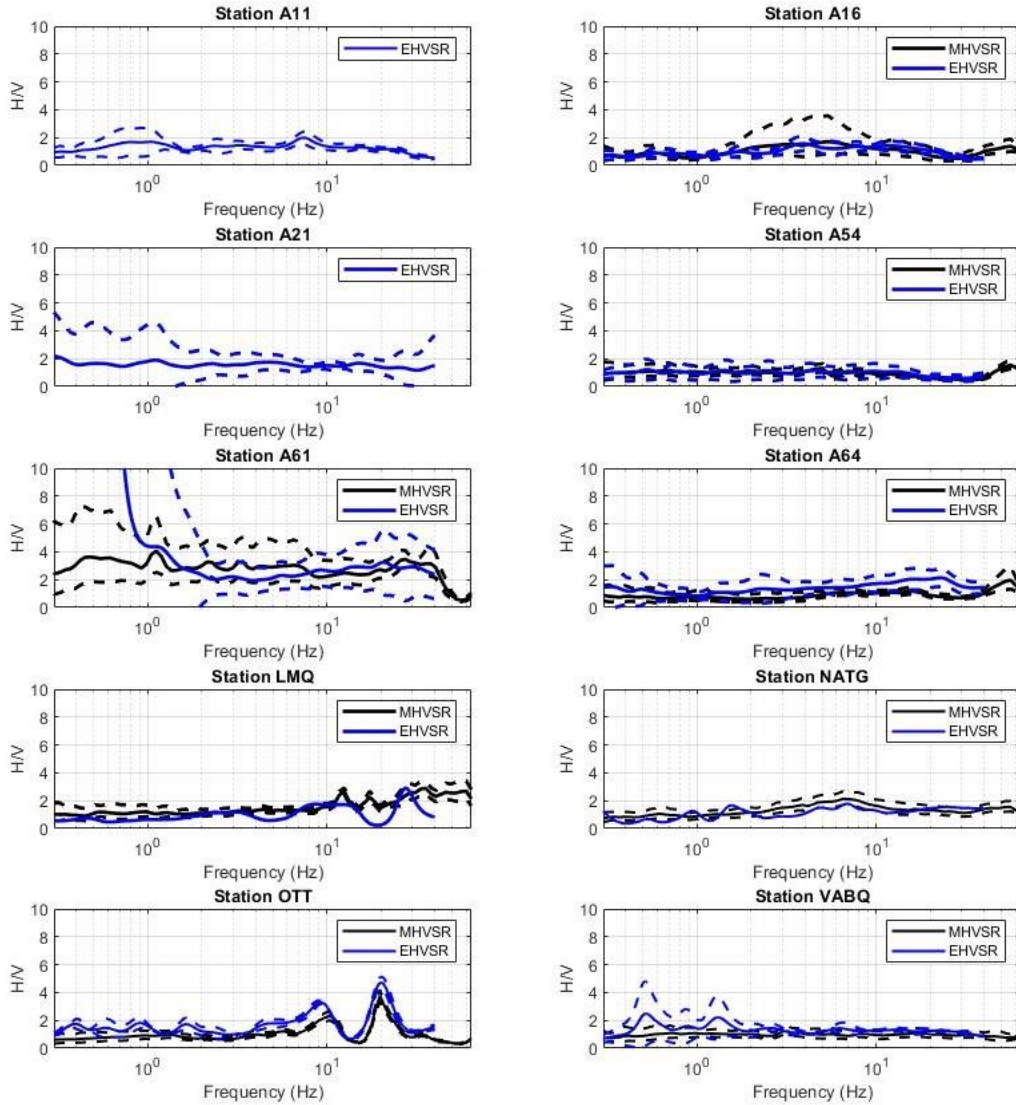
Figure 2.7: Average EHVSR (solid blue line) with standard deviation (dotted blue lines) compared to co-located average MHVSR (solid black line) with standard deviation (dotted black line) for select Eastern Canada seismograph stations.

2.4 Dispersion curves

Surface wave propagation in vertically heterogeneous media is controlled by geometric dispersion where waves of different frequency (and wavelength) travel at different phase velocities depending on the elastic properties of the subsurface (Foti et al., 2017). The distribution of phase velocities with frequency is defined as a dispersion curve. Surface wave propagation is a multimodal phenomenon where at different frequencies different modes of

vibration exist. The stations visited are in rocky conditions where lateral variability can play a role in the measurement conditions. Typically, the measurements were made at spacious areas of soil or gravel (to insert geophone spikes) overlaying rock near the station. For 23 of 25 stations, active- and/or passive-source array methods were performed to obtain dispersion estimates. Dispersion histograms of phase velocities estimated at each frequency are generated by the f-k method for active MASW shot gathers and by MSPAC processing for passive AVA recordings (these methods were described in section 1.5). A summary on the success of the surface wave array testing is presented in this section; dispersion histogram results for all stations are provided in Appendix B. For 16 of 23 stations, the fundamental mode dispersion curve could be identified and picked for these stations from either active and/or passive methods. Table 2.3 summarizes the frequency bandwidth over which reliable dispersion estimates were obtained from active and/or passive array methods at each station.

2.4.1 Passive AVA dispersion estimates

The applicability of passive seismic methods has been questioned for rock sites (e.g. Pileggi et al., 2011) due to the lack of a strong impedance contrast which eases surface wave generation at an undetectable amplitude (Poggi et al., 2017). AVA testing provides lower frequency dispersion estimates and is more likely to provide direct measurement of phase velocities in rock at depth, i.e., the rock velocity "top" of the dispersion curve, compared to the soil velocity "tail" from active MASW methods. When successful, the AVA method provides the most important and useful information in rock site characterization which is the Vs of the rock. At 7 out of the 22 stations, we were able to measure the "top" of the dispersion curve providing a direct measure of phase velocity at depth, assumed rock. Examples of the variation in AVA dispersion estimates is shown in Figure 2.8 with the method at times giving estimates solely of rock, the transition or dispersion curve into the shallower layers. For the majority of stations, no AVA dispersion estimates were obtained. For stations where AVA data acquisition was successful, the essential information of the rock velocity beneath the station was acquired. The dispersion estimates of the low frequency AVA data were then combined with the active high frequency MASW data set to build a dispersion curve.
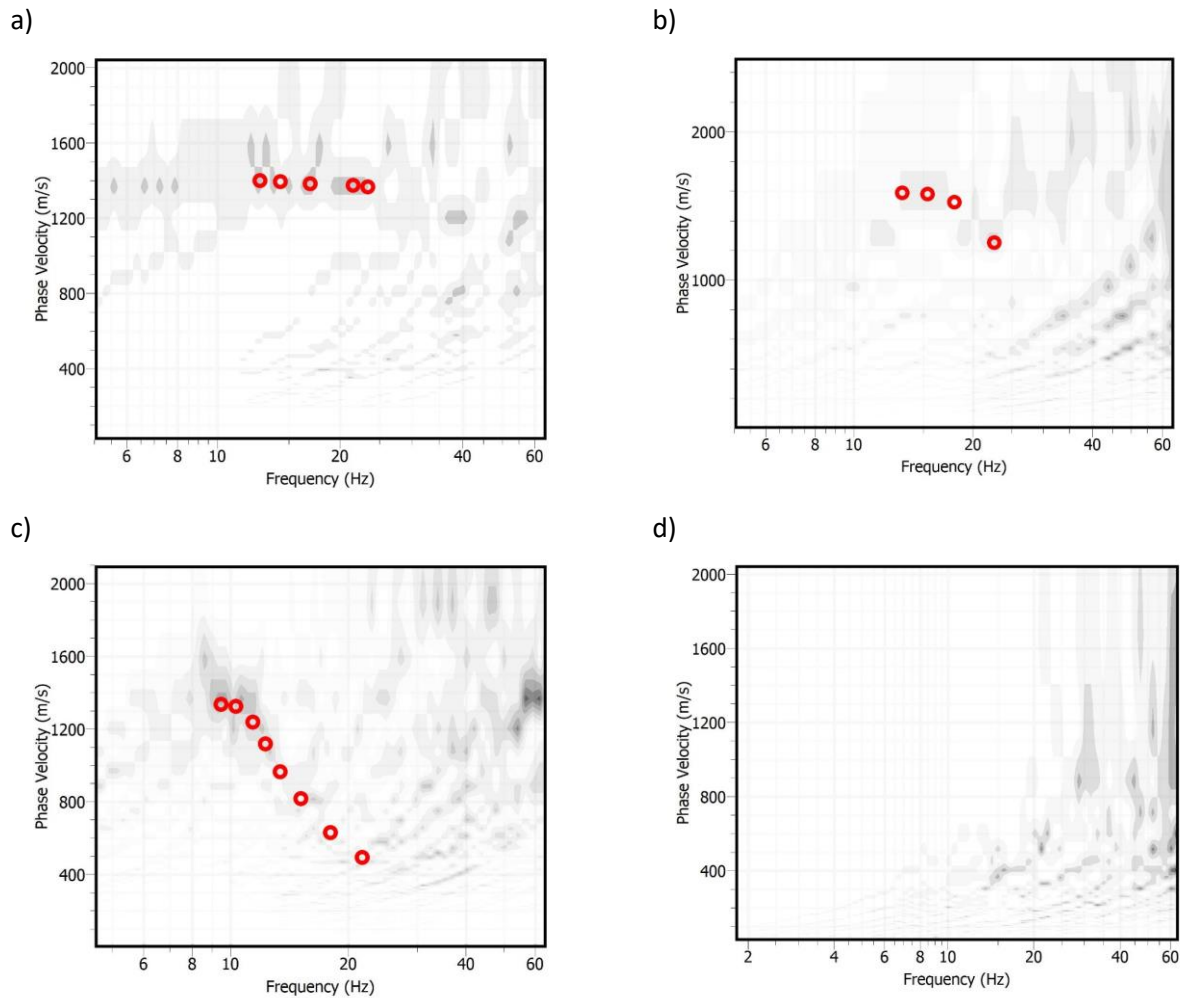
Figure 2.8: Examples of "top" rock velocity AVA dispersion estimates for stations a) QCQ, and b) ICQ. c) Mid-frequency dispersion estimates for station OTT and d) no AVA dispersion estimates for station MOQ.

2.4.2 Active MASW dispersion estimates

MASW data has been widely obtained in previous studies for rock site characterization. MASW has been successful at rock sites due to near surface impedance boundaries which are sensitive to high frequencies input into the ground. Rock velocity can be measured if enough energy is put into the subsurface and if dispersion can physically occur in the rock. MASW data was processed using f-k processing to get high frequency dispersion estimates. MASW methods were more successful than AVA in that velocities could be measured at all 23 stations. Variation was seen at the stations from measuring the rock velocity, getting the transition from soil to rock and measuring only shallow sediments (Figure 2.9). Enough dispersion information could be

resolved at 16 of 23 stations for inversion of a Vs profile. When combined with AVA dispersion estimates, a full dispersion curve could be built for 7 stations for inversion of a Vs profile. Nine stations produced MASW dispersion estimates for inversion. Some stations also had significant energy at lower frequencies indicating potential rock velocity measurements.
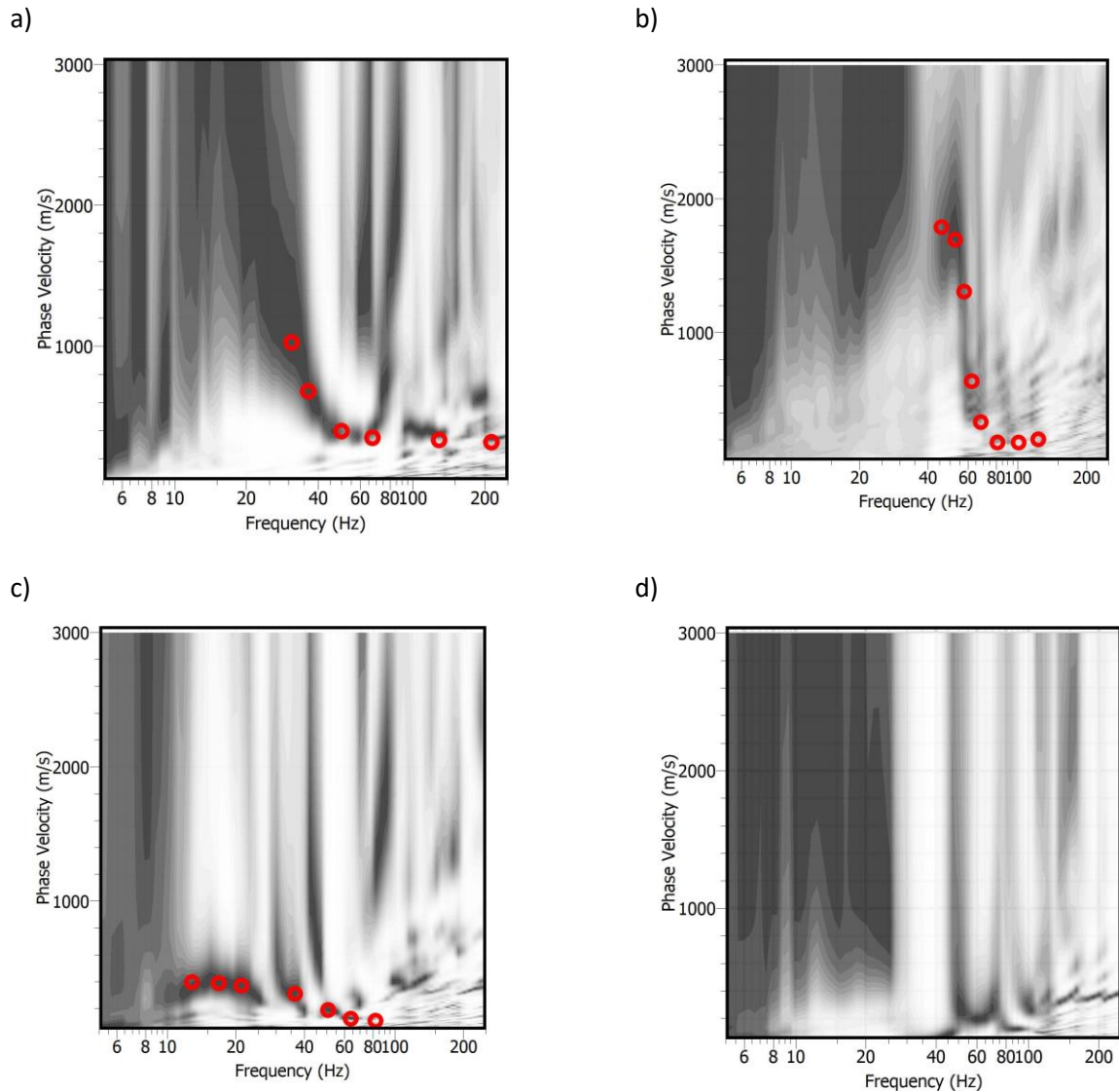
Figure 2.9: Example MASW dispersion estimates for stations a) ORIO, b) MCNB, and c) DAQ. d) Example of no MASW dispersion estimates for station MOQ.

2.5 Inversion methodology and results

Surface wave inversion requires a description of the ground model linked by physical and mechanical parameters connected to the experimental data. Rayleigh wave ellipticity and dispersion curves are influenced by Vs structure, they can both be used to solve for Vs through inversion independently or jointly. Surface wave inversions require knowledge of the layered

earth model where each layer is comprised of four elastic parameters: Vp, Vs, thickness, and density. Numerical computation of dispersion curves is applied using the Haskell-Thompson approach (Thompson 1950; Haskell 1953). The surface wave inverse problem is non-linear, mathematically ill-posed, and non-unique (Foti et al., 2014; Foti et al., 2017). Non-uniqueness is due to having more parameters than observations meaning an infinite number of solutions (Tarantola, 1987). Model parameterization to acquire a Vs profile is often unknown *a priori*. Too few parameters usually lead to underfitting the data and underestimating parameter uncertainties. Adopting too many parameters can over-fit the data leading to under determined parameters. Creating a more complex model adds more parameters and lowers the misfit but can lead to unrealistic models and should be avoided (e.g. Di Giulio et al., 2012).

Probabilistic Shear Wave Velocity Profiling (PSWP) and Geopsy's Dinver were two programs used to invert Rayleigh wave dispersion data to acquire Vs profiles for each station. Dinver was used to determine the optimal (best fitting) model while PSWP was used to analyze model parameter uncertainties. Dispersion data is first inverted using Dinver using one to two uniform velocity layers over a halfspace. PSWP was then initiated with two model parameterization options: two uniform velocity layers over a half space (a single layer over a halfspace is not available) and a powerlaw velocity gradient over a halfspace. The most appropriate parameterization is determined by the Bayesian Information Criterion (BIC) where it also applies a penalty for the number of parameters. When PSWP determined two uniform layers over a halfspace as the most appropriate model parameterization, the same multi-layer model was selected using Dinver. When PSWP determined a powerlaw velocity gradient over a halfspace as the most appropriate model parameterization, the selected Dinver model was a single uniform velocity layer over a halfspace. In this latter case, a sharp change in curvature of the dispersion data occurs and is best fit by each inversion routine given the model parameterization options. Since a single layer over a halfspace cannot be solved using PSWP, we re-run Dinver using the same powerlaw velocity gradient over a halfspace parameterization for comparison.

2.5.1 Modified Neighborhood Algorithm

Dinver uses a modified neighborhood algorithm, first developed by Sambridge (1999) and modified by Wathelet (2008). The Dinver inversion software is relatively quick and easy to use and was used to readily determine the lowest misfit model and the optimal rock velocity

estimate. The Dinver software is flexible in the number of layers used during the inversion compared to PSWP discussed in section 2.5.2.

Dinver is a stochastic direct search method to optimize the misfit function in a multi-parameter dimension space. Previously generated samples guide the search for improved models through the direct search method to optimize the misfit. Areas of the parameter space which are more promising are searched more than other areas. The neighborhood algorithm makes use of Voronoi cells to model the misfit function (Wathelet, 2005) across the parameter space. The misfit function for dispersion inversions is

$$misfit_{dis} = \sqrt{\frac{\sum_{i=1}^{n_F}(x_{di} - x_{ci})^2}{\sigma_i n_F}}, \tag{14}$$

where n_F is the number of frequency samples, x_{di} is the measured phase velocity at frequency f_i. x_{ci} is the theoretical phase velocity at f_i, and σ_i is the standard deviation of the frequency samples. If no uncertainty is provided, it is replaced by x_{di} in the equation. If additional dispersion modes are included in the inversion, the summation found in the numerator in Equation 14 is used. Joint inversion (including both dispersion and MHVSR curves) is performed in Chapter 4 where the misfit of the ellipticity function is calculated by

$$misfit_{ell} = \frac{(f_{peak})experimental - (f_{peak}) \, calculated}{(df_{peak})experimental}, \tag{15}$$

where f_{peak} is the peak frequency and df_{peak} is the standard deviation of the experimental peak. In the case of a joint inversion, the two misfits are combined as a global misfit:

$$misfit_{global} = (1 - \alpha)misfit_{dis} + (\alpha) \, misfit_{ell}. \tag{16}$$

This study used a weighting (α) of 50% to each of the two contributions to the joint inversion.

The forward models in Dinver solve for theoretical Rayleigh wave fundamental mode dispersion curves or Rayleigh wave ellipticity functions. The modified neighborhood algorithm is initiated by generating a pseudo-random seed number that samples a set of model parameters within the specified model parameter bounds (ns_0) to generate the first iteration of 50 forward models. The misfit for the 50 models is calculated using Voronoi cells (Figure 2.10). The number of cells with the lowest misfit (n_r) are selected within the total number of new models generated at each iteration (n_s) by using a Gibbs Sampler (or random walk) using a uniform probability density

function inside each cell. A random walk is a sequence of perturbations to the model along all axes where the modified model is statistically independent of the original model. An average of n_s/n_r new samples are generated with a uniform probability in each selected lowest misfit cell. More samples are generated within the selected space where the misfit function is calculated again for recently generated models. This is done with each run of the inversion algorithm. The neighborhood algorithm like all other Monte Carlo techniques relies on a pseudo-random generator. A random seed initializes a random generator with a uniform probability. In this study 3 independent inversion processes were initiated with different seeds to test the robustness of final models. Ns_0 and n_r were set to 50 as well with ns being set to 2500 which resulted in 2550 models generated for each iteration. Iterations were increased in the case where the misfit continually decreased per iteration. Once convergent and the lowest misfit was achieved, the inversion process was halted where the best fitting model was extracted and analyzed.
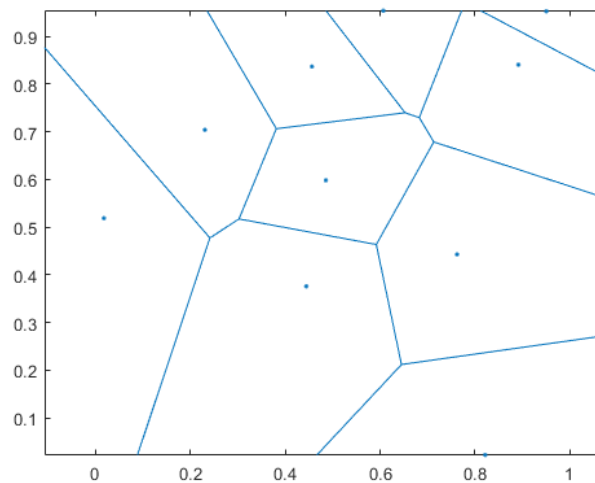
Figure 2.10: The parameter space is split into Voronoi cells where the misfit model is calculated (from Mathworks, 2006).

Model parameterizations consisted of one and two uniform velocity layer models overlaying a halfspace, and for a few stations a power law gradient layer over a halfspace was used. Uniform model parameter limits are set relatively wide. For example, Dinver's default 0.2-0.5 parameter range for Poisson's ratio was used and the default thickness of 100 m is used or reduced to 30 m for input dispersion data with high frequencies. Density is fixed to 2000 kg/m^3 for all layers. If available, refraction Vp of the rock was used to constrain the dispersion curve inversion. Several starting seeds were used to test the robustness of the final lowest misfit model. These tests

include different seeds but direct towards a similar model to counter non-uniqueness. Figure 2.11 shows the stations lowest misfit forward dispersion model and velocity profile in red.

2.5.2 Probabilistic Shear Wave Velocity Profiling (PSWP)

The second inversion software used is a Bayesian inversion software named PSWP (Probablistic Shear-Wave Velocity Profiling) developed by Molnar et al. (2010) and used for many applications in British Columbia (e.g. Molnar et al., 2012). The important points about this Bayesian inversion scheme is described fully in Molnar et al. (2010) and summarized here for the reader. Bayesian inversion evaluates data errors and model parameterization to produce the most-probable shear wave velocity profile together with quantitative uncertainty estimates from Rayleigh wave dispersion data. The Bayesian inversion approach draws models proportional to their probability but also provides rigorous estimation of data error statistics and an appropriate model parameterization. This software only inverts dispersion estimates (phase velocity vs frequency) where Rayleigh wave ellipticity cannot be independently or jointly inverted. For Eastern Canada rock sites, MHVSRs at the stations are flat and/or don't have distinct peaks and are therefore not useful for inversion (i.e., rock is rock and we cannot determine how much harder it may be from a flat MHVSR).

Bayesian inversion methods describe the inverse problem in terms of the posterior probability density (PPD) of a defined model's parameterization (Tarantola, 1987; Dosso, 2002). The PPD is defined for a given parameterization as the likelihood multiplied by prior knowledge divided by the evidence. They are considered random variables constrained by data and *a priori* information. Markov-chain Monte Carlo (MCMC) methods are used with an implementation of Metropolis-Hastings sampling to provide an unbiased sample from the PPD to compute parameter uncertainties and inter-relationships. The solution is quantified in terms of properties of the PPD that represent optimal parameter estimates (e.g. mean model) and parameter uncertainties and errors (variances). Computing these properties requires optimizing and integrating the PPD. Parameter uncertainties are calculated using MCMC methods unbiased from the PPD. Implementation of Metropolis-Hastings sampling is applied which draws parameter perturbations to the PPD.

Model parameterizations consisted of two uniform velocity layers overlaying a halfspace and a power law gradient layer over a halfspace. Uniform model parameter limits are set relatively wide and similar to the limits used for Dinver inversions. Poisson's ratio is constrained using a physical limit ($Vs \leq Vp/\sqrt{2}$). In a first stage, PSWP performs optimized inversion using an adaptive simplex simulated annealing (ASSA) algorithm. The most appropriate model parameterization is determined by calculating the BIC from each parameterization's optimal model. The optimal model with the lowest BIC is used as the starting model for the second stage Metropolis-Hastings sampling routine.

Figure 2.11 presents the optimal Vs model determined by Dinver with 66% and 95% credibility intervals determined from PSWP. The optimal (lowest misfit) Dinver model is plotted to compare with the models found through PSWP and falls into the range of the 95% credibility interval, as expected. Table 2.4 describes the velocities interpreted as rock measured using each inversion algorithm, including standard deviation from PSWP. Stations A54, A64, GAC, GBN, and LMQ had two rock velocities estimated from dispersion estimates as listed in Table 2.4.
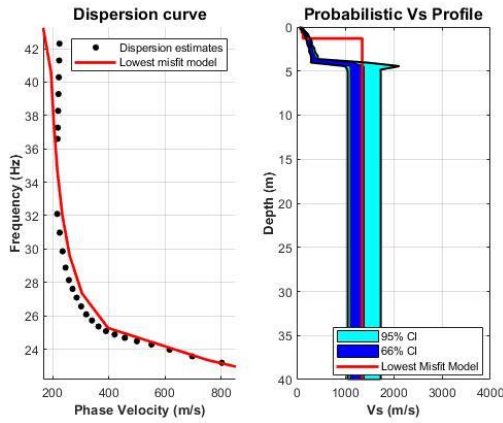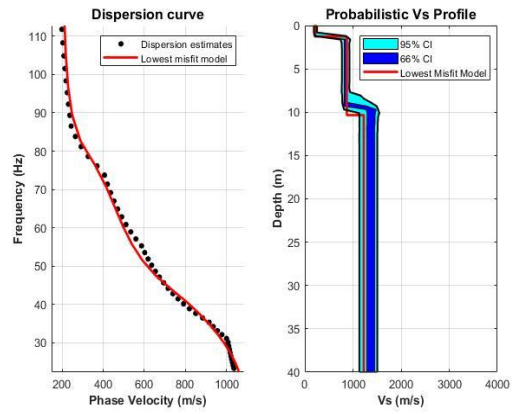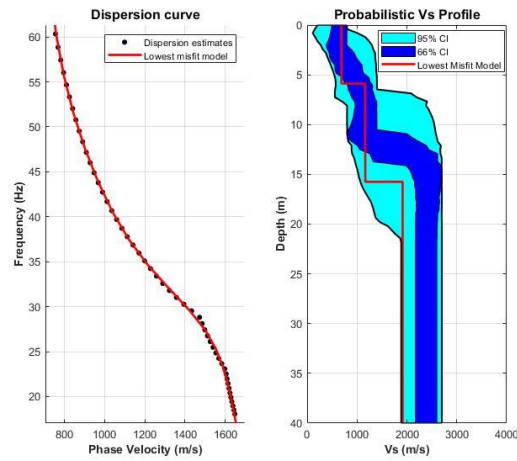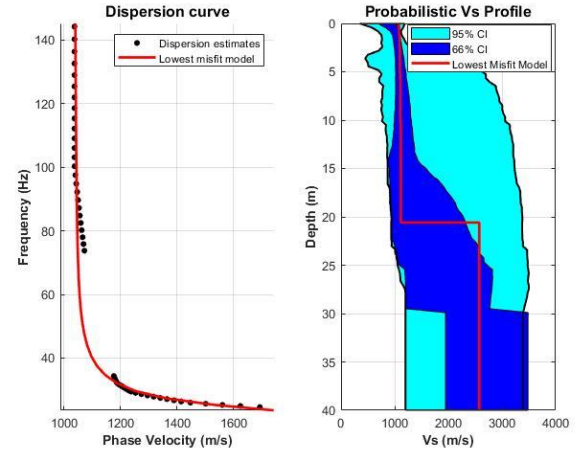
Figure 2.11: Left panels show dispersion estimates (black circles) plotted with the lowest misfit forward model in red. Velocity profiles derived from PSWP with stations a) A16, b) A54, c) A61, d) A64, e) BATG, f) BCLQ, g) DPQ, h) GAC, i) GBN, j) ICQ, k) KGNO, l) LMQ, m) MCNB, n) ORIO, o) OTT, and p) QCQ. The 66% and 95% credibility intervals are shown in blue and cyan respectively. The optimal Dinver model is shown in red.

g) DPQ
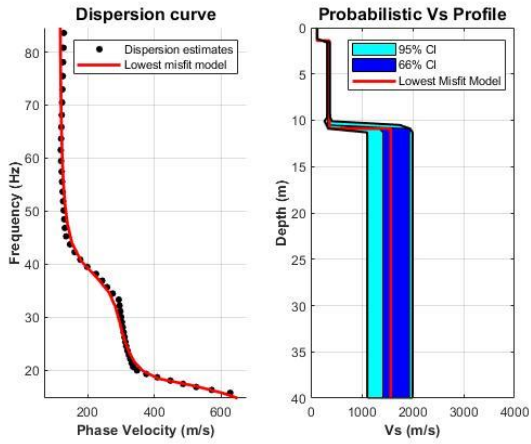
h) GAC
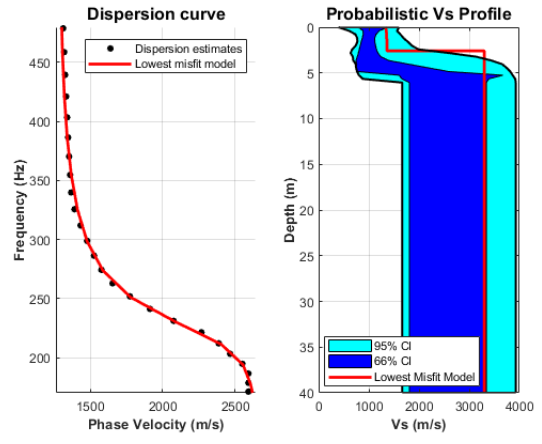
i) GBN
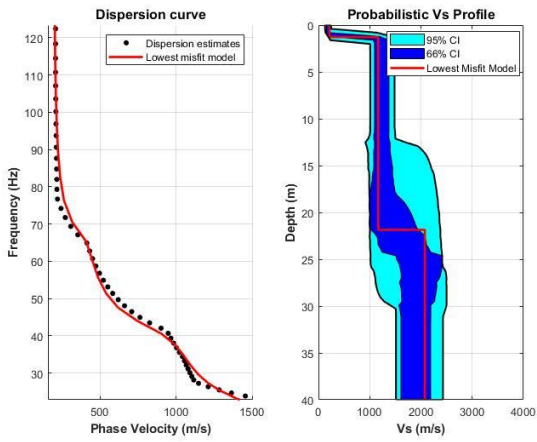
j) ICQ
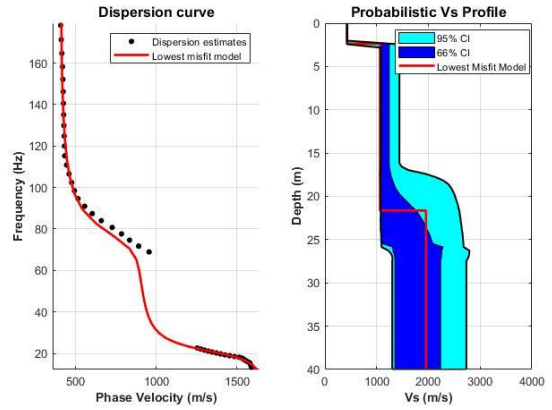
k) KGNO
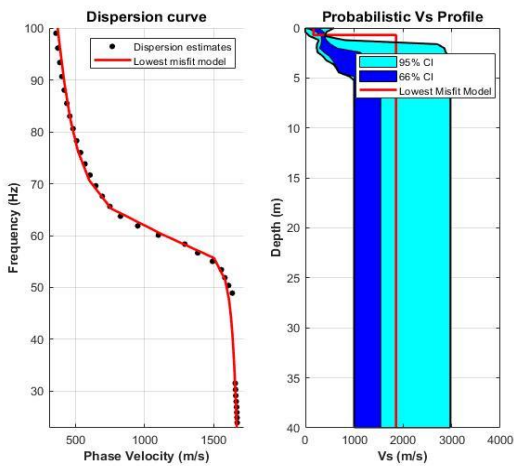
l) LMQ

Figure 2.11: Continued

59
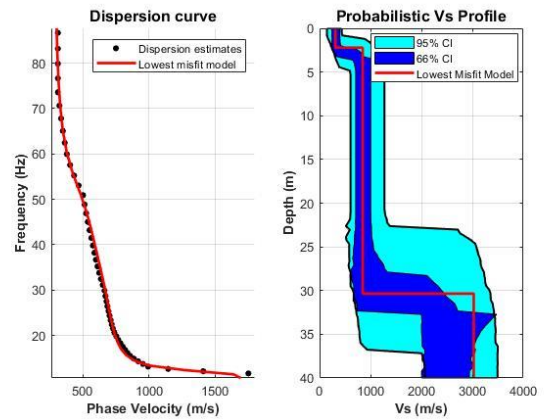
m) MCNB
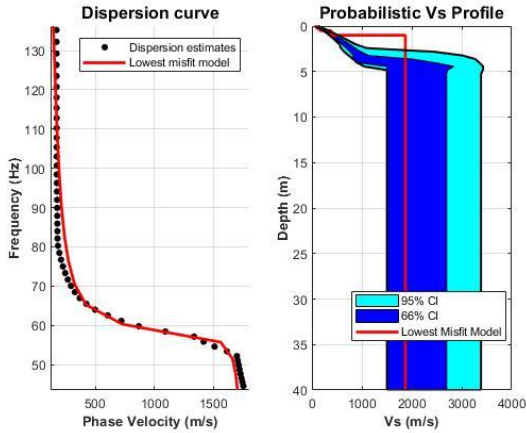
n) ORIO
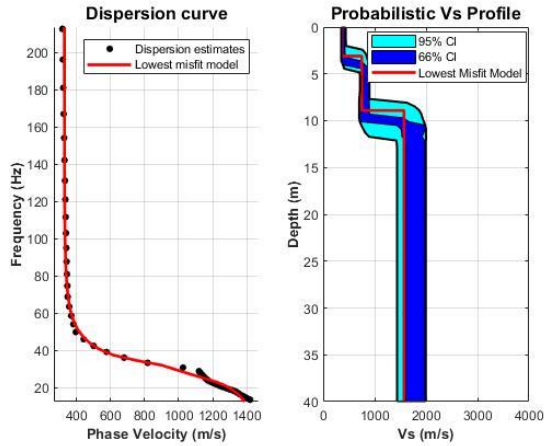
o) OTT
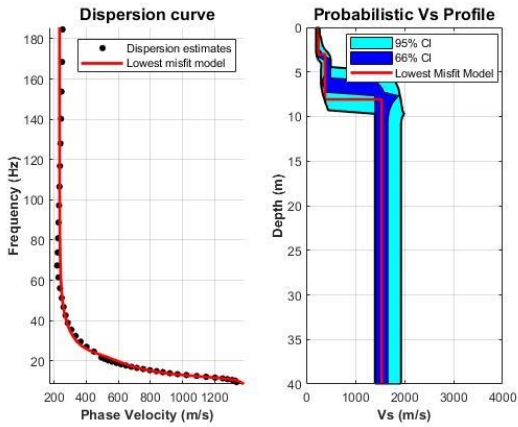
p) QCQ
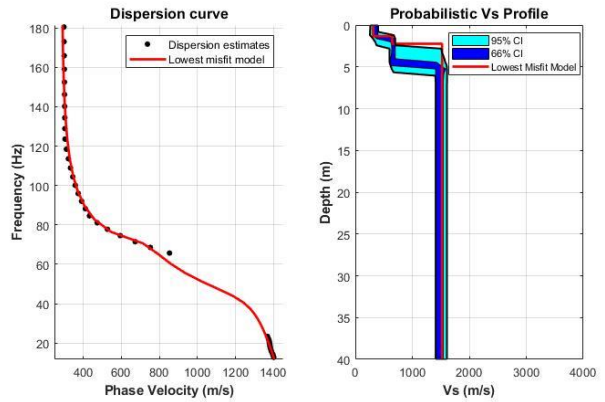
Figure 2.11: Continued

Table 2.4: Rock velocities determined under each station from inversion algorithms using Dinver and PSWP. Sites shaded in grey indicate that the rock velocity was measured by dispersion.

Station	Optimal rock velocity from Dinver (m/s)	Mean rock velocity (one standard deviation) from PSWP (m/s)
A16	1352	1336 (220)
A54	872 overlaying 1224	850 (38) overlaying 1357 (95)
A61	1915	2424 (557)
A64	1108 overlaying 2408	1020 (104) overlaying 2553 (686)
BATG	1379	1441 (227)
BCLQ	1339	1612 (300)
DPQ	1570	1574 (260)
GAC	1348 overlaying 3300	1080 (310) overlaying 2780 (685)
GBN	1164 overlaying 1936	1237 (133) overlaying 1976 (265)
ICQ	1954	1959 (260)
KGNO	1860	1553 (700)
LMQ	847 overlaying 3027	889 (174) overlaying 2717 (434)
MCNB	1870	2409 (600)
ORIO	1570	1708 (170)
OTT	1539	1612 (165)
QCQ	1523	1503 (60)

2.6 Vp Seismic refraction estimates

Vp refraction data was collected with the same equipment and array setup as MASW except a trigger switch and the stacking of five generated seismic signals was used. Measurements were performed where the Geode system could be deployed. For each shot gather, the first P wave arrivals were picked. Travel time analysis was performed in calculating layer velocities and thicknesses when possible. Seismic refraction was the most successful method to consistently obtain rock velocities with Vp > 1000 m/s (19 out of 20 stations). For 11 stations, velocity of the near surface material was also obtained and a Vp profile is obtained. The only station where reliable travel time picks could not be made was station CNQ. A sample of travel time picks made from a raw shot gather data set is shown in Figure 2.12. Velocities of rock and sediment were then compiled from forward and backward shots where the mean and standard deviation of each layer's velocity are calculated from Figure 2.13. If sufficient sampling in the surficial and rock layer was identified, a profile could be built (Figure 2.14) outlining the mean velocities and their standard deviation. Depth was calculated dependent upon the layering system interpreted from the data (i.e. dipping or flat interfaces) as shown in Figure 2.14 (briefly summarized in Chapter 1.5). Dipping interfaces were interpreted from variation in velocity and number of layers from picked arrival times of both forward and backward shots. Table 2.5 summarizes refraction Vp estimates outlining flat and dipping rock interfaces and indicates if a Vp profile could be built for the station. At some stations, we found two rock velocities from varying array spacing and is noted as upper and lower rock velocities. Upper rock velocity is the shallower rock interface (tighter array; shorter wavelength) while the lower rock velocity is the deeper rock. The average refraction Vp of the upper rock unit across all stations measured in Eastern Canada is 2684 m/s (800 m/s standard deviation) which does show a wide range in the units across a very large area.
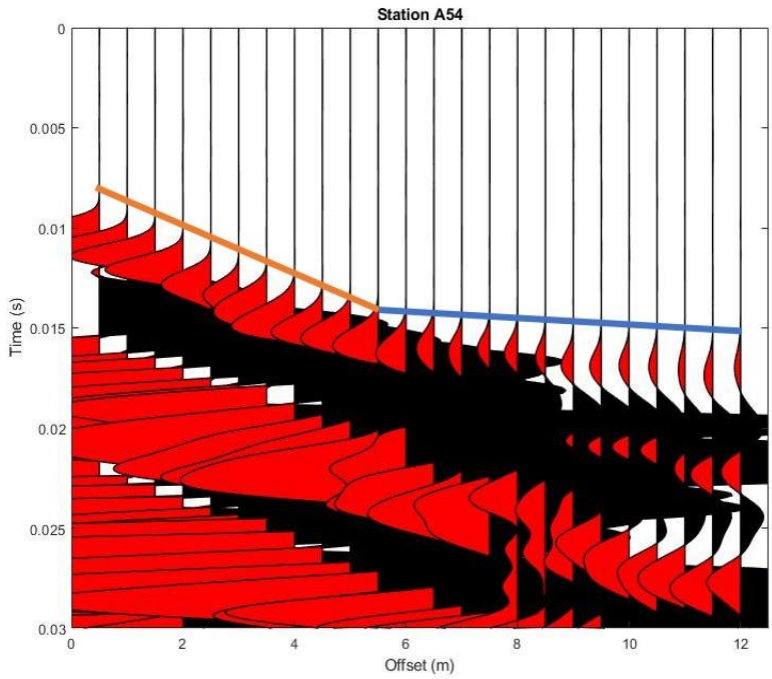
Figure 2.12: Sample of velocities determined for station A54 from 0.5 m array spacing. Orange and blue line indicate the direct wave and refracted wave arrivals, respectively.
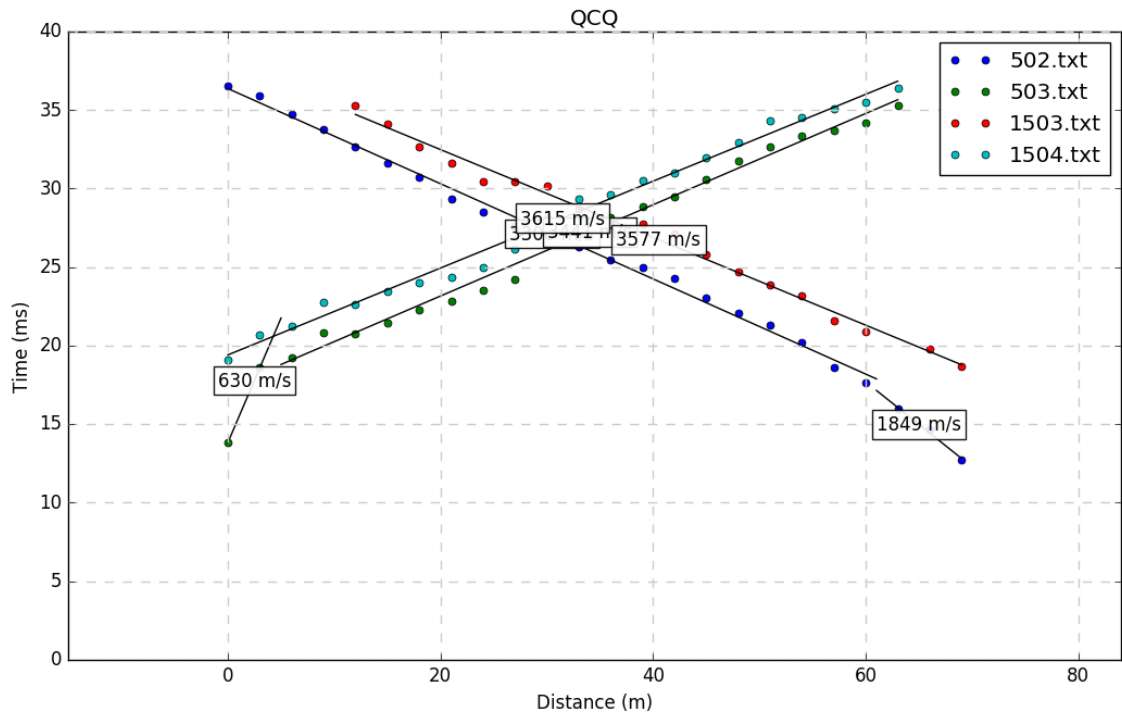
Figure 2.13: Sample of velocities (labelled on plot) determined for station QCQ from 3 m array spacing. File names beginning with 5 indicate 5 m source offsets whereas, names beginning with 15 indicate 15 m source offsets. End digits including 02, 03, or 04 indicate stacked file indicators.

a)
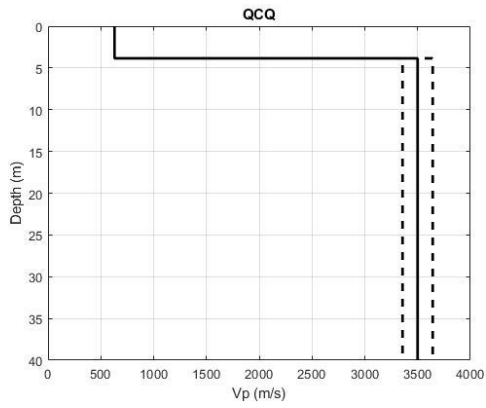
b)
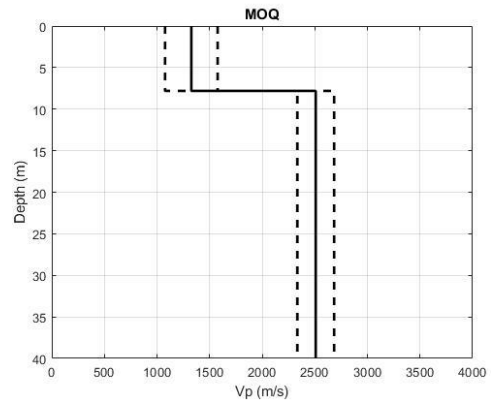
c)
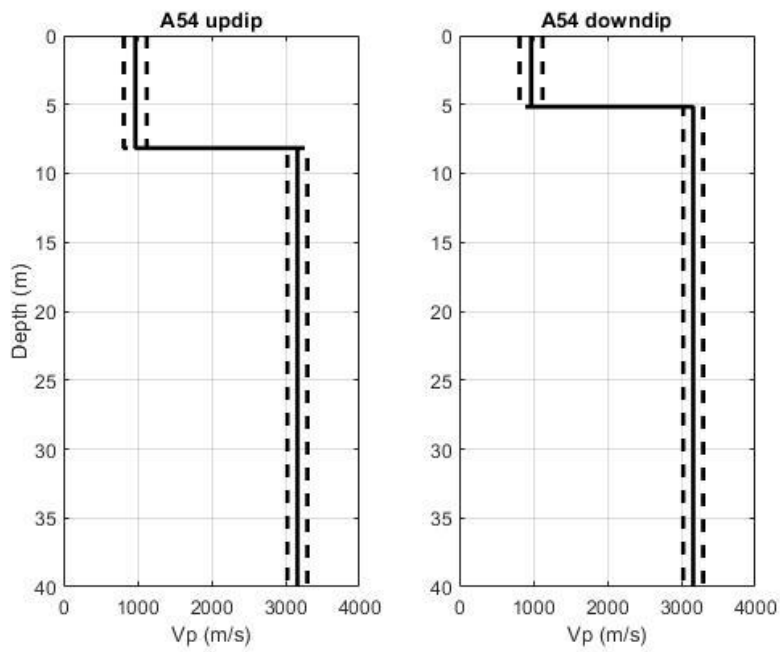
Figure 2.14: Sample mean Vp profiles (solid line) with one standard deviation (dashed lines) determined from refraction travel-times for stations (a) QCQ, and (b) MOQ. For station A54, two Vp profiles for the (c) downdip and (d) up-dip direction are determined.

Table 2.5: Summary of Vp refraction measurements in rock at stations in Eastern Canada.

Station	Upper Rock Velocity (m/s)	Lower Rock Velocity (m/s)	Vp profile	Rock interface
A16	2486 ± 112	Not measured	Rock Velocity only	Dipping
A54	3161 ± 135	Not measured	Profile	Dipping
A61	2500 ± 215	7000 ± 860	Profile	Flat
A64	4467 ± 401	Not measured	Rock Velocity only	Flat
BATG	1797 ± 350	3510 ± 345	Profile	Flat
BCLQ	1650 ± 225	2800 ± 850	Profile	Dipping
CNQ	Not successful	Not successful	Not successful	Not successful
DAQ	1945 ± 315	Not measured	Profile	Flat
DPQ	2610 ± 655	Not measured	Profile	Flat
GBN	2836 ± 481	Not measured	Rock Velocity only	Dipping
GSQ	1466 ± 466	Not measured	Rock Velocity only	Dipping
KGNO	3386 ± 930	Not measured	Rock Velocity only	Dipping
LMQ	2200 ± 240	Not measured	Profile	Flat
MCNB	3151 ± 387	Not measured	Rock Velocity only	Dipping
MOQ	2509 ± 175	Not measured	Profile	Flat
NATG	1711 ± 275	Not measured	Profile	Flat
ORIO	3750 ± 900	Not measured	Profile	Flat
OTT	2800 ± 900	4462 ± 581	Profile	Dipping
QCQ	3500 ± 142	Not measured	Profile	Flat
VABQ	3085 ± 444	Not measured	Rock Velocity only	Dipping

2.7   Poisson's ratio

Poisson's ratio is a fundamental metric to compare the performance of any material when strained elastically (Greaves et al., 2011). Poisson's ratio is defined as the shortening in the transverse direction to the elongation direction of applied force (Gercek, 2007). It is physically the ratio between transverse and longitudinal strain in an elastic material subjected to a uniaxial stress. The tendency of a material to expand or contract in a direction perpendicular to the compressive or tensile force direction is known as the "Poisson effect." Materials with different Poisson's ratios behave differently when under strain. The ratio defines properties of materials to range from rubbery to dilatational (anti-rubbery) where between the extremes are materials that are stiff (i.e. metals and minerals) and compliant (i.e. sponge). In measuring both Vp and Vs, Poisson's ratio (υ) is determined by

$$\upsilon = \frac{\frac{1}{2}\left(V_p^2 - 2V_s^2\right)}{V_p^2 - V_s^2}. \tag{17}$$

Poisson's ratio was calculated using Equation 17 at stations where both reliable rock Vp and Vs were measured. Poisson's ratio is reported in Table 2.6. Calculations were made using the rock Vs of the lowest misfit model from the Dinver inversion and the refraction Vp used to constrain the inversion. No standard deviation is calculated for stations where there is a high variability in the Vp measurements which makes the Vp close the Vs values. Those stations are indicated with a N/A in their standard deviation. The average Poisson's ratio (and standard error) calculated for stations in Eastern Canada is 0.36 (0.080).

Table 2.6: Calculated Poisson's ratio for Eastern Canada stations. N/A refers to stations without a standard deviation due to a single Vp refraction measurement.

Site	Average Poisson's Ratio	Standard Deviation
A16	0.29	0.04
A54	0.42	0.01
A61	0.46	0.01
A64	0.47	0.01
BATG	0.41	0.03
BCLQ	0.39	0.14
DPQ	0.22	N/A
GBN	0.40	0.06
KGNO	0.28	0.07
LMQ	0.41	0.01
MCNB	0.23	0.16
ORIO	0.37	0.11
OTT	0.32	0.26
QCQ	0.39	0.01

The NGA East project (Hashash et al., 2014) found the average Poisson's ratio in the region to be 0.28 ± 0.025 with values ranging from 0.24 to 0.33 for reference rock velocities in Eastern North America. Their Poisson's ratio values were calculated for reference rock site conditions which are assumed to be of Paleozoic age or older. Their mean Vs was 2951 ± 831 m/s likely due to sampling much older, stiffer rock compared to our mean Vs of all rock types of 1736 ± 602 m/s. Our average Poisson ratio value is slightly higher than those found by Hashash et al. (2014). There is a large range in the velocities at Eastern Canada stations, which directly relates to Poisson's ratio having variability as well. Hashash et al. (2014) determines a higher average observed rock Vs than ours which indicate their rock measurements likely being done on older rock compared to ours which is mainly Paleozoic. Variability amongst measurements is also a

factor especially with the majority of their measurements performed at more southern stations in the United States where ours are across a large range (distance) of stations in Eastern Canada.

2.8   Laboratory Vp measurements of rock samples

Laboratory ultrasonic wave transmission measurements were performed to determine the Vp of rock samples obtained at stations VABQ (near Ottawa), NATG (in the upper St. Lawrence), and A16 (in Charlevoix). Care was taken to obtain appropriate rock samples at the stations, representative of the rock composition the station resides on. Multiple small core samples were cut from the rock sample. The rock samples are assumed to be isotropic as only one direction could be measured. The core samples were cut and measured in the direction the grains were aligned, if evident.

Each core sample is put into a securing apparatus where an ultrasonic compressional wave pulse was transmitted through the sample to measure the travel time using a digital oscilloscope. The instrument was first calibrated without any sample in the apparatus and then an aluminum sample to measure the instrumental drift by measuring before and after the experiment. A gel is applied to both ends of the cut sample to couple well with the transmitter and receiver (detector pad) where it is clamped. An ultrasonic pulse is then applied through the sample and the first arrival time at the receiver is then picked from the recorded waveform. The true travel time is calculated by subtracting the travel time calculated with the sample by the travel time with no sample in the apparatus. We divide the true travel time by the length of the sample in order to then calculate Vp of the sample. This procedure is accomplished with multiple core samples extracted from the same rock sample taken from the field. The average Vp from these multiple core samples is then taken. A sample plot of a wave arrival is shown in Figure 2.15. A similar method of choosing travel times was performed for arrivals with and without rock samples.
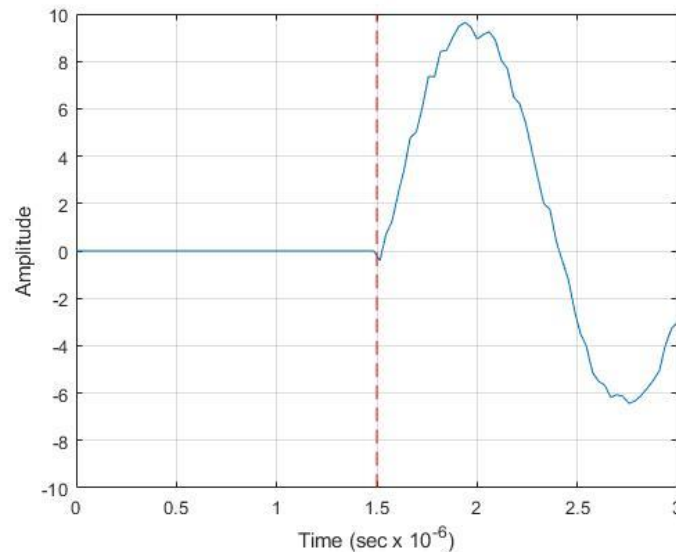
Figure 2.15: Example in the methodology in choosing first arrival travel times from waveforms (blue line) from Vp laboratory experiments. The dotted red line shows an example of how times were chosen as soon as the signal arrives.

Measurements are summarized in Table 2.7 with the average lab sample Vp and its standard deviation. A sample from station QCQ was obtained but crumbled when cut which caused the waveform to be incoherent and only one measurement was taken (no standard deviation obtained). This sample has similar velocities with both the refraction and laboratory Vp methods although unreliable. Station QCQ's refraction and lab measurement is likely similar in that the fractured core sample may replicate the conditions in the subsurface. 75% of our laboratory Vp values are much higher than those determined by the Vp refraction method. Figure 2.15 summarizes the *in situ* Vp refraction and laboratory Vp measurements. The laboratory Vp is approximately two times higher than our *in situ* Vp refraction measurements.

Due to the short length of the core samples, errors in choosing accurate first arrival microseconds apart can affect the measurement. For our study, coherent waveforms were only used to pick arrival times but nonetheless, can be a source of error. Brant et al. (2012) used the resonant frequency method with impulse excitation to calculate the velocity of 100 specimens of various rock types near New York City. That study also compares the laboratory results with low-strain *in situ* field seismic measurements. They concluded that laboratory specimens typically have a higher Vs than *in situ* measurements due to discontinuities present (joints and shears) in the *in situ* rock mass which are absent from laboratory specimens which are intact. Brant et al. (2012)

67

also found that laboratory Vp or Vs of rock samples to be almost two times the Vp or Vs *in situ* measurement for many rock types similar to our results.

Table 2.7: Summary of Vp lab measurements compared with Vp refraction results.

Station:	Average Rock Lab Sample Vp (m/s)	Standard Deviation (m/s)	Vp Refraction (m/s)	Standard Deviation (m/s)	Factor difference of Lab Sample with Refraction Vp
A16	5411	85	2486	112	2.17 (in situ is 46% of sample)
NATG	4950	481	1711	275	2.89 (in situ is 34% of sample)
VABQ	5427	319	3085	444	1.76 (in situ is 57% of sample)
QCQ	3526*	N/A	3500	142	1.00 (in situ is 99% of sample)

*Vp is estimated from incoherent measure of travel time.
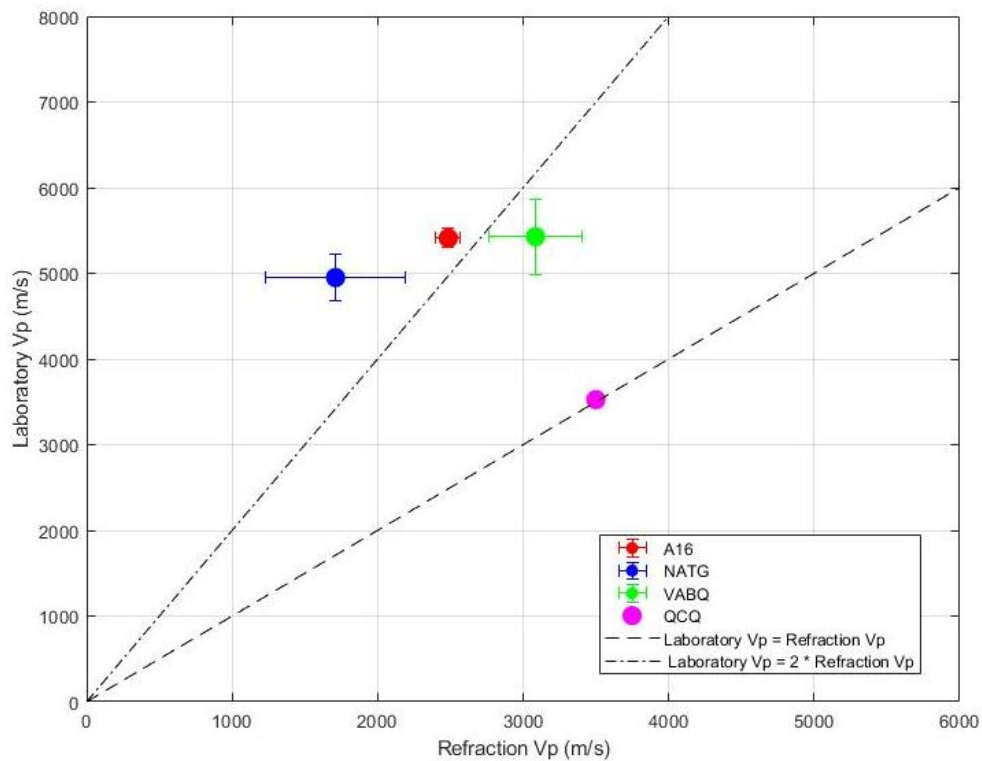
Figure 2.16: Comparison between refraction Vp and laboratory Vp measurements.

2.9   Discussion and Conclusions

This study incorporated a multi-method approach to characterize 25 seismograph stations situated on supposed hard rock in Eastern Canada. Multiple methods were used in attempts to acquire Vp and Vs of the station's rock using active and passive surface wave methods and active body wave methods. Surface wave methods used include active MASW and passive

AVA. Both active and passive surface wave methods were used to build a dispersion curve to be inverted for a Vs profile. Two inversion approaches were used including the modified neighborhood algorithm (Dinver) and a Bayesian inversion (PSWP). Dinver was used to provide the best fitting model and PSWP was used to analyze data errors and standard deviations to give a possible range of rock Vs, Vs profiles, Vs_{30}, and site class. Body wave Vp refraction was used to acquire Vp of the rock where Vp depth profiles were generated if the surficial layer was sampled sufficiently. Refraction Vp of rock was also used to constrain the parameterization of surface wave inversions. Poisson's ratio for the station rock was calculated from the inverted Vs and refraction Vp. Laboratory Vp measurements were performed using rock samples taken from the station with attempts to correlate it with the Vp calculated from seismic refraction. Dispersion estimates from AVA testing could be made at 7 out of 23 stations and the rock Vs could be measured at 6 stations. Dispersion estimates were obtained at all 23 stations using MASW, where only surficial soil and sediment was only measured at 7 of those stations. 16 out of 23 stations had reliable dispersion estimates where a transition from sediment to rock was observed in dispersion histograms and were inverted. Vp refraction was successful in providing rock Vp at 19 out of 20 stations. Active MASW and Vp refraction had the highest success rate in acquiring estimates of the rock velocity. Passive methods were less successful but included the important low frequency portion of the dispersion curve which typically provides the station's rock phase velocity.

Rayleigh wave dispersion curves could solely be built in having the most success with MASW and only having vertical component geophones. Other authors have had more success in obtaining rock Vs from jointly inverting Rayleigh wave dispersion curves with Love wave dispersion curves (Poggi et al., 2017; Martin et al., 2017). Love wave dispersion estimates can be reliably made through Love wave MASW (MAS_LW) to be jointly inverted (with Rayleigh wave dispersion data and/or ellipticity) or independently inverted for a Vs profile. Vs refraction is also a successful method used for site characterization at rock sites (e.g. Beresnev and Atkinson, 1997). From success seen in this study with Vp refraction, Vs refraction attempted at all sites would likely give reliable rock Vs for site characterization purposes. Due to not having horizontal geophones and a horizontal source, Vs refraction and MAS_LW could not be performed during this field campaign.

The use of different seismic sources has also been successful in measuring rock Vs instead of using a single source (e.g. Catchings et al., 2019). Catchings et al. (2019) used vertical sources such as an accelerated weight drop (AWD), 10 lb and 3 lb hammers, and seisguns to create 2-D models of the rocklike subsurface dams located in British Columbia. Shear sources for direct Vs measurements also were used and varied where an angled AWD, and a shear source were struck by 10 lb and 3 lb hammers to generate different energy levels. A sledgehammer may not be able to generate large enough wave amplitude to be detected by large offset geophones. The use of AWD would solve this site-specific issue where more energy is needed.

Comparing the Paleozoic and Precambrian rock velocities found from this study with those from Nastev et al. (2016) indicates similarities between both studies. The lowest misfit model is used in calculating the average Paleozoic rock to be 1671 ± 178 m/s (n=5) and the Precambrian rock to be 1935 ± 28 m/s (n=2). These compare with Nastev et al. (2016) with their Paleozoic rock velocity to be 1500 ± 500 m/s and Precambrian rock varying from 2500 ± 700 m/s. This study's measurements fall within the velocity ranges of both geologic Eons seen in Nastev et al. (2016) however sampling considerably less. Figure 2.17 shows our measured Vs compared to Nastev et al. (2016). Our average measured values do fall within the standard deviation range from Nastev et al. (2016) indicating similar measured rock velocities.
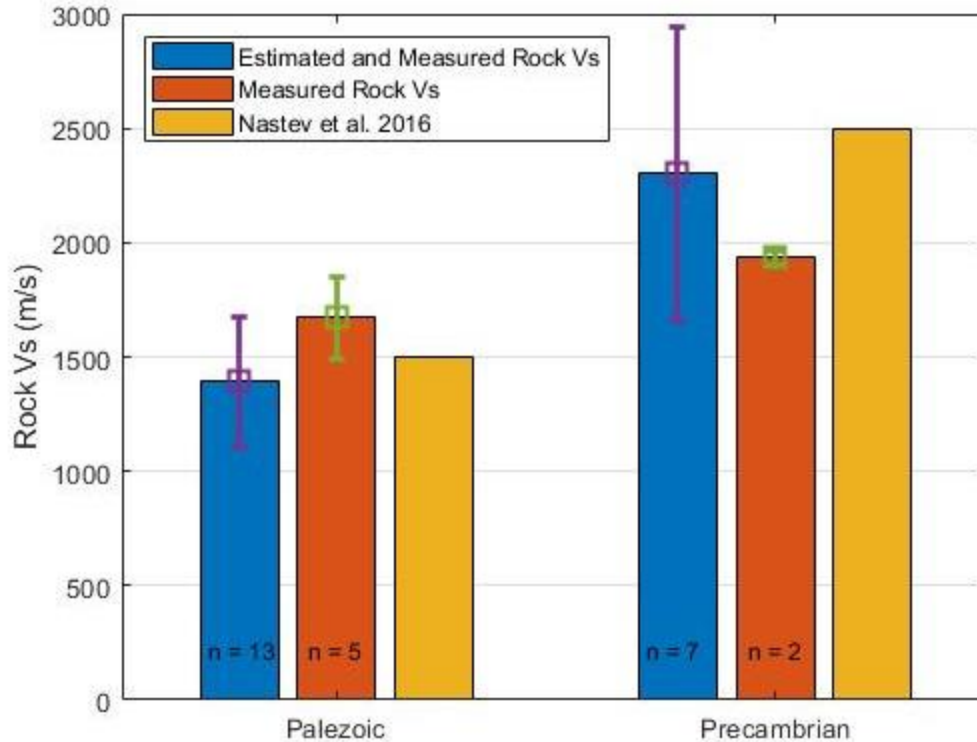
Figure 2.17: Comparison of Paleozoic and Precambrian rock Vs in Eastern Canada. Orange bars indicate stations where rock was measured through dispersion estimates. Blue bars indicate stations where rock was measured and estimated.

A Vs_{30} map has been created for the city of Ottawa (Motazedian et al., 2011) which also summarizes rock velocities found in the Ottawa area. Four stations near Ottawa are looked at in this study (e.g. OTT, ORIO, VABQ, and GAC) with OTT being in its municipality. From stations OTT and ORIO, the average rock Vs from our lowest misfit models are 1551 m/s which is lower than the majority of Paleozoic rock measurements found in Motazedian et al. (2011) with rock Vs being typically > 2000 m/s. Their study used downhole Vs, seismic reflection-refraction profiling, and high-resolution Vs reflection "landstreamer" profiling to measure Vs. Seismic Vs refraction at station OTT (Beresnev and Atkinson 1997) determined 30 m thick soft sedimentary rock with Vs of 1670 m/s overlays stiffer intrusive rock with Vs of 2700 m/s. We determine a dipping rock interface with our refraction data set at station OTT, where lateral heterogeneity can affect the accuracy of the sediment thickness. Our measured rock velocity of 1539 m/s with our lowest misfit model is comparable to their results. The other 10 stations investigated by Beresnev and Atkinson (1997) do not coincide with our stations but highlight the success of the Vs refraction technique in observing rock Vs.

71

Geological, geophysical, and geotechnical studies have been performed in Quebec City for the purpose of locating bedrock (e.g. Pugin et al., 2013) and for microzonation studies (e.g. Chagnon and Gilbert, 1990 and Perret and Lamarche, 2013). Vs of different subsurface materials are compiled and summarized in Nastev et al. (2016) where the average rock Vs in Quebec City is much lower (~ 980 m/s) compared to Ottawa and Montreal. Vs profiles are shown in Nastev et al. (2016) where the bottom-most rock has a Vs of ~1400 m/s. GPR (2005) conducted two downhole seismic surveys in Levis (south of Quebec City) where the rock Vs was measured. Rock Vs measurements as large as 1200 m/s were made in the area. Station QCQ is located at Laval University in Quebec City where the measured rock velocity of 1523 m/s matches well with Paleozoic rock Vs measurements seen in the Quebec City velocity profiles in Nastev et al. (2016). All studies including ours show similar, low rock Vs measured where Paleozoic rock is consistently measured near Quebec City.

No publicly available data is available for other Eastern Canada seismograph stations to compare our rock velocities with. Montreal has had extensive work done with boreholes drilled for geotechnical and microzonation studies, but we cannot compare as our closest station (MOQ) does not have successful Vs measurements. Similarly, for stations in Nova Scotia, New Brunswick, Charlevoix and the Upper St. Lawrence, no public data is available for comparison.

2.10 References

Atkinson, G. M. (1996). The high-frequency shape of the source spectrum for earthquakes in eastern and western Canada. *Bulletin of the Seismological Society of America*, *86*(1A), 106-112.

Atkinson, G. M., & Cassidy, J. F. (2000). Integrated use of seismograph and strong-motion data to determine soil amplification: response of the Fraser River Delta to the Duvall and Georgia Strait earthquakes. *Bulletin of the Seismological Society of America*, *90*(4), 1028-1040.

Beresnev, I. A., & Atkinson, G. M. (1997). Shear-wave velocity survey of seismographic sites in eastern Canada: Calibration of empirical regression method of estimating site response. *Seismological Research Letters*, *68*(6), 981-987.

Brant, L. C., Nikolaou, S., & Moss, C. (2013). Resonant frequency testing of New York City rock types. *Geotechnical Testing Journal*, *36*(4), 466-475.

Catchings, Rufus D., et al. (2019) "Two-Dimensional Seismic Velocities and Structural Variations at Three British Columbia Hydro and Power Authority (BC Hydro) Dam Sites, Vancouver Island, British Columbia, Canada." *USGS Open-File Report*, 2019, doi:10.3133/ofr20191015.

Chagnon, J. Y., & Gilbert, F. D. (1990). *Development of a Method of Seismic Microzonation Mapping Applicable to the Urban Areas of Canada*. Université Laval, Département de géologie, Faculté des sciences et de génie.

Di Giulio, G., Savvaidis, A., Ohrnberger, M., Wathelet, M., Cornou, C., Knapmeyer-Endrun, B., ... & Bard, P. Y. (2012). Exploring the model space and ranking a best class of models in surface-wave dispersion inversion: Application at European strong-motion sites. Exploring model space, ranking best models. *Geophysics*, *77*(3), B147-B166.

Dosso, S.E., (2002). Quantifying uncertainties in geoacoustic inversion I: A fast Gibbs sampler approach, J. acoust. Soc. Am., 111, 2166–2177

Foti, S., Lai, C., Rix, G. J., & Strobbia, C. (2014). *Surface wave methods for near-surface site characterization*. CRC press.

Foti, S., Hollender, F., Garofalo, F., Albarello, D., Asten, M., Bard, P. Y., ... & Forbriger, T. (2017). Guidelines for the good practice of surface wave analysis: A product of the InterPACIFIC project. *Bulletin of Earthquake Engineering*, *16*(6), 2367-2420.

Fulton, R. J. (1995). Surficial materials of Canada/Materiaux superficiels du Canada. Geological Survey of Canada. "A" Series Map 1880A, 1995, 1 sheet, https://doi.org/10.4095/205040 (Open Access) Ottawa, Ont.: Geological Survey of Canada.

Gercek, H. (2007). Poisson's ratio values for rocks. *International Journal of Rock Mechanics and Mining Sciences*, *44*(1), 1-13.

GPR Geophysics International Inc. (2005). *Down-hole Seismic Survey Rabaska Project, Lévis Quebec*. Technical report, Longueil, Teratech, 16 p

Greaves, G. N., Greer, A. L., Lakes, R. S., & Rouxel, T. (2011). Poisson's ratio and modern materials. *Nature materials*, *10*(11), 823.

Hashash, Y. M., Kottke, A. R., Stewart, J. P., Campbell, K. W., Kim, B., Moss, C., ... & Silva, W. J. (2014). Reference rock site condition for central and eastern North America. *Bulletin of the Seismological Society of America*, *104*(2), 684-701.

Haskell, N. A. (1953). The dispersion of surface waves on multilayered media. *Bulletin of the seismological Society of America*, *43*(1), 17-34.

Konno, K., & Ohmachi, T. (1995). A smoothing function suitable for estimation of amplification factor of the surface ground from microtremor and its application. *Doboku Gakkai Ronbunshu*, *1995*(525), 247-259.

Ladak, S., Molnar, S., Palmer, S., & Atkinson, G. (2019). Application of active and passive seismic methods for determining the shear wave velocity profile at hard rock sites in Eastern Canada. *Proceedings of the 12th CCEE (Canadian Conference on Earthquake Engineering) 2019*.

Martin, A., Yong, A. Stephenson, W. Boatwright,. J, Diehl,. J. (2017). Geophysical Characterization of Seismograph Station Sites in the United States – Importance of a Flexible Multi-Method Approach. In *Proc. from the 16th World Conf. on Earthquake Engineering*.

Mathworks. (2006). Voronoi diagram. Retrieved April 2019, from https://www.mathworks.com/help/matlab/ref/voronoi.html

 Molnar, S., Dosso, S. E., & Cassidy, J. F. (2010). Bayesian inversion of microtremor array dispersion data in southwestern British Columbia. *Geophysical Journal International*, *183*(2), 923-940.

Molnar, S., Dosso, S. E., Ventura, C. E., Finn, W. D. L., Taiebat, M., & Cassidy, J. F. (2012). Probabilistic site characterization based on Bayesian inversion of ambient vibration array recordings in SW British Columbia, Canada. In *15th World Conference on Earthquake Engineering*.

Motazedian, D., Hunter, J. A., Pugin, A., & Crow, H. (2011). Development of a Vs_{30} (NEHRP) map for the city of Ottawa, Ontario, Canada. *Canadian Geotechnical Journal*, *48*(3), 458-472.

Nastev, M., Parent, M., Benoit, N., Ross, M., & Howlett, D. (2016). Regional Vs_{30} model for the St. Lawrence Lowlands, Eastern Canada. *Georisk: Assessment and Management of Risk for Engineered Systems and Geohazards*, *10*(3), 200-212.

Natural Resources Canada. (2013). Geology Map of Canada. Retrieved from https://www.arcgis.com/home/item.html?id=4d2d5a2ebbde419ea2f928f6887e1d02.

Palmer, S.M., and Atkinson, G.M. (2018) Bedrock Site Conditions and Kappa in Charlevoix, Quebec. Seismological Research Letters: Volume 89 Number 2B, pp 750 and 821.

Palmer, S. M., & Atkinson, G. M. (2020). The High-Frequency Decay Slope of Spectra (Kappa) for M≥ 3.5 Earthquakes on Rock Sites in Eastern and Western Canada. *Bulletin of the Seismological Society of America*, *110*(2), 471-488.

Perret, D., & Lamarche, L. (2013). Microzonage sismique des villes de Québec - Ancienne-Lorette et réserve indienne Wendake (période de vibration des terrains), Québec. *Natural Resources Canada*. doi: 10.4095/292641

Pileggi, D., Rossi, D., Lunedei, E., & Albarello, D. (2011). Seismic characterization of rigid sites in the ITACA database by ambient vibration monitoring and geological surveys. *Bulletin of Earthquake Engineering*, *9*(6), 1839-1854.

Poggi, V., Burjanek, J., Michel, C., & Fäh, D. (2017). Seismic site-response characterization of high-velocity sites using advanced geophysical techniques: application to the NAGRA-Net. *Geophysical Journal International*, *210*(2), 645-659.

Pugin, A. J. M., Pullan, S. E., & Hunter, J. A. (2013). Shear-wave high-resolution seismic reflection in Ottawa and Quebec City, Canada. *The Leading Edge*, *32*(3), 250-255.

Sambridge, M. (1999). Geophysical inversion with a neighbourhood algorithm—I. Searching a parameter space. *Geophysical journal international*, *138*(2), 479-494.

Tarantola, A., (1987). Inverse Problem Theory: Methods for Data Fitting and Model Parameter Estimation, Elsevier, Amsterdam.

Thomson, W. T. (1950). Transmission of elastic waves through a stratified solid medium. *Journal of applied Physics*, *21*(2), 89-93.

Wathelet, M. (2005). Array recordings of ambient vibrations: surface-wave inversion. *PhD Diss., Liége University*, *161*.

Wathelet, M. (2008). An improved neighborhood algorithm: parameter conditions and dynamic scaling. *Geophysical Research Letters*, *35*(9).

Chapter 3 Site Classification at "Hard Rock" Stations in Eastern Canada

3.1 Introduction

Characterizing seismograph stations is important in developing GMM's and estimating the site response in the event of an earthquake. The NBCC prioritizes the use of Vs_{30} as a site classification parameter for rock sites compared to other geotechnical parameters as part of the seismic guidelines in Canada. Chapter 2 introduced our multi-method seismic testing approach to obtain velocity depth profiles at selected seismograph stations across Eastern Canada. This Chapter focuses on performing earthquake site classification (Vs_{30}, site period, site amplification) first for the tested sites, then specific to the seismograph station itself. The velocity profiles start at the ground or rock surface; the seismograph is installed on the rock surface. The appropriate site classification of the seismograph location itself is determined in section 3.3.1 by removing low velocities of surficial soils (not present below the seismograph) and using the station's rock velocity to calculate the appropriate Vs_{30}. MHVSR and EHVSR have become a popular technique in estimating site amplification, and authors have developed a site period classification scheme instead of Vs_{30} (Zhao et al. 2006; Di Alessandro et al. 2012). MHVSRs are also used here to determine site period classification of the selected seismograph stations. This Chapter concludes with combining site classification approaches (Vs_{30}, site period) with our multi-method seismic testing to document earthquake site characterization of the selected Eastern Canada seismograph stations.

3.2 Preliminary Vs_{30} site classification from dispersion estimates

A preliminary Vs_{30} site classification is performed using Rayleigh wave phase velocity (dispersion) estimates. The relation of Martin and Diehl (2004) is

$$Vs_{30} = 1.045 * V_{R40}, \tag{18}$$

where Vs_{30} is calculated based on the measured Rayleigh phase velocity with a 40-m wavelength (V_{R40}). Figure 3.1 shows all the dispersion estimates for measurement locations near the seismograph stations. Using the measured V_{R40} at each station, Vs_{30} is solved via Equation 18 and reported in Table 3.1. Stations that achieve at least a 40 m wavelength are assigned a site class; stations below 40 m have an estimated site class from their trend. Figure 3.1 shows that the

Vs_{30} of most stations corresponds to site class B (soft rock, 760-1500 m/s) with Vs_{30} of two stations related to site class C (dense soil, 360-760 m/s) and three stations related to hard rock class A (> 1500 m/s). This method is used as a quick and preliminary estimate of Vs_{30} site class with no inversion required of the dispersion curve. These dispersion measurements were taken at a distance from the station with soil at the surface, which is later looked at again to calibrate the measurements to those of the station in section 3.3.1. We compare these preliminary Vs_{30} estimates with 'robust' Vs_{30} estimates determined from inverted Vs profiles in section 3.3.

Table 3.1: Preliminary Vs_{30} of Eastern Canada seismograph stations.

Station	V_{R40} (m/s)	Vs_{30} (m/s)	Site Class
A16	No Data	No Data	B[*]
A54	1026	1072	B
A61	1297	1355	B
A64	1218	1273	B
BATG	844	882	B
BCLQ	No data	No data	B[*]
DPQ	No data	No data	C[*]
GAC	No data	No data	A[*]
GBN	1123	1174	B
ICQ	1182	1235	B
KGNO	1657	1732	A
LMQ	766	800	B
MCNB	No Data	No Data	A[*]
ORIO	1127	1178	B
OTT	683	714	C
QCQ	1267	1324	B

*station measurements did not achieve a 40 m wavelength and are estimated.
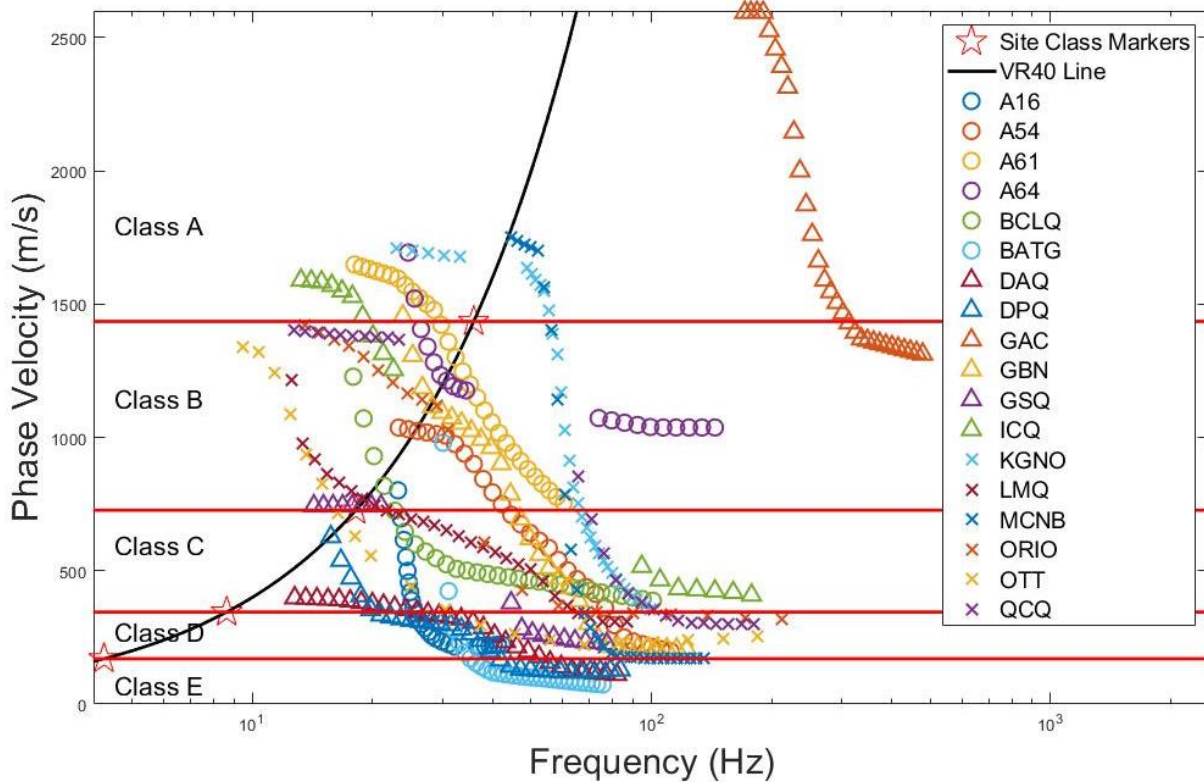
Figure 3.1: Preliminary Vs$_{30}$ site classification based on Rayleigh phase velocities (symbols) measured at each station. The Rayleigh wave velocity with a 40-m wavelength is shown by the black line ("V$_{R40}$ line") and corresponding V$_{R40}$ limits of Vs$_{30}$ classes (horizontal lines) are labelled.

3.3   Robust Vs$_{30}$ site classification from Vs profiles

In the previous section, active and passive surface wave methods were used to build a full dispersion curve and are assigned a preliminary Vs$_{30}$ site class from the dispersion estimates. Inverted Vs profiles from Chapter 2 (section 2.5) are applied and converted to 'robust' Vs$_{30}$ values here. Dispersion curves were inverted using two algorithms to acquire Vs profiles. Vs$_{30}$ is calculated using the lowest misfit model from the Dinver inversion (Table 3.2). For the PSWP inversion, a subset of 10,000 models are drawn from the posterior probability density (PPD) to calculate Vs$_{30}$. The mean Vs$_{30}$ and one standard deviation is reported in Table 3.2. PSWP also calculates the probability of each site class from this sample of Vs$_{30}$ values. The preliminary site classes concluded from the V$_{R40}$ estimate correspond to the same robust Vs$_{30}$ site classes estimated from inverted Vs profiles except for two stations. It is important to note these inverted Vs profiles and Vs$_{30}$ values correspond to the seismic testing location (on ground or rock surface), which are some distance away from the seismograph and/or located on different ground

conditions (surficial soils) compared to the seismograph. They are appropriate to the seismograph 'site'.

Table 3.2: Robust Vs_{30} determined from inverted Vs profiles.

Station	Optimal Vs_{30} (m/s)	Mean Vs_{30} with one std. dev. (m/s)	Site class probability
A16	890	799 ± 111	65 % Class B, 35 % Class C
A54	922	984 ± 100	99 % Class B
A61	1226	1507 ± 207	57 % Class B, 43 % Class A
A64	1352	1464 ± 360	65 % Class B, 34 % Class A
BATG	835	894 ± 72	99 % Class B
BCLQ	989	423 ± 66	92% Class C
DPQ	607	600 ± 31	99 % Class C
GAC	2936	2418 ± 512	98 % Class A, 2% Class B
GBN	1071	1094 ± 91	99 % Class B
ICQ	1075	1172 ± 93	100 % Class B
KGNO	1504	956 ± 450	77 % Class B, 10 % Class A
LMQ	751	792 ± 125	50 % Class B, 50 % Class C
MCNB	1380	1459 ± 205	56 % Class B, 44 % Class A
ORIO	1007	1052 ± 68	100 % Class B
OTT	752	828 ± 63	87 % Class B, 13 % Class C
QCQ	1197	1150 ± 55	100 % Class B

3.3.1 Station appropriate Vs_{30} site classification

The Vs_{30} estimates in the previous two sections are calculated from seismic array measurements performed at a distance from the station with soil and other sediment overburden present. These Vs_{30} estimates may not be accurate to the seismograph site conditions, installed on rock. Additional steps are performed in this section to determine Vs profiles representative of the outcropping rock the seismograph stations are placed on and shown in Figure 3.2. At stations where our surface wave methods penetrated 30 m or more into rock, Vs_{30} is calculated from the measured rock velocity from the station's (inverted) Vs profile. At stations where our surface wave methods penetrated rock less than 30 m, two approaches are used to estimate Vs_{30} which provide minimum and maximum Vs_{30} bounds. The first is to simply extend the inverted rock velocity down to 30 m depth and assume it is accurate of the station's Vs_{30}. Extending the same constant rock Vs at shallower depth to 30 m is a conservative (lower Vs_{30} and site class) approach because velocity generally increases with depth in the earth. A less conservative approach is to extrapolate the measured average velocity at the maximum measured depth further to 30 m depth. Ahdi et al. (2017) summarizes various Vs_{30} extrapolation models from authors who have applied non-invasive and invasive seismic data to create correlations between Vs_{30} and

time-averaged Vs measurements at a depth z (Vs_z). The first extrapolation model was made by Boore (2004) where 135 geophysical borehole measurements from California were used to develop a linear correlation between logarithmic Vs_{30} and depth. Other authors have developed correlations depending on the region such as in Japan (Boore et al., 2011; Midorikawa and Nogi, 2015) and California and Turkey (Dai et al., 2013). Boore et al. (2011) is the most suitable correlation to be used in our study due to Japanese KiK net stations having a tendency to be on stiff soil or rock similar to our stations in Eastern Canada situated on rock.
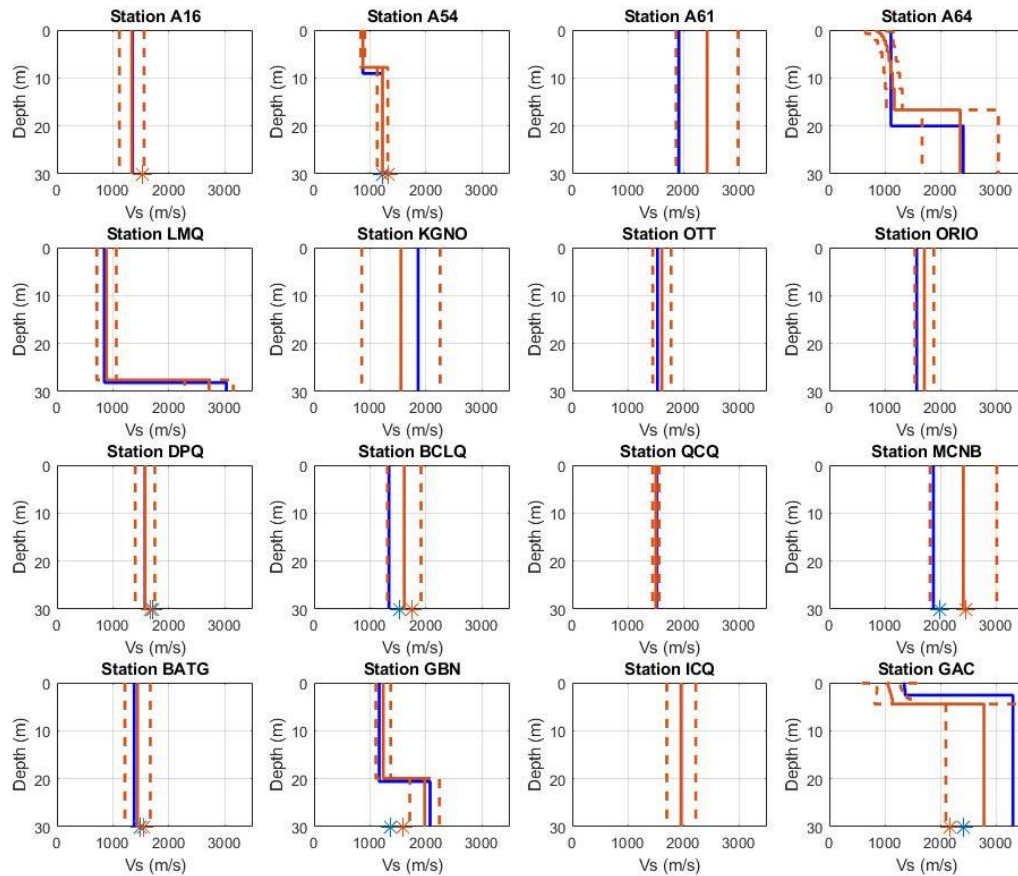
Figure 3.2: Extended Vs profiles representative beneath each station including measured rock (Vs of surficial sediment and overburden are removed, not shown). Optimal Dinver Vs profile is shown by solid blue lines and mean PSWP Vs profile in solid orange with the standard deviation shown by dashed lines Stars indicate extrapolated Vs_{30} values.

For the purpose of this study, velocities corresponding to material the station is not residing on (e.g. surficial soil/gravel layers) is removed from the velocity profiles determined in section 2.5 to determine station appropriate Vs profiles shown in Figure 3.2. This decreases the depth resolution of our Vs profiling at some stations, but we are able to extrapolate to 30 m depth using correlations between Vs_{30} and Vs_z.

Boore et al. (2011) built a Vs_{30} extrapolation model using 635 velocity models from Japan (KiK-Net) stations placed on rock and stiff soil. A second order-polynomial was developed to correlate Vs_z with Vs_{30} at 1 m depth intervals starting at 5 to 29 m,

$$logVs_{30} = c_0 + c_1 logVs_z + c_2 (\log Vs_z)^2. \qquad (19)$$

This logarithmic second-order polynomial relation requires measures of Vs_z. Coefficients (c_0, c_1, and c_2) were developed from the Kik-Net station Vs data (Table 3.3). The standard deviation of residuals is shown in the last column of Table 3.3 and exemplifies that when deeper Vs is measured, the lower the uncertainty in Vs_{30}.

Table 3.3: Depth (z) of maximum Vs_z and respective coefficients used in Equation 19 (Boore et al. 2011) to extrapolate to Vs_{30}.

z (m)	c0	c1	c2	Standard Deviation of Residuals
5	0.205	1.318	-0.117	0.119
6	-0.061	1.482	-0.142	0.111
7	-0.274	1.607	-0.160	0.103
8	-0.372	1.649	-0.163	0.097
9	-0.494	1.707	-0.169	0.090
10	-0.544	1.715	-0.167	0.084
11	-0.601	1.727	-0.165	0.078
12	-0.608	1.707	-0.158	0.072
13	-0.632	1.698	-0.152	0.067
14	-0.612	1.659	-0.142	0.062
15	-0.578	1.611	-0.130	0.056
16	-0.543	1.565	-0.119	0.052
17	-0.528	1.535	-0.112	0.047
18	-0.496	1.494	-0.102	0.043
19	-0.455	1.447	0.092	0.038
20	-0.406	1.396	-0.081	0.035
21	-0.383	1.365	-0.073	0.030
22	-0.353	1.331	-0.066	0.027
23	-0.316	1.291	-0.058	0.023
24	-0.274	1.250	-0.049	0.019
25	-0.223	1.202	-0.039	0.016
26	-0.177	1.159	-0.031	0.013
27	-0.135	1.120	-0.023	0.009
28	-0.090	1.080	-0.015	0.006
29	-0.046	1.040	-0.008	0.003

The maximum resolution depth (z_{max}) of surface wave dispersion methods is based on an assumption many authors (e.g. Park et al., 1999) use where $z_{max} \approx \lambda_{max}/2$ where λ_{max} is the maximum achieved wavelength from the AVA or MASW survey. For all stations, λ_{max} is calculated from dispersion curve V_R at the lowest frequency ($\lambda_{max} = V_R/f$) and halved to

determine z_{max} (Table 3.4). Sediment thickness (if present) is subtracted from z_{max} to calculate the penetration depth into rock, i.e., z of Vs_z. The average rock velocity is known from the inverted velocity profiles in Chapter 2 (Table 2.4).

Table 3.4 summarizes z_{max}, depth to rock and penetration depth into rock at the survey location for each station. If the stations rock penetration depth is less than 30 m, Equation 19 is used to extrapolate Vs_z given the known penetration depth z to estimate Vs_{30}. The resolution depth at stations DAQ and GSQ indicate that dispersion estimates could be made but only soft sediment was measured.

Table 3.4: Determination of penetration depth (z) into rock. Rows shaded grey indicate measured rock velocity. Red font indicates that dispersion estimates were made but depth to rock was not determined.

Station	z_{max} (m)	Sediment thickness from lowest misfit model (m)	Penetration depth into rock (m)
A16	17.40	1.30	16.10
A54	22.25	1.27	20.98
A61	45.67	15.78	29.89
A64	34.44	0	34.44
BATG	34.27	10.87	23.40
BCLQ	16.03	0.37	15.66
DAQ	15.58	Not measured	Not measured
DPQ	19.94	10.90	9.04
GAC	7.57	0	7.57
GBN	30.51	1.3	29.21
GSQ	26.04	Not measured	Not measured
ICQ	60.03	21.60	38.43
KGNO	37.05	0.70	36.35
LMQ	48.56	2.67	45.89
MCNB	19.69	1.01	18.68
ORIO	52.43	9.00	43.43
OTT	70.61	8.10	62.51
QCQ	55.11	2.24	52.87

Vs_{30} is determined using Vs profiles from both Dinver and PSWP inversion. The Dinver optimal rock Vs profile is used to calculate the representative Vs_{30} for the seismograph station. The mean Vs_{30} and its standard deviation is calculated from the PSWP subset of 10,000 Vs profiles. For stations with Vs profiles to 30 m depth or more, the measured Vs profile is used to calculate Vs_{30}. When the station's Vs profile is less than 30 m, Vs_{30} is calculated in two ways, by extending the base rock Vs to 30 m (provides a minimum Vs_{30} bound) or by extrapolation using the relation of Boore et al. (2011) given penetration depth into rock, i.e., Vs_z reported in Table

3.4 for each station (provides a maximum Vs_{30} bound). The station appropriate calculated Vs_{30} value(s) is reported in Table 3.5. In Table 3.5 some stations are noted to be A/B (or B/A) which indicates that their mean value is within A (or B) and their standard deviation goes into site class B (or A).

Table 3.5: Station appropriate Vs_{30} estimates. Grey shading indicates stations where rock Vs was directly measured by dispersion estimates.

Station	Optimal Vs_{30} (m/s), Site Class	Extended optimal Vs_{30} (m/s), Site Class	Extrap. optimal Vs_{30} (m/s), Site Class	Mean Vs_{30} (1 std. dev.) (m/s), Site Class	Extended mean Vs_{30} (1 std. dev.) (m/s), Site Class	Extrapolated mean Vs_{30} (1 std. dev.) (m/s), Site Class
A16		1352, B	1530, A		1336 (220) B/A	1532 (280), A/B
A54		1091, B	1232, B		1174 (95), B	1316 (115), B
A61	1915, A			2424 (557), A		
A64	1352, B			1464 (340), B/A		
BATG		1379, B	1480, B		1441 (226), B/A	1543 (317), A/B
BCLQ		1339, B	1530, A		1612 (300), A/B	1747 (309), A/B
DPQ		1570, A	1711, A		1574 (260), A/B	1670 (224), A/B
GAC		2936, A	2405, A		2418 (512), A	2170 (355), A
GBN		1350, B	1364, B		1573 (265), A/B	1587 (221), A/B
ICQ	1954, A			1959 (260), A		
KGNO	1860, A			1553 (700), A/B		
LMQ	887, B			940 (485), B/C		
MCNB		1870, A	1991, A		2409 (600), A	2461 (720), A
ORIO	1570, A			1708 (170), A		
OTT	1539, A			1612 (165), A/B		
QCQ	1523, A			1503 (60), A/B		

Figure 3.3 summarizes calculated Vs_{30} from both inversion methods and by extension or extrapolation, if applied. Eleven of the 16 stations (69%) correspond to site class A whereas, the remaining 5 stations fall under site class B based on the optimal Vs_{30}. The mean PSWP Vs_{30} at 12 out of 16 stations (75%) corresponds to class A but the standard deviation indicates that some stations span across to class B. It is interesting to note that when we have not measured or estimated station-appropriate Vs to 30 m depth, and need to either extend or extrapolate the base Vs to 30 m, there is consistency in the determined site class. The exception is for stations BATG and BCLQ where the Vs_{30} estimates are close to the A-B class boundary.

For the 16 Eastern Canada seismograph stations in Table 3.5 and Figure 3.3, we recommend that the end-user report or use the optimal Vs_{30} value for the station. Vs_{30} should always be rounded to the nearest 5 m/s. If applicable, it is recommended to report or use the extended Vs_{30} value

rather than the extrapolated Vs30 value as it is more conservative. In addition, the end-user shall report or use the determined standard deviation in Vs30 for the station with the optimal Vs30. If applicable, the larger standard deviation from either extending or extrapolating the Vs profiles shall be used.
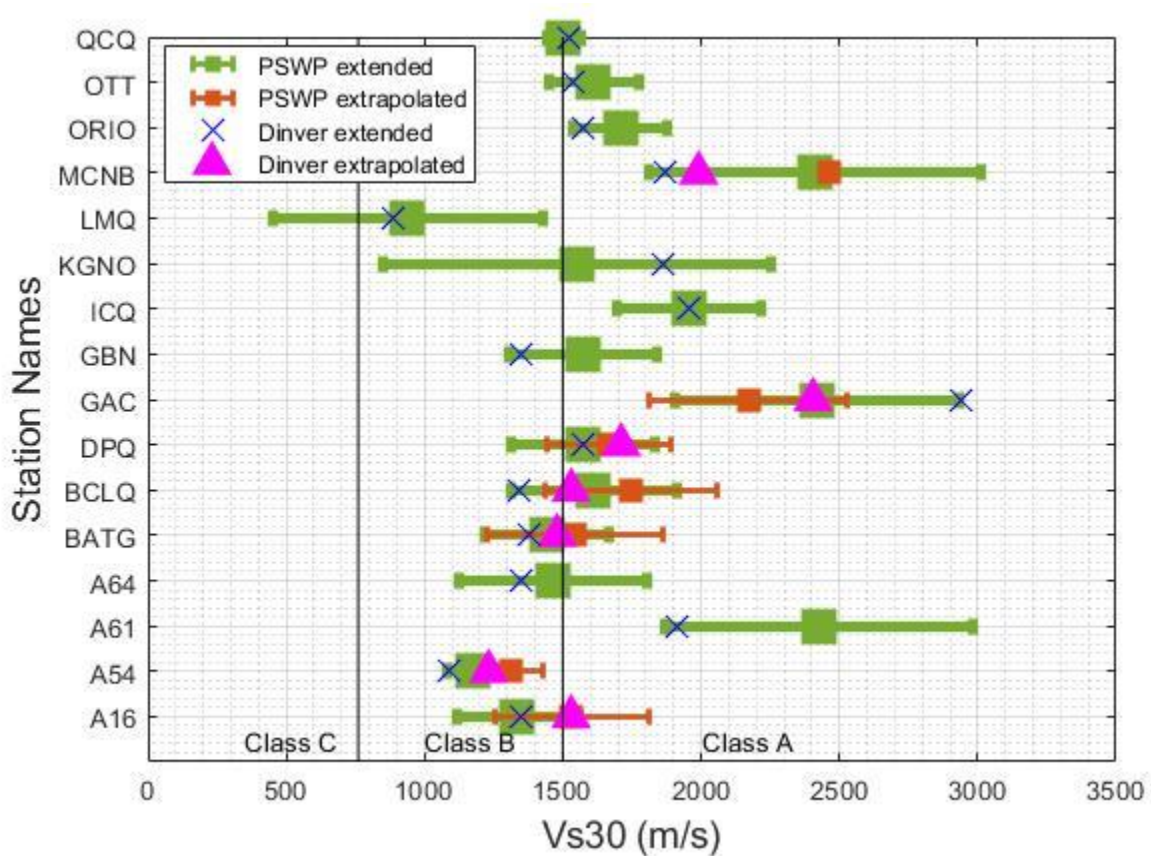

Figure 3.3: Station appropriate Vs30 estimates.

3.4 Alternative site period site classification from amplification functions

Chapter 2 compared the station MHVSRs and EHVSRs and generally portrayed that both methodologies agree with each other and the EHVSRs at some stations being higher in amplitude than MHVSRs. A site-period-based site classification scheme could assist in identifying potential sturdy rock (i.e., no amplification or site period) from softer rock (e.g., broadband amplification) as well as potential site effects (e.g., short site period due to thin soils present). An alternative site period classification scheme is applied here for all stations, but is particularly useful where Vs profiles and calculated Vs30 could not be determined because array measurements were not

performed (no applicable testing location). This situation is typical of stations on outcropping rock.

The site period classification scheme (Table 1.2) of Di Alessandro et al. (2012) is applied to visited CNSN stations. Class (CL)-I indicates a site period greater than 0.2 s. Classes higher than IV are not based on a distinct site period. CL-V indicates a flat amplification response and CL-VI indicates broadband amplification. CL-VII describes multiple peaks occurring over the frequency bandwidth. Site period is determined from both MHVSRs and EHVSRs and the corresponding site classification is reported in Table 3.6. Stations where microtremor measurements were performed on soil and other terrain are not accurate of the stations conditions. A correction is applied to stations where it is observed that the site response is not indicative of rock due to the measurement not being able to be performed on that interface. For example, station ORIO is placed on outcropping rock in a field, the measurement was done near the station but on soil where a high frequency peak is shown which is related to the thin soil layer; that peak is ignored when determining the classification as it is not indicative of the station conditions.

Site period classifications are similar using either the MHVSR or EHVSR. 8 out of 23 stations were classified as CL-V or no amplification (flat), as expected for rock sites. The flat or CL-V stations re-affirm that the stations are located on a sturdy rock surface. 5 out of 23 stations exhibit broadband amplification (CL-VI) indicative of fractured rock at the surface with the shortening of shear wavelengths. 8 out of the 25 stations had no access or results not indicative of the geology at the station and need to be revisited in order to get an accurate site response measurement. Stations A61 and DAQ exhibited high amplification across majority of its frequency bandwidth (CL-VII) in their MHVSR and A61's EHVSR that can be indicative of softer or weathered rock in the amplified response. Station GBN had its measurement performed on rock yet a high frequency ~ 50 Hz peak (CL-I) was present which can be indicative of weathered rock at the surface. Some stations located on hills (e.g. A11 and A21) had clear wind effects during the microtremor measurement and site period cannot be determined. High frequency noise at ~ 10 and 20 Hz was observed at station OTT in both microtremor and earthquake recordings and should be looked at further to mitigate this noise affecting the seismograph recordings. Site period also could not be determined for QCQ, LMQ, and MOQ due

to potential noise exciting the vertical component of the instrument. It should be looked at further at those stations if the noise was only during the visit or is prolonging.

Table 3.6: Site-period-based site classification using MHVSR and EHVSRs. Grey shading indicates that a correction was applied due to being on a surface not representative of what the station is placed on.

Station	MHVSR Classification	MHVSR Appropriate Classification	EHVSR Classification
A11	N/A – Wind effects	N/A – Wind effects	CL-V
A16	CL-V	CL-V	CL-V
A21	N/A – Wind effects	N/A – Wind effects	CL-V
A54	CL-V	CL-V	CL-V
A61	CL-VII	CL-VII	CL-VII
A64	CL-V	CL-V	CL-I
BATG	CL-VII	CL-VI	Not provided
BCLQ	CL-VII	CL-VII	Not provided
CNQ	CL-VI	CL-VI	Not provided
DAQ	CL-VII	CL-VII	Not provided
DPQ	CL-V	CL-V	Not provided
GAC	CL-I	CL-V	Not provided
GBN	CL-I	CL-I	Not provided
GSQ	CL-V	CL-V	Not provided
ICQ	CL-VI	CL-VI	Not provided
KGNO	N/A – no access	N/A – no access	Not provided
LMQ	N/A – noise at the station	N/A – noise at the station	CL-I
MCNB	N/A – no access	N/A – no access	Not provided
MOQ	N/A – noise at the station	N/A – noise at the station	Not provided
NATG	CL-VI	CL-VI	CL-V
ORIO	CL-I	CL-V	Not provided
OTT	N/A - noise at the station	N/A - noise at the station	N/A - noise at the station
QCQ	N/A - noise at the station	N/A - noise at the station	Not provided
SMQ	CL-VI	CL-VI	Not provided
VABQ	CL-V	CL-V	CL-VI

3.5 Multi-method site characterization of Eastern Canada seismograph stations

Maps of the MHVSR response, rock Vp, and Vs_{30} are generated (Figures 3.4 to 3.6, respectively) to examine trends among stations regionally. Figure 3.4 summarizes the station site period classifications. Stations along the upper St. Lawrence exhibit a common trend in broadband amplified response. The Ottawa area exhibits consistent flat MHVSRs. For the Charlevoix region, all stations have a flat response, except station A61. Figure 3.5 displays the average (forward and reverse surveying) rock Vp measured at each station where refraction was able to

be performed. At north-east-most stations (BATG, GSQ, and NATG), rock Vp is < 2000 m/s. The Ottawa and Charlevoix regions ("central" Eastern Canada) exhibits moderate rock Vp values (> 2300 m/s) except for station LMQ where lower Vp is identified. There also appears to be a trend in the highest rock Vp values at the southern-most stations (KGNO, MCNB, GBN) which are not geographically close to each other. Figure 3.6 shows the station appropriate Vs_{30} of the lowest misfit model (columns 1 and 3 of Table 3.5). Similar Vs_{30} values are observed in the Ottawa area (Vs_{30} 1500-1700 m/s). The Charlevoix region shows a variety of Vs_{30} values in a small area, Vs was directly measured from dispersion estimates at only A61.
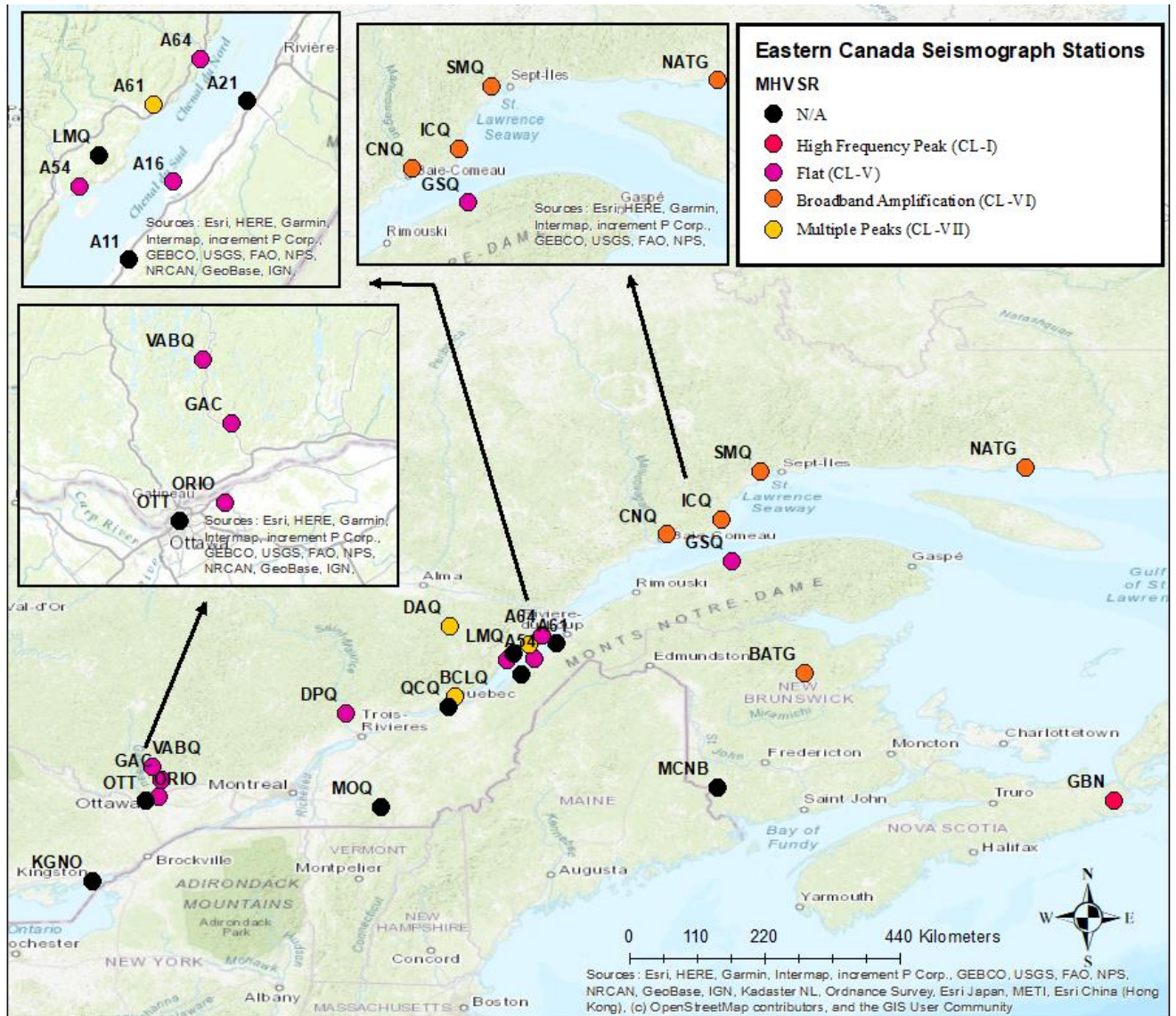

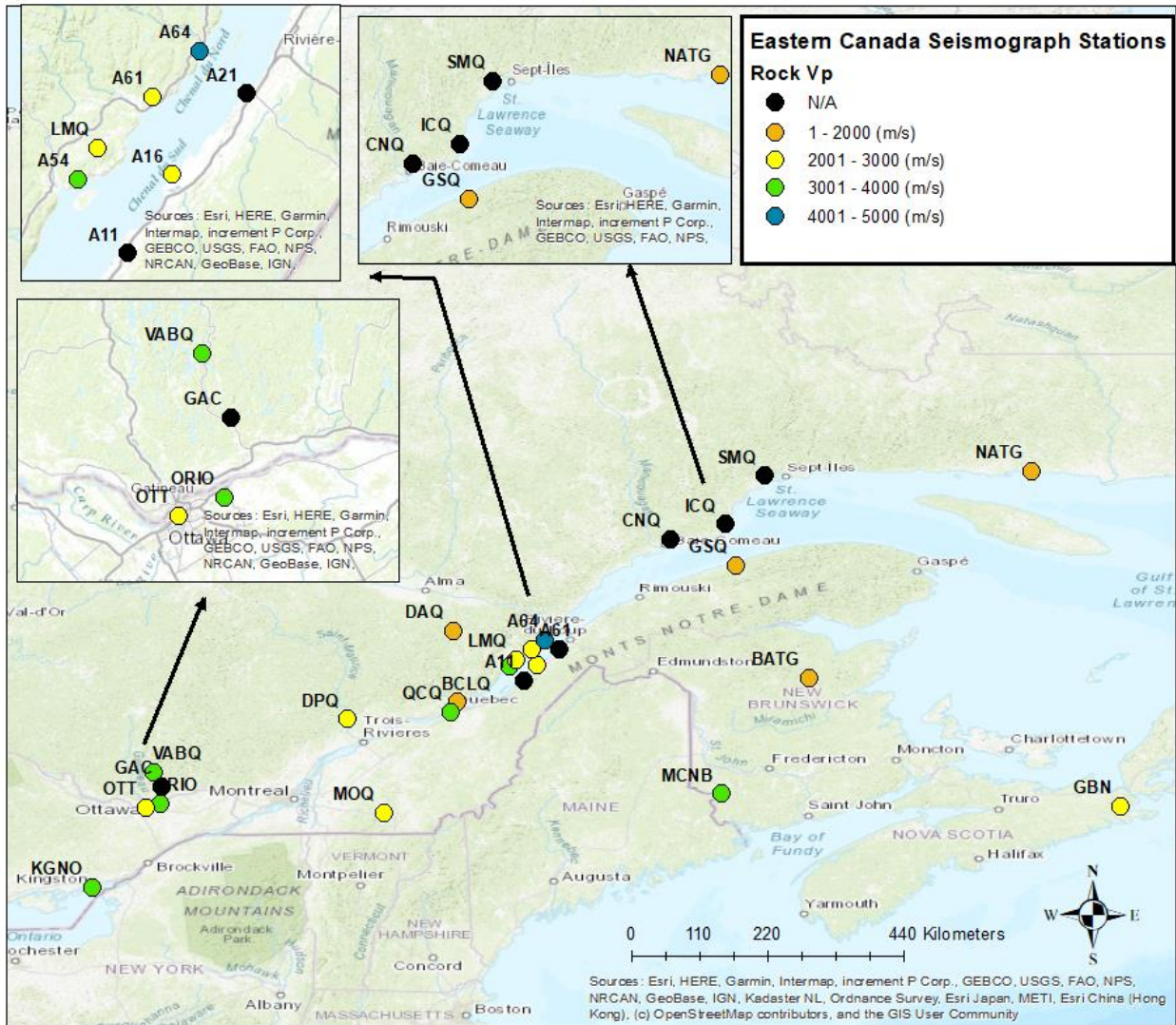**Figure 3.4: MHVSR site period classification map of Eastern Canada stations.**

86

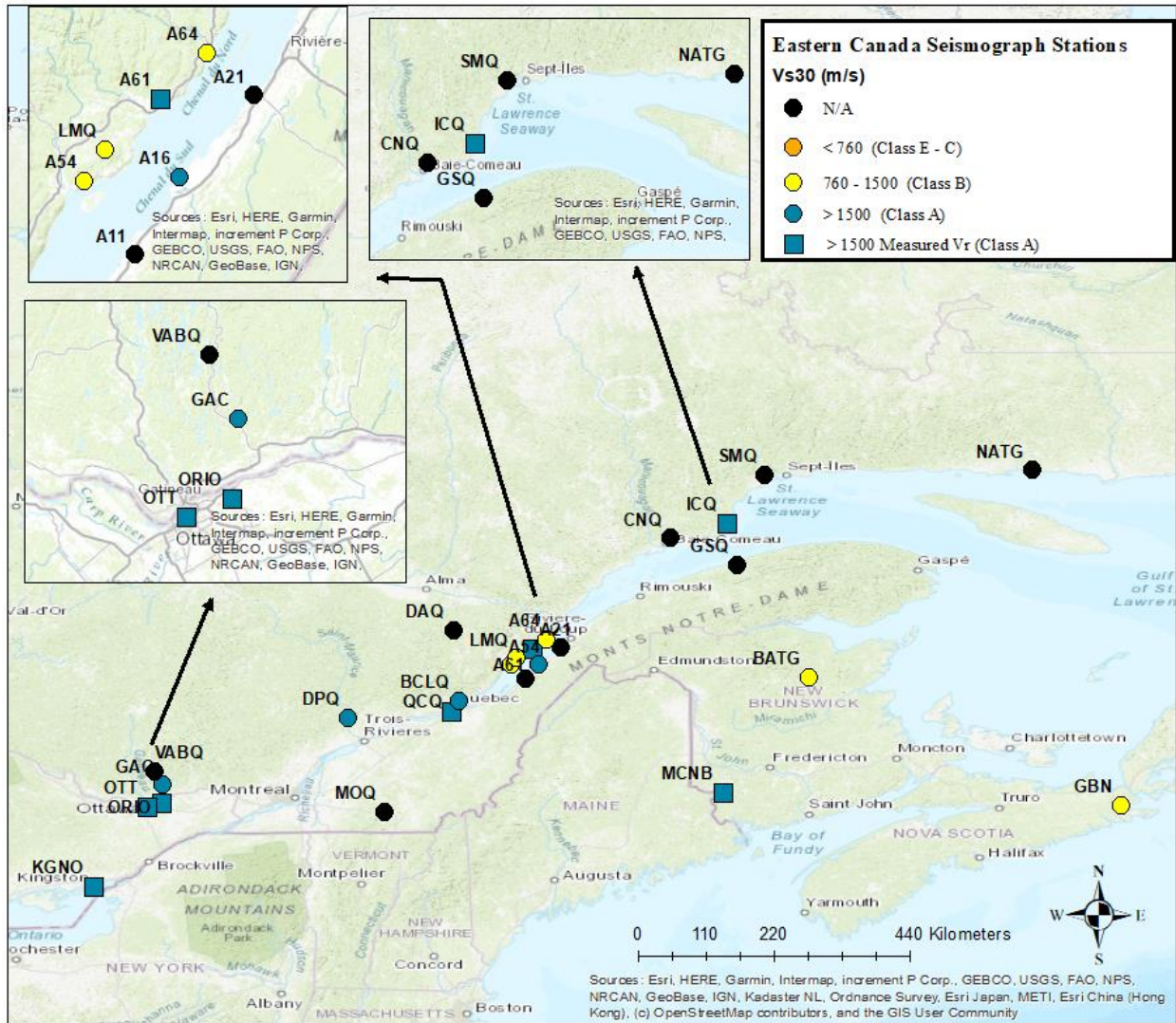**Figure 3.5: Rock Vp map of Eastern Canada seismograph stations.**

Figure 3.6: Vs₃₀ map of Eastern Canada seismograph stations.

A multi-method (MM) site characterization metric is introduced in this section to utilize all performed methods in earthquake site characterization of the stations. The MM site metric is calculated by combining (summing) results from all methods performed at each station. The components of the metric are exemplified in Table 3.7 where each method's outcomes are assigned a value between 0 and 1 corresponding to harder and softer rock conditions, respectively. Hence the lower the summed MM site metric, the harder the rock conditions indicated from the multi-method testing. The maximum value of the MM site metric is 4.5. More emphasis is placed on parameters controlling the Vs beneath the station in having two parameters: Vs₃₀ and rock Vs. All assigned values of the MM outcomes representative of the station are summed together to calculate the MM site characterization metric. The MM site

88

characterization metric for the visited stations in Eastern Canada is reported in Table 3.8. Some stations have less information than others; the metric is normalized to be used at a comparison level where stations with limited information (e.g. A11) can be compared with stations with more information (e.g. LMQ). Through normalization, a metric value below 0.5 is indicative of sturdy or hard rock conditions whereas values above 0.5 relate to softer rock conditions. Figure 3.7 displays the normalized MM site metric calculated for each station. A total of 17 stations (68%) portray harder rock site conditions with a MM site metric less than 0.5. Five stations portray softer rock conditions with a MM site metric above 0.5. Three stations are indeterminate or correspond to intermediate rock conditions with a MM metric close to 0.5. Figure 3.8 shows a map of the MM site metric applied to stations to determine if there is a spatial trend in softer and harder rock regionally. The upper St. Lawrence has two stations with a MM site metric less than 0.5. Station LMQ in Charlevoix, GBN in New Brunswick, and MOQ near Montreal all have a MM site metric less than 0.5. The MM site metric conveys that these five stations deviate the most from the assumed default assumption of hard rock conditions.

Table 3.7: Values between zero and one (in brackets) assigned to each method's site characterization outcome which are summed to calculate the MM site characterization metric.

Vs_{30} site class (value)	Site period class (value)	Rock Vs (m/s) (value)	Rock Vp (m/s) (value)	Rock age (value)
Class A (0)	CL-V flat (0)	> 2000 (0)	> 3000 (0)	Precambrian (0)
Class A/B (0.2)	CL-VII multiple peaks (0.25)	1500-2000 (0.25)	2000-3000 (0.5)	Paleozoic (0.5)
Class B/A (0.4)	CL-VI broadband (0.75)	1000-1500 (0.75)	< 2000 (1)	
Class B (0.6)	CL-I high frequency peak (1)	< 1000 (1)		
Class B/C or C/B (0.8)				
Class C (1)				

Table 3.8: MM site characterization metric for each Eastern Canada station.

Station	MM site metric	# methods	MM site metric normalized
A11	0.50	3	0.33
A16	1.95	5	0.43
A21	0.50	5	0.33
A54	1.85	4	0.41
A61	0.50	2	0.11
A64	1.65	5	0.37
BATG	2.20	4	0.49
BCLQ	1.95	5	0.43
CNQ	0.75	2	0.50
DAQ	1.00	2	0.40
DPQ	1.20	5	0.27
GAC	0.00	3	0.00
GBN	2.45	5	0.54
GSQ	1.00	3	0.50
ICQ	1.00	2	0.29
KGNO	0.95	5	0.27
LMQ	3.05	2	0.68
MCNB	0.50	5	0.14
MOQ	1.00	4	0.67
NATG	1.38	4	0.55
ORIO	0.95	5	0.21
OTT	1.45	4	0.41
QCQ	1.20	4	0.34
SMQ	1.25	3	0.83
VABQ	0.38	5	0.09
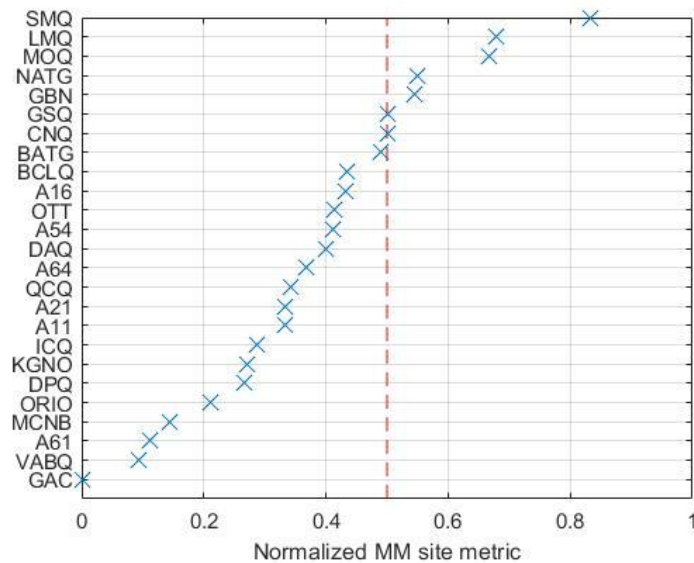
Figure 3.7: Normalized MM site metric for Eastern Canada stations. Red dashed line indicates transition between harder (left) and softer rock (right) conditions stations.
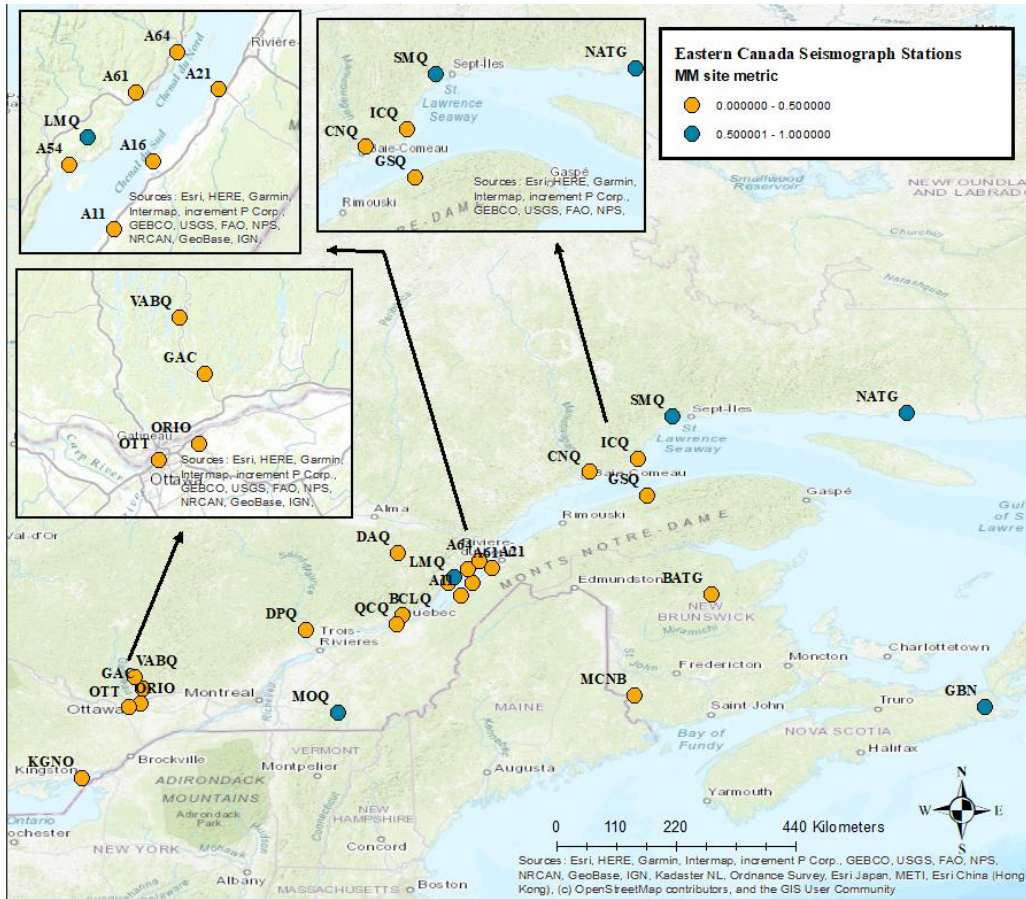
Figure 3.8: Map of normalized MM site metric applied to Eastern Canada seismograph stations.

3.5.1 Ottawa-Kingston region

The Ottawa and Kingston, Ontario area contains a cluster of seismic stations to monitor seismic activity in the area. Table 3.9 summarizes the rock velocities and site amplification obtained for these stations. In general, velocities are measured at stations on Paleozoic rocks compared to stations on Precambrian rocks. In contrast, interpretable site amplification (MHVSR or EHVSR) is accomplished at stations on Precambrian rocks compared to stations on Paleozoic rock. Our methods were most successful in this area in acquiring reliable rock Vs by measuring the "top" of the dispersion curve. Reliable rock velocity estimates corresponding to site class A are determined at stations KGNO, ORIO, and OTT on Paleozoic rocks in Kingston and Ottawa similar to previous studies (e.g. Beresnev and Atkinson, 1997). The average Vs_{30} (with one standard deviation) found for these three stations using the Dinver lowest misfit models is 1656 (177) m/s. At station VABQ, only low Vs sediments were measured using surface wave methods (no station appropriate Vs_{30}) whereas refraction Vp of rock was measured. The average rock Vp (with one standard deviation) of Precambrian rock is 3085 (444) m/s. The average rock Vp and

91

Vs (with one standard deviation) of Paleozoic rock is 3312 (525) m/s and 1617 (246) m/s. The average rock Vp of these two rock age categories overlaps within their standard deviations, hence there is no significant difference in the measured rock velocities by rock age. Overall Vs_{30} based site class is not well constrained but is consistently class A at stations in the Kingston and Ottawa region. At station OTT, evident high frequency noise (~10 and 25 Hz) likely caused by the station installed in a building was observed in both MHVSR and EHVSR measurements, and operators should be aware of this effect.

High Rayleigh phase velocities (> 1000 m/s) are determined for station GAC and combined with a flat MHVSR indicates rock site conditions. Having the lowest MM site metric (0) is strong evidence that GAC is placed on hard rock. Station VABQ also did not have rock Vs information but it had rock Vp measurements and both had a calculated MHVSR and EHVSR. Its EHVSR that have low frequency peaks (0.55 and 2.5 Hz) from multiple earthquakes indicating potential site effects present at the station but a flat MHVSR. Through its MM site metric being low (close to 0) from Vp and site period classes station VABQ is placed on hard rock. Stations KGNO and OTT do not have MHVSR or EHVSR data but have high rock Vs (and Vp) and class A Vs_{30} site class that indicates hard rock site conditions with a MM site metric less than 0.5. Station ORIO has rock Vs and Vp and site period information indicating sturdy rock conditions. The MM site metric for station ORIO is low indicating sturdy rock conditions.

Table 3.9: Summarized site characterization for stations in the Ottawa and Kingston area. Grey shading indicates dispersion estimates did provide rock velocity measurements.

Station	MHVSR	EHVSR	Rock Vs (m/s)	Vs_{30} (m/s) (Site Class)	Rock Vp (m/s)	Rock type	MM site metric norm.
GAC	CL-V	No Data	1080 ± 310 overlaying 2780 ± 685	2170 ± 355, A	No data	Precambrian	0
KGNO	No data	No Data	1553 ± 700	1553 ± 990 (A/B)	3386 ± 930	Paleozoic	0.27
ORIO	CL- V	No Data	1708 ± 170	1708 ± 240 (A/B)	3750 ± 900	Paleozoic	0.21
OTT	N/A - noise	No Data	1612 ± 165	1612 ± 233 (A/B)	2800 ± 900	Paleozoic	0.41
VABQ	CL-V	CL-VI	No Data	No Data	3085 ± 444	Precambrian	0.09

3.5.2 Montreal - Quebec City region

Eastwards towards Montreal and Quebec City, 5 stations were visited to acquire a proper site classification (Table 3.10). The average rock Vs_{30} using the Dinver lowest misfit models is 1588 $\pm$ 107 m/s in the region. All stations where dispersion curves were built and inverted provides a calculated Vs_{30} corresponding to site class A. Rock Vs was not measured directly by dispersion estimates in this region with the exception of Station QCQ at Laval University. The average rock Vp (with one standard deviation) of Precambrian rock is 2277 (363) m/s. The average rock Vp and Vs (with one standard deviation) of Paleozoic rock is 2936 (293) m/s and 1557 (305) m/s, respectively.

No rock Vs data was acquired at station DAQ but its low rock Vp and moderate (~4) broadband amplification indicate site effects present. Its moderate MM site metric (0.4) indicates intermediate rock conditions compared to mapped Precambrian rock. Similarly, at station MOQ, rock Vs was not acquired but intermediate rock Vp was acquired. A higher MM site metric (0.67) indicates this station is on softer rock from its rock Vp and Paleozoic rock age. Station BCLQ had low (~2) broadband amplification at multiple frequencies for its MHVSR. Its Vs_{30} occurs between site classes A and B. Hence its moderate MM site metric indicates intermediate rock conditions underneath the station. Stations DPQ and QCQ have similar stiff rock Vp and Vs but differ in their mapped rock age. Station DPQ has a flat MHVSR which reaffirms the placement of the station on rock. Both DPQ and QCQ have lower MM site metrics indicating harder rock site conditions.

Table 3.10: Multi-method site characterization for stations in the Montreal and Quebec City area. Grey shading indicates dispersion estimates did provide rock velocity measurements.

Station	MHVSR	EHVSR	Rock Vs (m/s)	Vs_{30} (m/s) (Site Class)	Rock Vp (m/s)	Rock type	MM site metric norm.
BCLQ	CL-VII	No Data	1612 $\pm$ 300	1747 $\pm$ 309 (A/B)	2800 $\pm$ 850	Paleozoic	0.43
DAQ	CL-VII	No Data	No Data	No Data	1945 $\pm$ 315	Precambrian	0.4
DPQ	CL-V	No Data	1574 $\pm$ 260	1670 $\pm$ 224 (A/B)	2610 $\pm$ 655	Precambrian	0.27
MOQ	N/A - noise	No Data	No Data	No Data	2509 $\pm$ 175	Paleozoic	0.67
QCQ	N/A - noise	No Data	1503 $\pm$ 60	1503 $\pm$ 85 (A/B)	3500 $\pm$ 142	Paleozoic	0.34

3.5.3 Charlevoix region

Northeast of Montreal and Quebec City is the Charlevoix region of Quebec, the most seismically active region in Eastern Canada. 7 stations are monitoring the seismicity in the region on both west and east sides of the St. Lawrence River. Table 3.11 summarizes the rock velocities and site amplification obtained for these stations. The average rock Vs_{30} from the optimal Dinver model is 1347 m/s and varies between site class A and B amongst the stations (370 m/s standard deviation). Stations on Paleozoic rocks tend to have lower Vs_{30} values than station A61 on Precambrian rock. The average rock Vs is higher for stations on Precambrian rock (2564 m/s) compared to Paleozoic rock (1408 m/s). A factor affecting the average rock Vs is the differing geology west and east of the St. Lawrence River. East of the St. Lawrence River typically has sedimentary rock compared to the west which typically contains metamorphic or igneous rock. The average Paleozoic rock Vp (with one standard deviation) also varies greatly in the region similar to Paleozoic rock Vs with an average of 3078 (500) m/s. With the exception of stations A61 and LMQ, MHVSRs and EHVSRs in Charlevoix are generally flat in the region portraying that the stations are placed on harder rock.

Stations A11 and A21 are both located on high topography outcropping rock where *in situ* array measurements could not be performed. The only information available from these stations is the EHVSR which is flat for both stations, confirming harder rock conditions. Station A16 is placed on stiff rock determined by site period and its rock Vs leading to its low MM site metric, although relatively low rock Vp from refraction demonstrates variability in measured rock velocities. Station A61 has moderate (> 2) amplification seen in its MHVSR and EHVSR across multiple frequencies but with a high measured rock Vs and Vp determines a low MM site metric to indicate harder rock conditions. Station A54 exhibits no (flat) site amplification and a high rock Vp, but with an intermediate rock Vs and Vs_{30} a moderate MM site metric is determined. Station A64 also has an intermediate MM site metric due to variability in site amplification and rock velocities. The station on softest rock conditions is station LMQ with a MM site metric of 0.68. Short period site amplification combined with lower rock velocities on Paleozoic rocks leads to this high MM site metric.

Table 3.11: Multi-method site characterization of stations located in Charlevoix, Quebec. Grey shading indicates dispersion estimates did provide rock velocity measurements.

Station	MHVSR	EHVSR	Rock Vs (m/s)	Vs$_{30}$ (m/s) (Site Class)	Rock Vp (m/s)	Rock type	MM site metric norm.
A11	N/A - noise	CL-V	No Data	No Data	No data	Paleozoic	0.33
A16	CL-V	CL-V	1336 ± 220	1532 ± 280 (A/B)	2486 ± 112	Paleozoic	0.43
A21	N/A - noise	CL-V	No Data	No Data	No data	Paleozoic	0.33
A54	CL-V	CL-V	850 ± 38 overlaying 1357 ± 95	1316 ± 115 (B)	3161 ± 135	Paleozoic	0.41
A61	CL-VII	CL-VII	2424 ± 557	2424 ± 363 (A)	2500 ± 215	Precambrian	0.11
A64	CL-V	CL-I	1020 ± 104 overlaying 2553 ± 686	1464 ± 340 (B/A)	4467 ± 401	Paleozoic	0.37
LMQ	N/A	CL-I	889 ± 174 overlaying 2717 ± 434	940 ± 174 (B)	2200 ± 240	Paleozoic	0.68

3.5.4 Upper St. Lawrence region

North of Charlevoix are 5 seismograph stations of the Upper St. Lawrence and their rock velocities and site amplification are summarized in Table 3.12. Similar to Charlevoix, our methods were not very successful in this area. Only surficial Vs was measured at stations CNQ, GSQ, NATG, and SMQ with no measured velocities of underlying rock. Broadband site amplification is observed at all stations except GSQ, indicative of weathered or softer rock conditions consistent with lower measured rock Vp. The Paleozoic and Precambrian rock Vp average (with one standard deviation) in the region is 1466 (466) m/s and 1700 (275) m/s, respectively. The average rock Vp does not differ significantly from Paleozoic to Precambrian rock but is found to be lower in this region than others. Overall most stations correspond to a high MM site metric (0.5 or greater) due to broadband site amplification occurring at majority of the stations and low rock Vp. Site characterization at station ICQ is the most constrained with high rock Vs and Vs$_{30}$ confidently measured. The low MM site metric indicates the station is

placed on harder rock but still broadband amplification at the station suggests potential weathered rock.

Table 3.12: Multi-method site classification of stations located in the Upper St. Lawrence River in Quebec. Grey shading indicates dispersion estimates did provide rock velocity measurements.

Station	MHVSR	EHVSR	Rock Vs (m/s)	Vs_{30} (m/s) (Site Class)	Rock Vp (m/s)	Rock type	MM site metric norm.
CNQ	CL-VI	No Data	No Data	No Data	No Data	Precambrian	0.5
GSQ	CL-V	No Data	No Data	No Data	1466 ± 466	Paleozoic	0.5
ICQ	CL-VI	No Data	1959 ± 260	1959 ± 368 (A)	No data	Precambrian	0.29
NATG	CL-VI	CL-V	No Data	No Data	1700 ± 275	Precambrian	0.55
SMQ	No Data	No Data	No Data	No Data	No data	Precambrian	0.83

3.5.5 New Brunswick - Nova Scotia region

The most eastern stations visited are located in New Brunswick and Nova Scotia. These three stations (Table 3.13) are a considerable distance apart monitoring seismicity for the national network. All stations have a $Vs_{30} > 1500$ m/s (class A) and are mapped on Paleozoic rock. The average Vs_{30} of the region using the Dinver optimal model (with one standard deviation) is 1611 (333) m/s. The average rock Vp and Vs (with one standard deviation) of Paleozoic rock is 3165 (235) m/s and 1695 (218) m/s. Consistent Paleozoic Vs and Vp rock velocities were measured with little variance.

Station BATG's MM site metric is moderate from the combination of a relatively low mean rock Vs and broadband amplification compared to high rock Vp and Vs_{30} site class A. Station GBN is very similar with high frequency amplification observed in its MHVSR. Station MCNB had direct rock velocity measurements with high rock Vs, Vs_{30}, and Vp which consistently indicate harder rock conditions with a low MM site metric.

Table 3.13: Multi-method site classification of stations located in the New Brunswick and Nova Scotia. Grey shading indicates dispersion estimates did provide rock velocity measurements.

Station	MHVSR	EHVSR	Rock Vs (m/s)	Vs_{30} (m/s) (Site Class)	Rock Vp (m/s)	Rock type	MM site metric norm.
BATG	CL-VI	No Data	1441 ± 227	1543 ± 317 (A/B)	3510 ± 345	Paleozoic	0.49
GBN	CL-I	No Data	1237 ± 133 overlaying 1976 ± 265	1587 ± 221 (A/B)	2836 ± 481	Paleozoic	0.54
MCNB	No data	No Data	2409 ± 600	2461 ± 720 (A)	3151 ± 387	Paleozoic	0.14

3.6 Discussion and Conclusions

This Chapter focused on performing earthquake site classification (Vs_{30}, site period, site amplification) of Eastern Canada seismograph stations. Based on Vs profiles and calculated Vs_{30}, 16 of 23 stations (70%) were classified, 7 stations (30%) were classified confidently by measuring rock velocity directly from dispersion estimates and 9 stations (40%) classified less confidently where only the transition to rock (dispersion curve) was measured. Nine stations out of 25 (36%) were unable to be classified with Vs_{30} but other site information was acquired such as rock Vp and/or an estimate of the site amplification from spectral ratios. Figure 3.9 shows the calculated upper and lower range in Vs_{30} values from inverted PSWP Vs profiles. For comparison, the USGS Vs_{30} values from topographic slope (USGS, 2019 https://earthquake.usgs.gov/data/Vs30/) are also shown for each station. These topographic slope Vs_{30} values are essentially proxy measures of Vs_{30} and can be regarded as *a priori* Vs_{30} estimates, prior to our *in situ* Vs_{30} estimation. The difference between our *in situ* Vs_{30} values and the proxy-based Vs_{30} values is significant. Overall the Vs_{30} values based on topographic slope are too low and capped at 900 m/s. The USGS maximum 900 m/s Vs_{30} also does not correspond to our highest *in situ* Vs_{30} estimates (no correlation). The USGS global mapping of Vs_{30} based on topographic slope is therefore inappropriate for rock classification in Eastern North America. It is best advised for *in situ* velocity and site amplification measurements to be performed for station classification at rock sites than using proxy-based remote-sensing type methods.
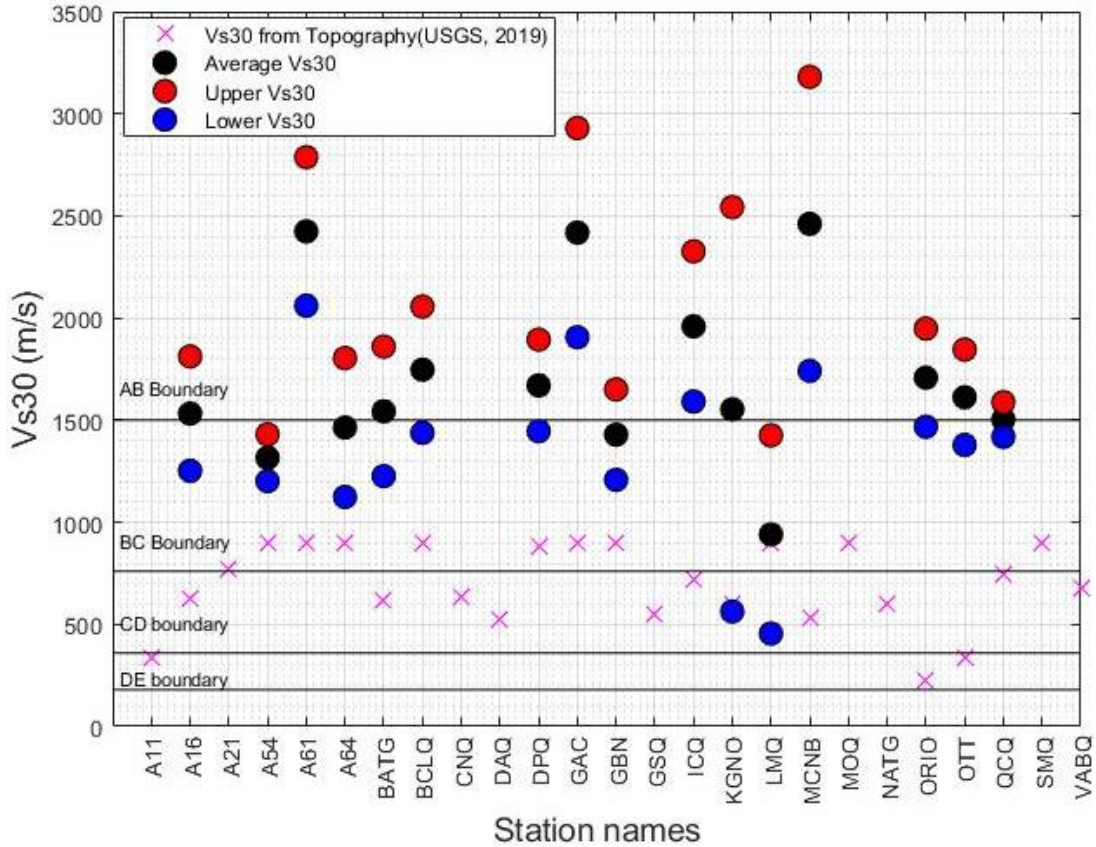
Figure 3.9: Summary of Vs$_{30}$ site classification showing average and standard deviation. Proxy Vs$_{30}$ values based on topographic slope are shown for comparison.

Figure 3.10 summarizes Vs$_{30}$ site classes observed for the two ages of rock at each station determined from the bedrock map of Canada. Precambrian rocks are typically highly metamorphosed igneous and metamorphic rocks of the Canadian shield and most likely to have been heavily deformed (very stiff). In comparison, Paleozoic rocks are typically sedimentary with low-to-moderate metamorphism, and we interpret to be less heavily deformed (more variable range in stiffness but lower stiffness than Precambrian rocks). Stations placed on Precambrian rocks typically have a Vs$_{30}$ > 1500 m/s indicating site class A conditions, as assumed. Stations on Precambrian rock may correspond to site class B, but on the 'high end' of class B, i.e., class A/B. Stations on Paleozoic rocks can correspond to class A or class B, but dominantly have Vs$_{30}$ at the class A-B boundary of 1500 m/s (class A/B or B/A). Figure 3.10 shows there is much more variability in the rock velocity of Paleozoic rocks, as expected. There is greater variation in Paleozoic rock types and their velocity which may be more easily weathered than Precambrian rock.
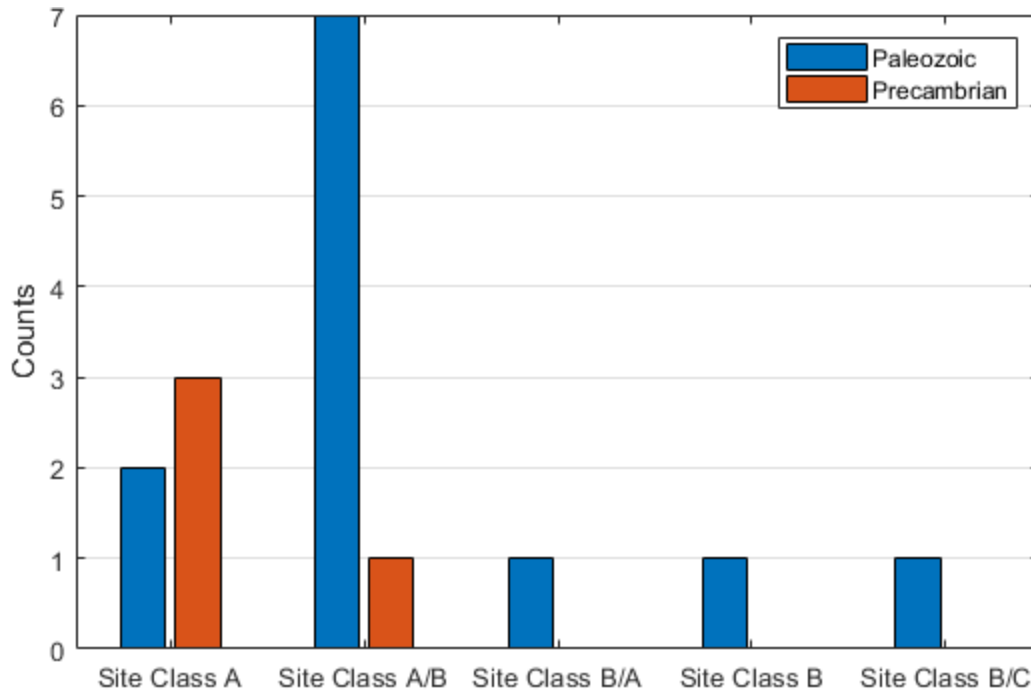
Figure 3.10: Summary of Vs$_{30}$ site class by rock age.

Figure 3.11 shows site-period-based site classifications compared to Vs$_{30}$. There is no clear trend or correlation between site period and Vs$_{30}$ site classifications. We would expect CL-I (peak amplification at short period) and CL-VI (broadband amplification) to correspond to lower Vs$_{30}$; this is true of the one CL-I station. In contrast, we would expect CL-V (no amplification, flat) and CL-VII (multi-peak) to correspond to more "rocky" conditions and higher Vs$_{30}$. Many stations where reliable velocity measurements were made had external noise during their microtremor recording (N/A category) and the two site classifications cannot be compared directly. Peak frequency was also compared with Vs$_{30}$, but no trend was identified. Hassani and Atkinson (2016) demonstrated increasing f$_{peak}$ correspond to higher velocities at Eastern North American stations.
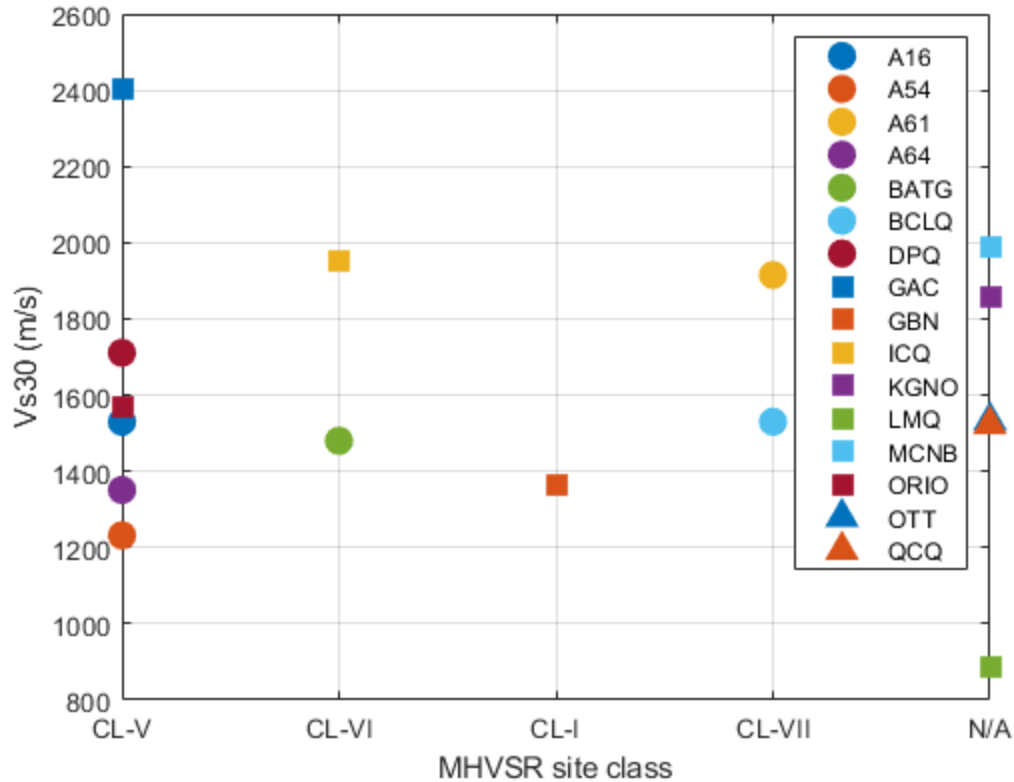
Figure 3.11: Site period site classes from MHVSRs compared to Vs$_{30}$.

A multi-method non-invasive seismic methodology was applied to acquire rock velocity and site amplification measurements to provide site characterization of Eastern Canada seismograph stations. Other authors previously found success in using Vs refraction to directly obtain rock Vs estimates and generating Love wave dispersion curves from MAS$_L$W to include in the inversion with Rayleigh wave dispersion estimates (e.g. Hollender et al., 2018; Poggi et al., 2017). Generating both Love and Rayleigh wave dispersion curves and including higher modes to be jointly inverted constrains the inversion procedure and reduces the non-uniqueness of surface wave inversions. Due to not having a shear-wave source and horizontal component geophones, those methods could not be performed but they have had abundant success in Vs based site classification at rock sites with the other methods we have presented (e.g. Martin et al., 2017). Using a multi-method approach was also applied in Catchings et al. (2019) in using MAS$_L$W, MAS$_R$W, Love and Rayleigh wave AVA, and Vs and Vp refraction. The use of different seismic sources has also been successful (e.g. Catchings et al., 2019). Varying energy sources and angling of source energy are known to improve dispersion estimates. A higher sampling rate is also encouraged to capture higher modes for inversion as well as for sites with a very thin layer

of sediment over rock; Catchings et al. (2019) found a 250 Hz sampling rate to be too sparse. For example, a 1024 Hz sampling rate was used with fewer Tromino sensors (smaller array) at station GAC, resulting in dispersion estimates being observed and made at higher frequencies.

It is recommended to revisit the stations to perform refraction Vs and MAS$_L$W measurements to acquire the rock Vs and further constrain Vs$_{30}$. Varying the source's energy is also encouraged to access different frequency bandwidths with a multi-method approach. Table 3.14 lists the stations and the recommended measurements to be (re)performed at each station. MHVSRs should reperformed at stations where noise was detected previously. Vs measurements need to be performed at most stations with refraction Vs and/or MAS$_L$W or at a different location to measure the rock velocity successfully. Vp measurements also need to be (re)performed at stations where measurements were not successful or could not be performed.

Table 3.14: Summary of previous testing and recommended future testing at Eastern Canada stations. Gray shading indicates the measurement does not need to be performed and white indicates an initial or more accurate measurement needs to be performed.

Station	MHVSR	Vs Measurement	Vp Measurement
A11			
A16			Gray
A21			
A54	Gray		Gray
A61	Gray		
A64	Gray		Gray
BATG	Gray		Gray
BCLQ	Gray		
CNQ	Gray		
DAQ			Gray
DPQ			Gray
GAC	Gray		
GBN	Gray		
GSQ	Gray		
ICQ	Gray	Gray	
KGNO		Gray	Gray
LMQ			Gray
MCNB		Gray	
MOQ			Gray
NATG	Gray		Gray
ORIO	Gray	Gray	Gray
OTT		Gray	Gray
QCQ		Gray	Gray
SMQ	Gray		
VABQ	Gray		Gray

The NGA East project (Goulet et al., 2018) highlighted that only 84 of 1,379 (6%) seismograph stations in Central and Eastern North America have a directly measured Vs_{30}. Many stations have an 'assigned' Vs_{30} of 2000 m/s. Our study highlights the importance and difficulty of *in situ* Vs measurements at rock sites to acquire a constrained Vs_{30} value and associated site classification. An increased and concerted effort is required to properly characterize rock sites in Eastern Canada and confirm the general assumption that they are of "hard rock" site class A. We demonstrate that the majority of our stations correspond to site class A but some stations also have a probability of site class B (A/B or B/A). We conclude the default "hard" rock class A assumption is biased slightly too high. The use of a multi-method approach is encouraged to acquire proper site characterization of rock sites.

3.7 References

Ahdi, S. K., Stewart, J. P., Ancheta, T. D., Kwak, D. Y., & Mitra, D. (2017). Development of Vs Profile Database and Proxy-Based Models for Vs_{30} Prediction in the Pacific Northwest Region of North America. *Bulletin of the Seismological Society of America*, *107*(4), 1781-1801.

Boore, D. M. (2004). Estimating Vs_{30}(or NEHRP site classes) from shallow velocity models (depths< 30 m). *Bulletin of the seismological society of America*, *94*(2), 591-597.

Boore, D. M., Thompson, E. M., & Cadet, H. (2011). Regional correlations of Vs_{30} and velocities averaged over depths less than and greater than 30 meters. *Bulletin of the Seismological Society of America*, *101*(6), 3046-3059.

Catchings, Rufus D., et al. (2019) "Two-Dimensional Seismic Velocities and Structural Variations at Three British Columbia Hydro and Power Authority (BC Hydro) Dam Sites, Vancouver Island, British Columbia, Canada." *USGS Open-File Report*, 2019, doi:10.3133/ofr20191015.

Dai, Z., Li, X., & Hou, C. (2013). A shear-wave velocity model for Vs_{30} estimation based on a conditional independence property. *Bulletin of the Seismological Society of America*, *103*(6), 3354-3361.

Di Alessandro, C., Bonilla, L. F., Boore, D. M., Rovelli, A., & Scotti, O. (2012). Predominant-period site classification for response spectra prediction equations in Italy. *Bulletin of the Seismological Society of America*, *102*(2), 680-695.

Goulet, C., Bozorgnia, Y., Abrahamson, N., Kuehn, N., Al Atik, L., Youngs, R., … Atkinson, G. (2018). *Central and Eastern North America Ground-Motion Characterization - Nga-East Final Report*. Berkeley, California: Pacific Earthquake Engineering Research Center (PEER).

Hassani, B., & Atkinson, G. M. (2016). Applicability of the site fundamental frequency as a VS 30 proxy for central and eastern North America. *Bulletin of the Seismological Society of America*, *106*(2), 653-664.

Hollender, F., Cornou, C., Dechamp, A., Oghalaei, K., Renalier, F., Maufroy, E., ... & Boutin, V. (2018). Characterization of site conditions (soil class, Vs_{30}, velocity profiles) for 33 stations from the French permanent accelerometric network (RAP) using surface-wave methods. *Bulletin of Earthquake Engineering*, *16*(6), 2337-2365.

Martin, A. J., & Diehl, J. G. (2004). Practical experience using a simplified procedure to measure average shear-wave velocity to a depth of 30 meters (Vs$_{30}$). In *13th World Conf. on Earthquake Engineering*. Tokyo: International Association for Earthquake Engineering.

Martin, A., Yong, A. Stephenson, W. Boatwright. J, Diehl. J. (2017). Geophysical Characterization of Seismograph Station Sites in the United States – Importance of a Flexible Multi-Method Approach. In *Proc. from the 16th World Conf. on Earthquake Engineering*.

Midorikawa, S., & Nogi, Y. (2015). Estimation of Vs$_{30}$ from shallow velocity profile. *J. Japan Assoc. Earthq. Eng.*, (2), 91-96.

Park, C. B., Miller, R. D., & Xia, J. (1999). Multichannel analysis of surface waves. *Geophysics*, *64*(3), 800-808.

Poggi, V., Burjanek, J., Michel, C., & Fäh, D. (2017). Seismic site-response characterization of high-velocity sites using advanced geophysical techniques: application to the NAGRA-Net. *Geophysical Journal International*, *210*(2), 645-659.

Zhao, J. X., Irikura, K., Zhang, J., Fukushima, Y., Somerville, P. G., Asano, A., ... & Ogawa, H. (2006). An empirical site-classification method for strong-motion stations in Japan using H/V response spectral ratio. *Bulletin of the Seismological Society of America*, *96*(3), 914-925.

Chapter 4 Site Characterization at Stiff Ground Sites in Vancouver

4.1 Introduction

A multi-year seismic microzonation mapping project for Metro Vancouver is underway. A portion of work for this project is presented here to characterize sites (including some strong motion stations) that are geologically complex, including stiff ground conditions. Simplified geology of Metro Vancouver is shown in Figure 4.1. Majority of Vancouver is overlain by glacial Pleistocene sediments with softer Holocene sediments present in south-most Richmond and Tertiary and Pre-Tertiary bedrock present in northern Vancouver. Ten 'complex geology' sites are examined here (Table 4.1) and are compared with the current microzonation map to update Vs_{30} and amplification hazard ratings. These 10 sites are located across the city of Vancouver, which is predominantly an upland area comprised of a sequence of glacial and interglacial sediments from several glaciation periods. These sites are in addition to initial AVA and MASW testing at schools in southwestern British Columbia (Jackson 2017) and are part of the Metro Vancouver seismic microzonation project (Assaf et al. 2019; Molnar et al. 2020).
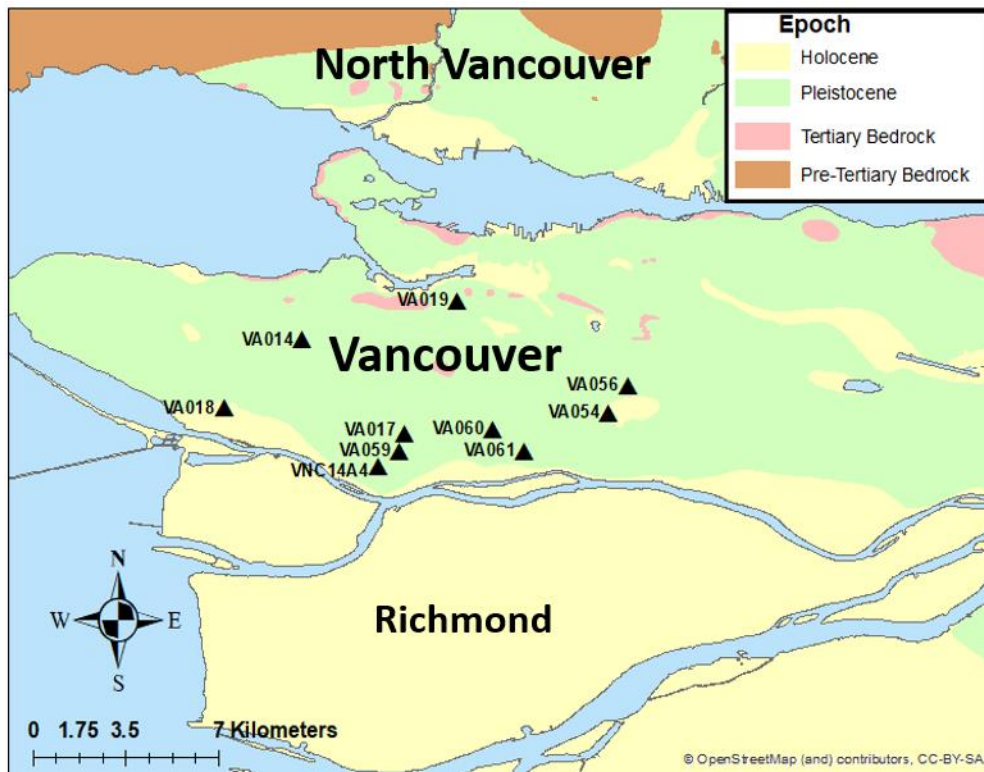
Figure 4.1: Map of examined sites and surficial geology (updated from Molnar et al. 2020).

Table 4.1: List of Vancouver sites investigated with multi-method seismic testing.

Site Name	Latitude (°N)	Longitude (°E)
VA014	49.25142	-123.16140
VA017	49.22087	-123.12656
VA018	49.22924	-123.18784
VA019	49.26417	-123.10865
VA054	49.22758	-123.05726
VA056	49.23662	-123.05098
VA059	49.21511	-123.12825
VA060	49.22218	-123.09655
VA061	49.21522	-123.08605
VNC14A4	49.20996	-123.13575

4.2 Non-invasive seismic testing

A similar multi-method seismic testing campaign is performed at 10 sites across Vancouver as at Eastern Canada seismograph stations (presented in Chapter 2). Both passive AVA and active MASW surface wave array testing was performed. MASW data was collected with 0.5, 1, and 3 m spacing at all sites. Seismic waves were generated by striking an aluminum plate vertically with a 10 lb. sledgehammer at 5 m offset from each end of the MASW survey line. For the longest array (geophones with 3 m spacing), seismic waves were also generated at the array mid-point (Figure 4.2a). Passive AVA recordings were typically acquired using 7 Trominos® arranged in a circular array with 5, 10, 15, and 30 m radial spacing (Figure 4.2b). The array aperture is adjusted several times to measure over various wavelengths (wide frequency bandwidth). Active MASW and passive AVA recordings were pre-conditioned and processed as described in Chapter 2. Active MASW was processed using HRFK while passive AVA was processed using MSPAC to generate Rayleigh wave phase velocity estimates with frequency (histogram plots). The details for each processing method are outlined in Section 1.5. Array average MHVSRs were also calculated for each array site.
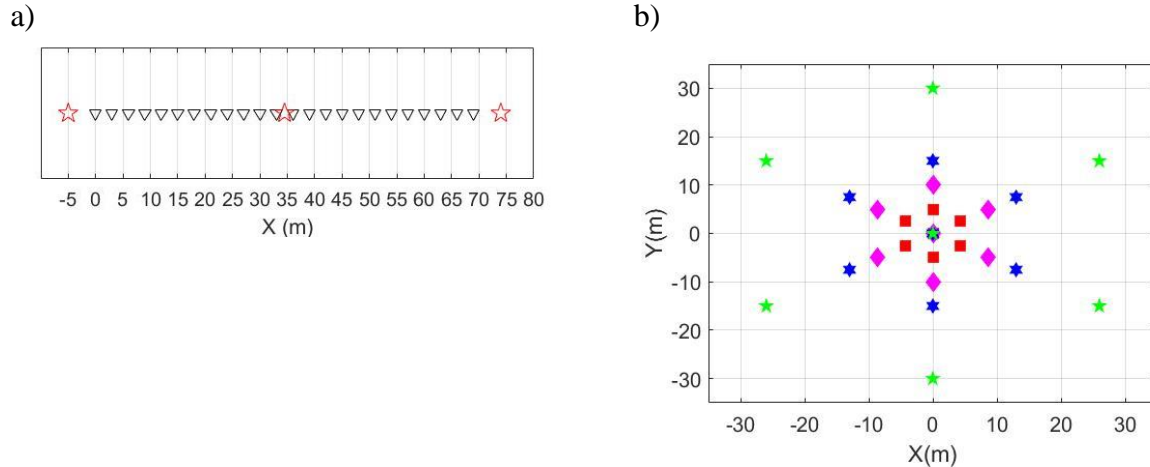
Figure 4.2: Example array spacing and shot locations for a) active MASW and b) passive AVA testing at Vancouver sites. In a) 3 m spacing of geophones (triangles) is shown and shot locations are shown with red stars. In b) the circular arrays of 7 sensors are shown for 5 m (squares), 10 m (diamond), 15 m (hexagon), and 30 m (stars) radial spacing.

4.3   Active and passive dispersion curves

Figure 4.3 shows dispersion histograms generated through HRFK and MSPAC processing for active MASW and passive AVA, respectively. Both active and passive surface wave techniques were used to build a dispersion curve from multiple spacing with each method. AVA estimates were not obtained at sites VA056 and VA061; MASW was the only successful method at these sites.

AVA histogram plots from MSPAC processing are shown in the left-most column of Figure 4.3 with histograms from each array spacing stacked together. Time synchronization between the sensors was an issue and was fixed for 9 out of 10 sites. VA056 and VA061 were the only sites where reliable AVA dispersion picks could not be made. At some sites (VA017, 054, 059 and VNC14A4), a mid-frequency plateau or 'hump' in the dispersion estimates occurs. This is selected as the fundamental mode (Molnar et al. 2020), indicative of a low velocity zone (or velocity reversal with depth) within the glaciated upland Pleistocene sediment package which is geologically feasible since the sequence includes several glaciations (advances and retreats) and likely reversals in sediment stiffness. An alternative interpretation is the mixing of modes resulting in an apparent or effective mode (e.g. Martin et al., 2017 and Asten and Hayashi, 2018). For the majority of sites (7 of 10; 70%), low site amplification is observed and phase velocities at the lowest frequencies (longest wavelengths) span 400-1000 m/s indicating firm to stiff ground

106

conditions. Four sites (VA 014, 018, 056, 060) display moderate peak amplification above 1 Hz with relatively low phase velocity estimates indicating a significant seismic impedance contrast with lower velocity sediments present.
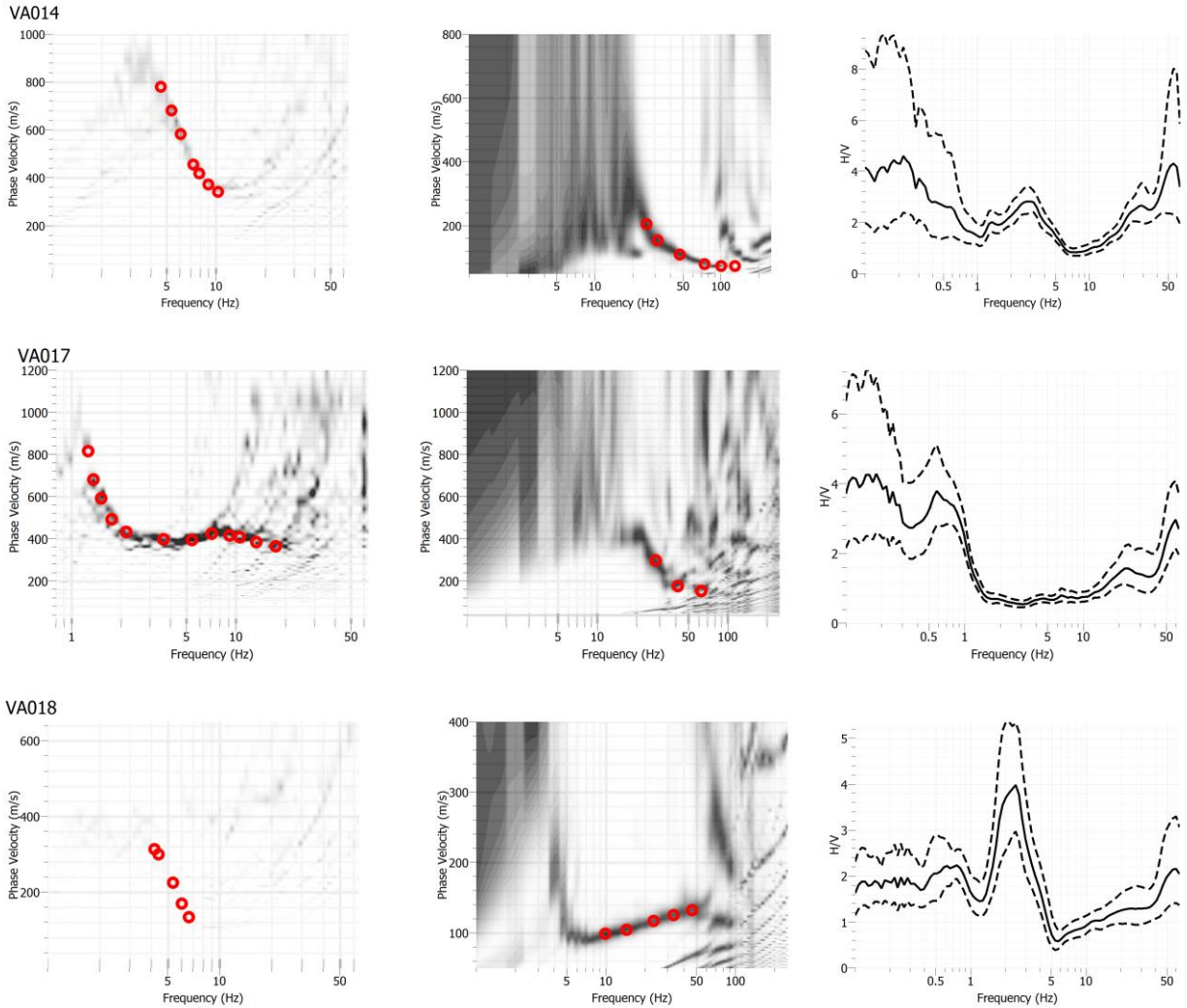
Figure 4.3: Summary of AVA (left) and MASW (middle) dispersion estimates with applicable picked dispersion estimates in open red circles. Darker shading indicates higher histogram counts. Array averaged MHVSRs with one standard deviation are shown in the right-most panel.
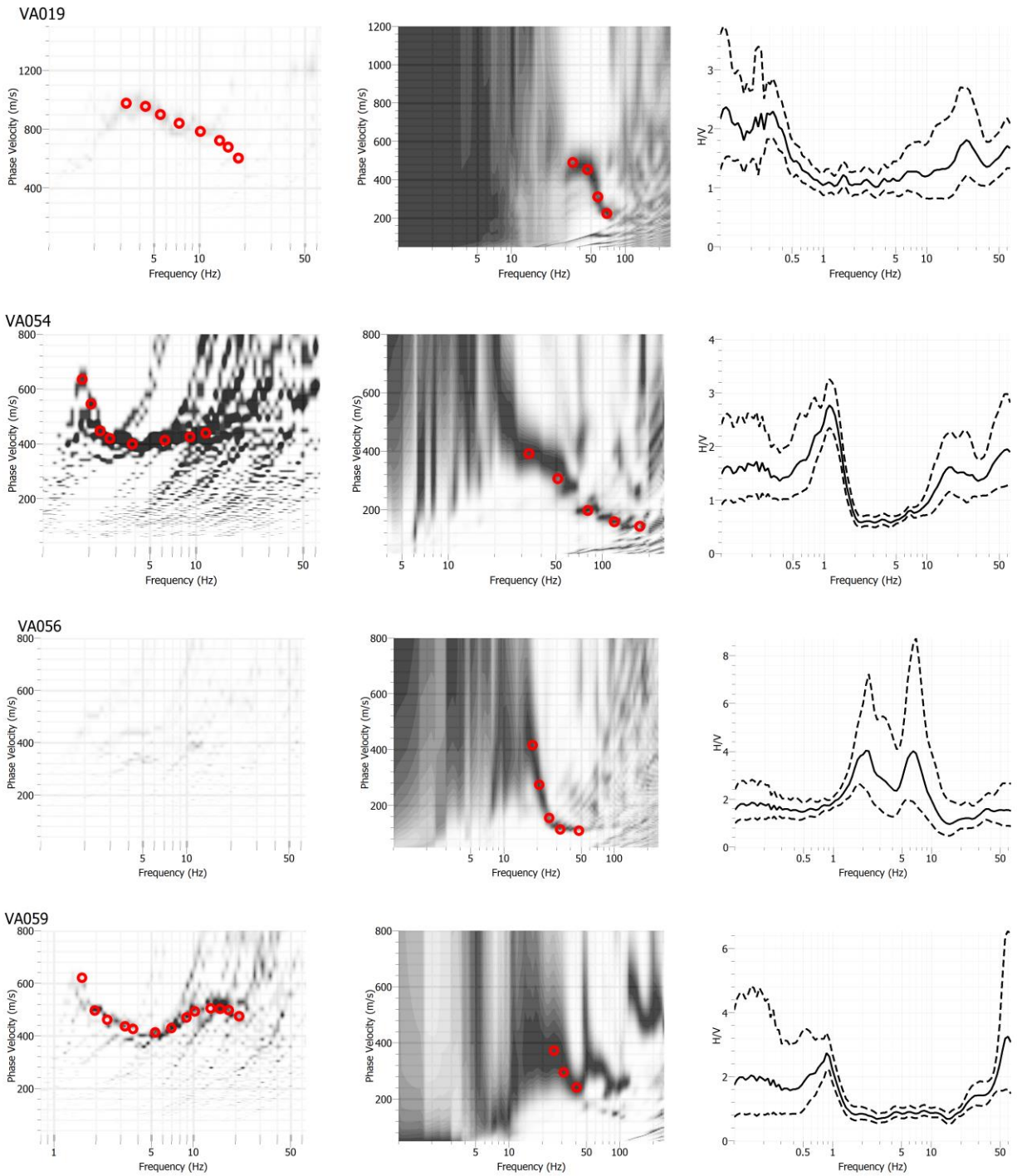
Figure 4.3 Continued
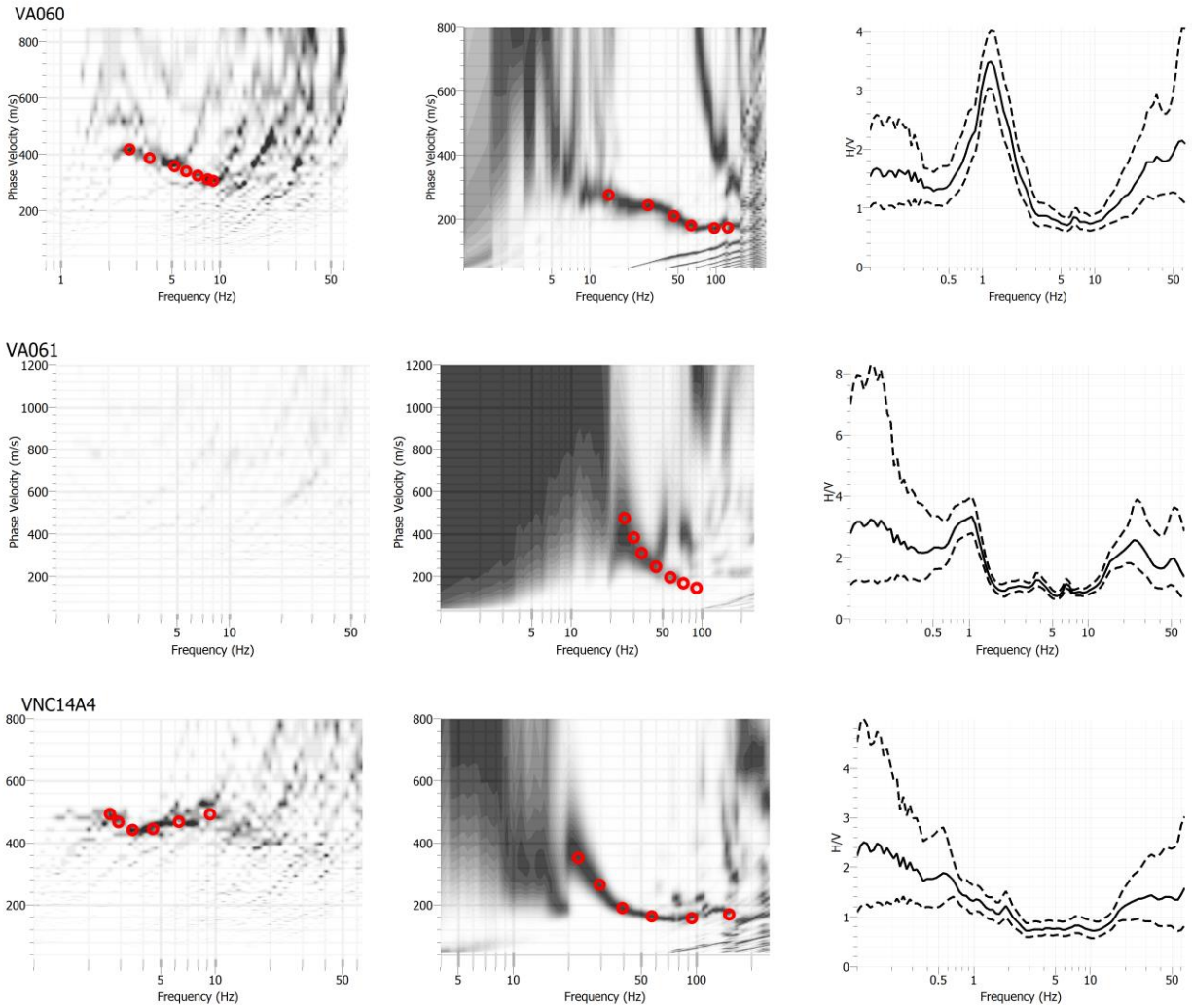
Figure 4.3 Continued

4.3.1 Preliminary Vs₃₀ site classification from dispersion estimates

Dispersion curves for all sites are plotted together in Figure 4.4 and preliminary V_{s30} estimates are determined from V_{R40} (Equation 18; Martin and Diehl, 2004). From preliminary analysis of dispersion estimates, 8 of the sites correspond to site class C (V_{s30} 360-760 m/s) as expected with 2 sites correspond to softer site class D (V_{s30} 180-360 m/s). Dispersion measurements at VA056 and VA061 did not reach the 40 m wavelength to calculate a preliminary V_{s30} but likely correspond to class C. Table 4.2 reports resolution depth limits of the measured dispersion estimates at each site based on the $\lambda_{max}/2$ criterion from Section 3.3.1. Sites with less than 30 m resolution depth are sites where AVA was not successful in providing dispersion estimates and only active MASW was successful.
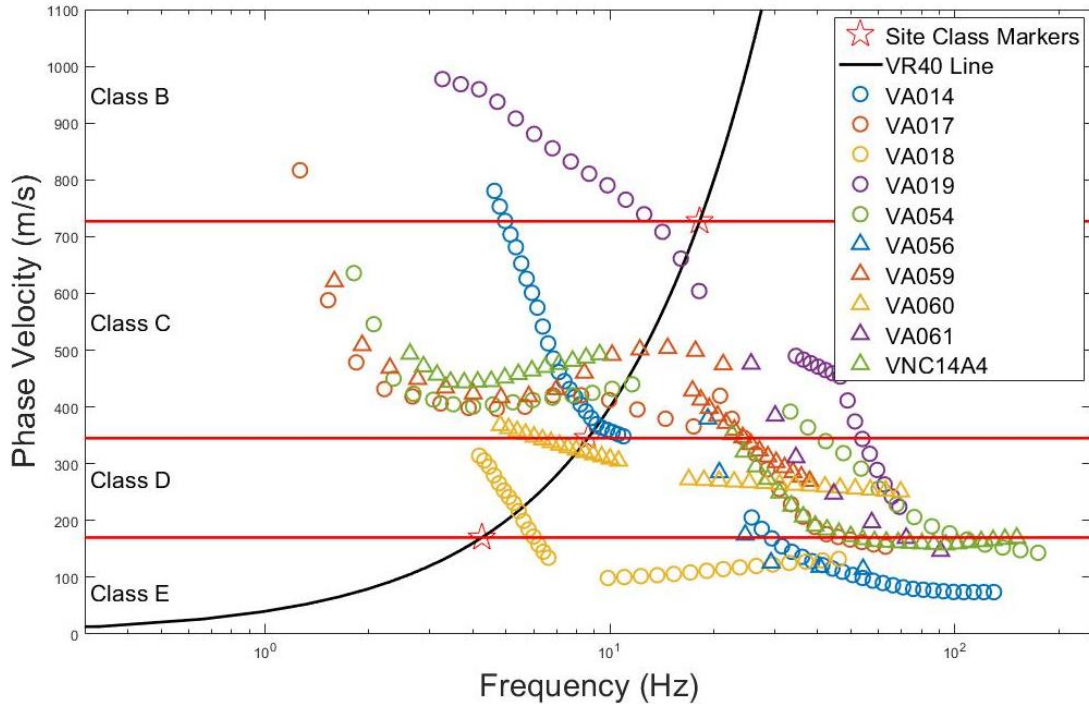
Figure 4.4: Compiled dispersion curves from active and passive surface wave methods are plotted and compared to the V_{R40} line to assign a preliminary site class.

Table 4.2: Calculated maximum wavelength and resolution depth of dispersion estimates.

Site	Maximum wavelength (m)	Resolution depth (m)
VA014	150	75
VA017	647	323.5
VA018	75	37.5
VA019	300	150
VA054	351	175.5
VA056	19	9.5
VA059	391	195.5
VA060	75	37.5
VA061	18	9
VNC14A4	187	93.5

4.4   Joint inversion of dispersion curves and MHVSRs

Robust Vs profiles from inversion of dispersion and/or MHVSRs are sought for Vs_{30} calculation and site classification. Joint inversions were performed using the Dinver software routine (Wathelet, 2008) with dispersion and MHVSR estimates. Sites VA019 and VNC14A4 had MHVSRs that were flat and/or no amplification was observed so only dispersion estimates were inverted.

Surface wave inversion is an ill-posed, non-linear, mixed determined, and non-unique problem. *A priori* information (e.g. geotechnical boreholes or well logs) is typically used to constrain inversion parameters (i.e. layering) but was not available at the Vancouver sites. A 'layering ratios' method has been proposed by Cox and Teague (2016) to systematically vary inversion parameterizations to identify feasible layered earth models for a site based on the measured dispersion data. The layering ratio method applies constraints of the minimum and maximum potential depth for each layer. The minimum and maximum depth of each layer i is determined by one-third and one-half of the resolved wavelength respectively (i.e. $\lambda_{max}/3$ and $\lambda_{max}/2$) from the measured dispersion data. Equations 20 and 21 for the minimum (d_{min}) and maximum (d_{max}) depth are

$$d_{min,i} \approx \begin{cases} \dfrac{\lambda_{min}}{3} & for\ i = 1 \\ d_{max,i-1} & for\ i > 1 \end{cases} \tag{20}$$

$$d_{max,i} \approx \begin{cases} \dfrac{\lambda_{min}}{2} & for\ i = 1 \\ d_{min,i} + \Xi\left(\dfrac{\lambda_{min}}{2}\right) & for\ i = 2 \\ d_{min,i} + \Xi(d_{max,i-1} - d_{min,i-1}) & for\ i > 2 \end{cases} \tag{21}$$

In this way, the depth (thickness) range of each layer is based on the depth range of the layer directly above it; thinner layers will be determined near surface and thicker layers with depth. The layering ratio, Ξ, varies depending on the number of layers the user selects. Layers are added until the maximum resolution is reached of the specified site ($\lambda_{max}/2$). For the Vancouver sites, a layering ratio of 7 or 9 is typically used, generating 4 layer models. Using the layering ratio method to determine layer depth limits for the appropriate model parameterization, dispersion curves are jointly inverted with MHVSRs to acquire Vs profiles. Relatively wide model parameter limits are used and density is fixed at 2000 kg/m^3, as described in section 2.5.1. Velocities were fixed to increase with depth. Hence for sites with potential velocity reversals (VA017, 054, 059, VNC14A4), observed as mid-frequency dispersion 'hump' or plateau, we seek to fit these estimates as a plateau (cannot decrease).

Figure 4.5 shows joint inversion results of the 1,000 lowest misfit models for the 8 sites with full dispersion curves. Theoretical dispersion curves fit dispersion estimates appropriately. The top of the dispersion curve is typically not measured leading to increased Vs variability at depth.

MHVSR peak frequency estimates used in the joint inversion were also fit appropriately. Some MHVSRs are not included in the inversion as they are either flat (e.g. VA019) or likely do not represent subsurface conditions (e.g. VA017 and VNC14A4). For these three sites only dispersion curve inversion is performed. Figure 4.6 compares the resulting optimal Vs profile for the 8 sites. The average Vs (with one standard deviation) of sediment layers (< 800 m/s) is 438 (135) m/s. This coincides with stiff glaciated sediment found in Monahan and Levson (2001) with the average value (with one standard deviation) of 475 m/s (78 m/s). The average maximum depth (with one standard deviation) of the sediment layers is 98 (54) m. The spatial locations of these sites are presented in the next section. The most northern site, VA019, determines rock ($\geq$ 1000 m/s) closest to surface (~20 m). The south central sites (e.g. VA017, VA059, and VNC14A4) contain the thickest sediments (average of 134 ± 19 m), with rock deepest from the surface.

Site	Dispersion	Ellipticity	Vs profile
VA014			
VA017			
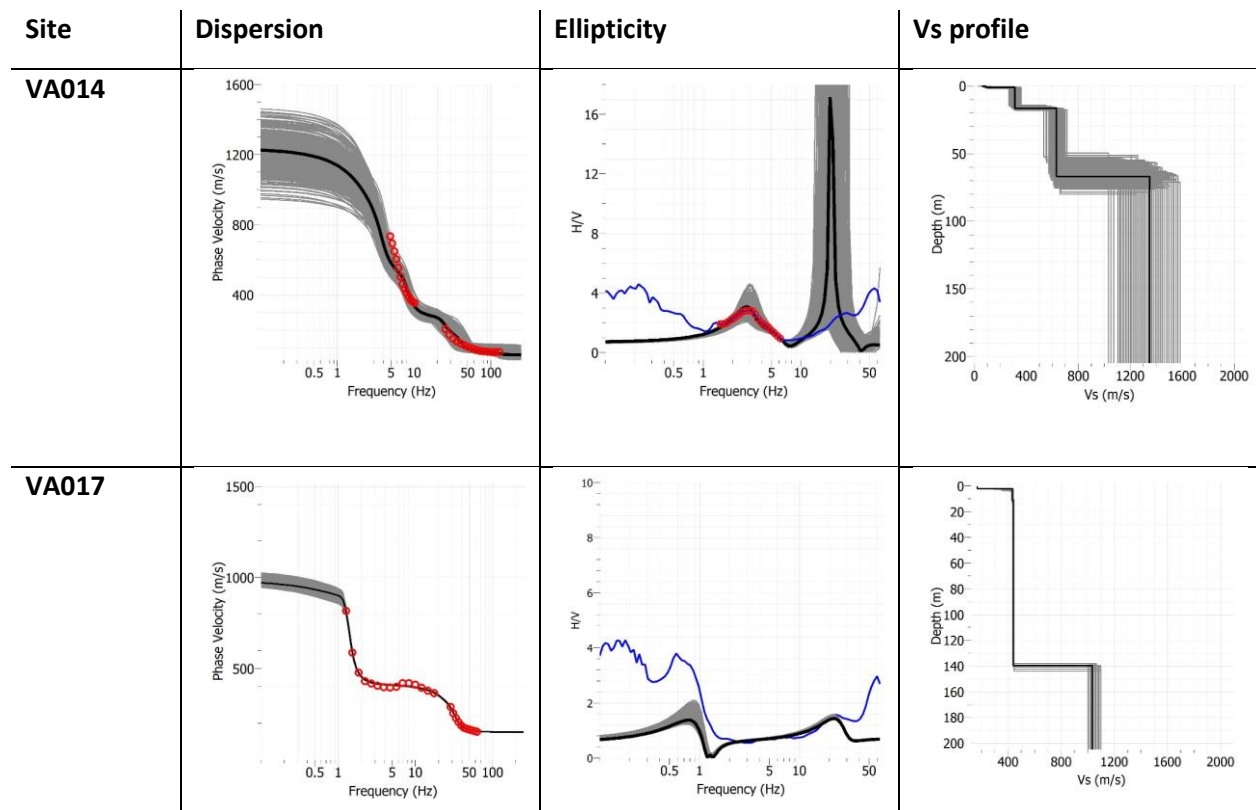
Figure 4.5: Joint inversion of dispersion and MHVSR data (open circles) for 10 Vancouver sites. Theoretical dispersion and ellipticity functions and Vs profiles of the optimal (black line) and 1,000 lowest misfit models (grey lines) are shown. The observed MHVSR is shown with blue lines.

VA018

VA019

VA054

VA059

Figure 4.5 Continued

VA060

VNC14A4
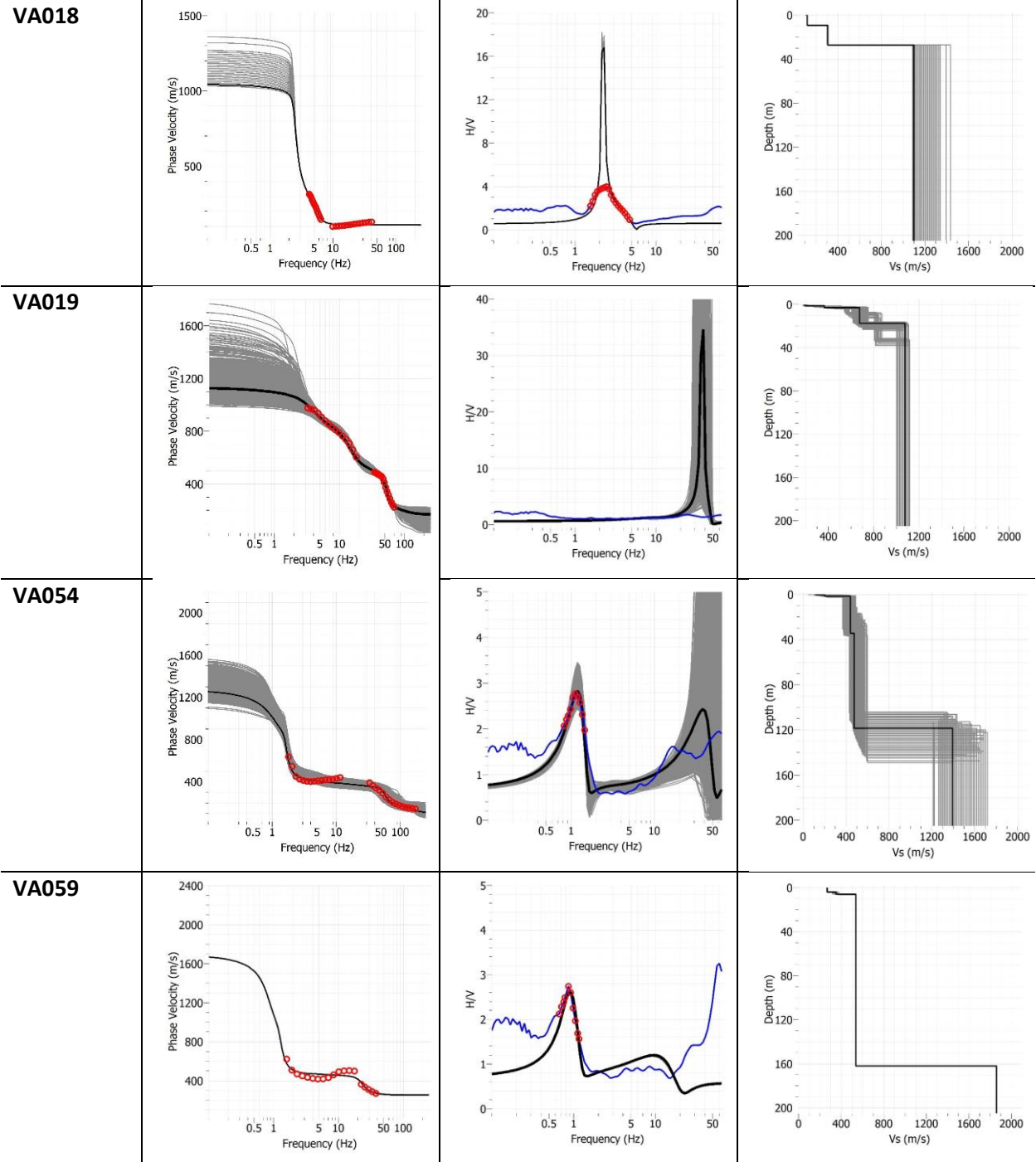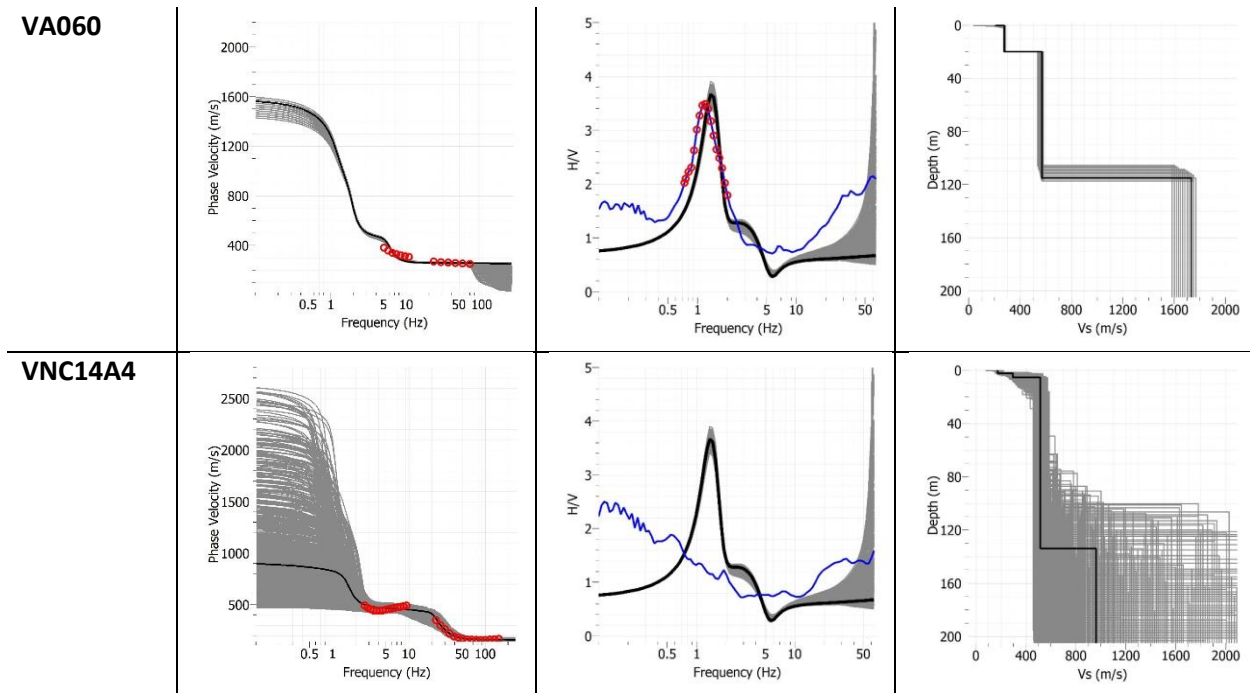
Figure 4.5 Continued
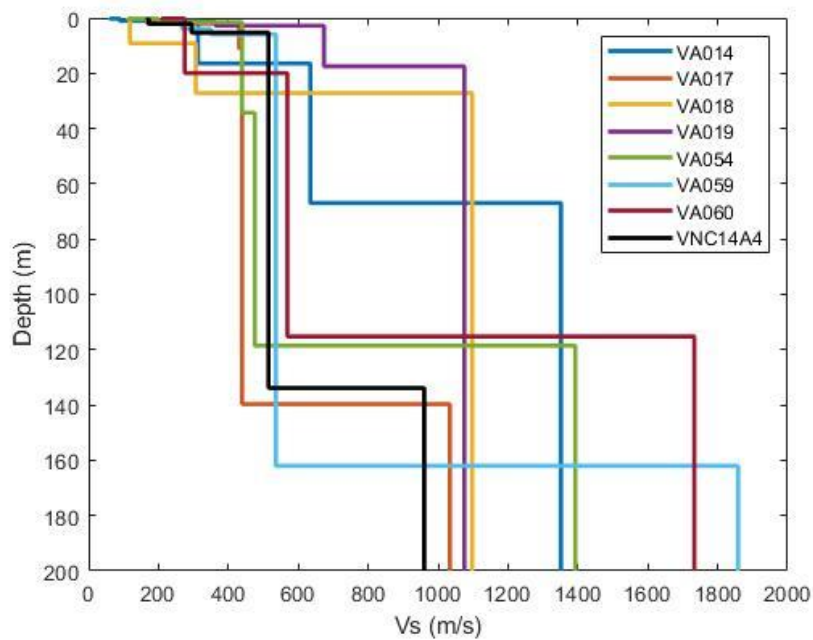
Figure 4.6: Lowest misfit Vs profiles from Vancouver sites.

4.4.1 Robust Vs$_{30}$ site classification from Vs profiles

Vs$_{30}$ calculations are performed using the optimal Vs profile and reported in Table 4.3. Most sites (8) correspond to site class C ($360 < $ Vs$_{30} < 760$ m/s), as expected for stiff glaciated ground.

The site classes from our preliminary V_{R40} site classification provides the same site class as the inverted Vs profile. Overall our inverted Vs profiles determine similar site classification as the current amplification hazard map of Taylor et al. (2006); for the three "softer" site class (D-E) sites of Taylor et al. (2006) we also determine softer site classification for two of these sites. There are deviations between the current site class map and our calculated Vs_{30} for a few sites (VA018, VA054, VA060). There is no consistent trend in "under" or "over" prediction in site classification relative to the current classification (our site classes are higher for two sites and lower for one site). The classification ratings of Taylor et al. (2006) are determined from Vs measurements for the same geologic unit within the region (may or may not have been measured at that exact location). Hence, we have greater confidence in our site-specific *in situ* determined Vs_{30} compared to the current classification map.

Table 4.3: Summary of Vs_{30} site classification for investigated Vancouver sites.

Site	Prelim. Site Class from V_{R40}	Vs_{30} (m/s), Site Class (This Study)	Site Class (Taylor et al. 2006)
VA014	C/D	358, D	D
VA017	C	395, C	C
VA018	D	216, D	E
VA019	C	676, C	C
VA054	C	407, C	E
VA056	Likely C	No Data	C
VA059	C	458, C	C
VA060	D	332, D	C
VA061	No Data	No Data	C
VNC14A4	C	421, C	C

Figure 4.7 shows a map of the sites and their corresponding Vs_{30} site classification. The northern most site VA019 is the stiffest ground with the highest Vs_{30} estimate (seismic bedrock at 20 m). Five sites correspond to the lower range of site class C and the remaining three sites correspond to the upper bound of site class D.
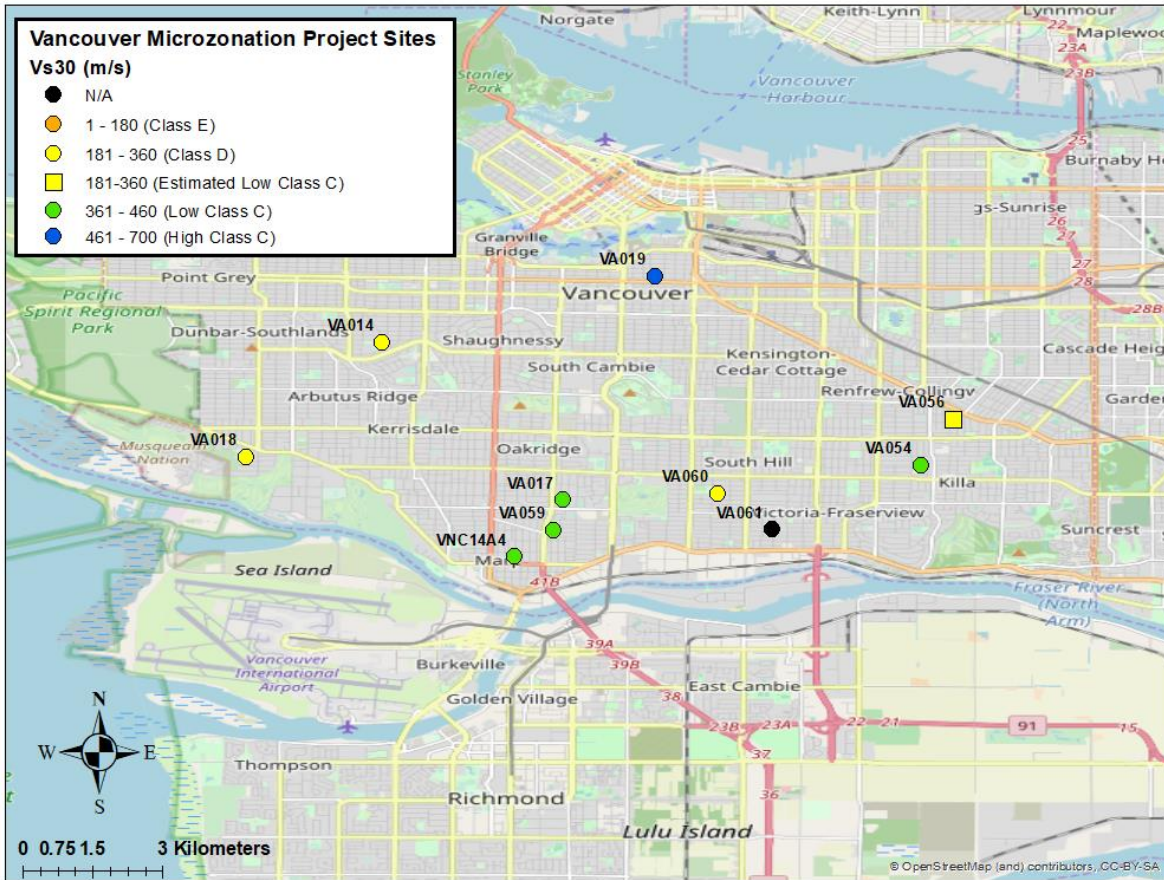
Figure 4.7: Map of investigated Vancouver sites with Vs$_{30}$ site class determined in this study. At two sites, Vs$_{30}$ was not determined as dispersion estimates did not meet the required 30 m resolution depth (Table 4.2).

4.5 Discussion and Conclusions

There has been an effort to improve the current seismic microzonation map and to perform in-depth site characterization across Greater Vancouver (e.g. Jackson, 2017; Assaf et al., 2019) due to the high seismic risk poised in the region. The current amplification hazard map of Greater Vancouver is based on surficial geology and limited geotechnical (Vs) information (Taylor et al., 2006). Part of improving the current map is to obtain *in situ* Vs measurements in areas where information is limited, including the glaciated upland area of Vancouver. A multi-method seismic testing campaign is performed at 10 sites across Vancouver including MHVSR site amplification and active MASW and passive AVA dispersion estimates. Overall the seismic testing was successful - MASW and AVA dispersion estimates are obtained at all 10 and 8 sites, respectively. Low-to-moderate site amplification is observed but we only have confidence in the MHVSR estimates at 5 sites (50%). Difficulty in interpreting dispersion estimates (mid-

frequency plateau or 'hump') and MHVSRs highlights the geologic complexity of these Vancouver sites.

Joint inversion of dispersion and peak amplification estimates generally provided constrained Vs profiles to significant depth ($\geq$ 100 m). From the 10 sites investigated, we determine an average Vs of 438 m/s for the glaciated sediments beneath Vancouver which vary in thickness from 20 m to over 100 m from north to south. The predominant Vs_{30} site class is C, as expected and in agreement with current site classification mapping. We also determine variability in Vs_{30} amongst these site class C sites; the northernmost site has the highest Vs_{30} related to shallower depth to rock. Few sites correspond to lower Vs_{30} site class D, related to softer sediments near surface which are also currently mapped as softer than class C.

The Vs profiling and site classification for 10 sites in Vancouver is a good first step, but the region with the highest seismic risk in Canada requires a finer grid of *in situ* Vs measurements for urban site class mapping. This study highlights the importance in determining the appropriate site classification for sites in the region to develop a detailed map of the hazard posed from earthquakes. The Vs profiles and Vs_{30} site classification obtained will be combined with other non-invasive seismic testing results within the project's geodatabase. Geotechnical and geophysical data is compiled from several organizations per annum. The supplement of geotechnical data in the region will assist in constraining future inversions.

4.6   References

Assaf, J., Molnar, S., Naggar, H., Sirohey, A. (2019). Site Characterization at Strong Motion Stations in Metro Vancouver. *Proceedings of the 12th CCEE (Canadian Conference on Earthquake Engineering) 2019.*

Asten, M. W., & Hayashi, K. (2018). Application of the spatial auto-correlation method for shear-wave velocity studies using ambient noise. *Surveys in Geophysics*, *39*(4), 633-659.

Cox, B. R., & Teague, D. P. (2016). Layering ratios: a systematic approach to the inversion of surface wave data in the absence of a priori information. *Geophysical Journal International*, *207*(1), 422-438.

Jackson, Frederick Andrew. (2017). "Assessment of Earthquake Site Amplification and Application of Passive Seismic Methods for Improved Site Classification in the Greater Vancouver Region, British Columbia" *Electronic Thesis and Dissertation Repository*. 4938. https://ir.lib.uwo.ca/etd/

Martin, A. J., & Diehl, J. G. (2004). Practical experience using a simplified procedure to measure average shear-wave velocity to a depth of 30 meters (Vs_{30}). In *13th World Conf. on Earthquake Engineering*. Tokyo: International Association for Earthquake Engineering.

Martin, A., Yong, A. Stephenson, W. Boatwright,. J, Diehl,. J. (2017). Geophysical Characterization of Seismograph Station Sites in the United States – Importance of a Flexible Multi-Method Approach. In *Proc. from the 16th World Conf. on Earthquake Engineering*.

Molnar, S., J. Assaf, A. Sirohey, S. Adhikari (2020). Overview of local site effects and seismic microzonation mapping in Metropolitan Vancouver, British Columbia, Canada. *Engineering Geology*, 270, 105568.

Taylor, G. W., Monahan, P., White, T. W., & Ventura, C. E. (2006). British Columbia school seismic mitigation program. Dominant influence of soil type on life safety of greater Vancouver and lower mainland schools of British Columbia. 8th U. S. National Conference on Earthquake Engineering, San Francisco, California.

Wathelet, M. (2008). An improved neighborhood algorithm: parameter conditions and dynamic scaling. *Geophysical Research Letters*, *35*(9).

Chapter 5 Conclusions

Accurate (*in situ*) site characterization is important in developing GMM's, particularly at seismograph stations, and in both regional and site-specific seismic hazard assessment. The objective of this thesis was two-fold in characterizing seismograph stations in Eastern Canada using a multi-method approach and applying similar multi-method techniques to characterize stiff ground sites as part of the Metro Vancouver seismic microzonation mapping project. The importance of having *in situ* velocity and site amplification measurements to characterize sites that are rocky and more geologically complex than simple normally-consolidated sediment deposition is presented here to advance cost-effective and non-destructive non-invasive seismic site characterization methods.

In Chapter 2, we introduce the various methods performed within our multi-method approach for characterizing seismograph stations in Eastern Canada. We performed Vp refraction, Vp measurements of laboratory rock samples, active MASW and passive AVA dispersion analysis, and calculated site amplification as HVSRs using both microtremor and earthquake recordings. Each method provided value to site characterization of various rock types amongst the stations visited across Eastern Canada. Poisson's ratio, a useful metric in measuring the ratio between transverse and longitudinal strain, was calculated for rock beneath particular stations when both Vp and Vs was measured. Rayleigh wave dispersion curves were generated from surface wave methods and were inverted to obtain Vs profiles. Two inversion programs were used. Dinver was used to determine the lowest misfit velocity profile and obtain the rock velocity which best fits the dispersion data. PSWP was used to determine an appropriate model parameterization prior to performing Bayesian inversion to obtain a range of probable Vs profiles. We compare the measured rock velocities in sub-regions across Eastern Canada and by rock age (Paleozoic or Precambrian rock). Our measured average Paleozoic rock was found to be 1671 ± 178 m/s (n = 5) and the Precambrian rock to be 1935 ± 28 m/s (n = 2) which falls within the Vs ranges determined by Nastev et al. (2016) for these same rock ages. The rock velocities determined in Chapter 2 are applied in Chapter 3 to obtain a station appropriate Vs profiles for site classification.

Site classification is performed in Chapter 3 using Vs_{30} and site period based approaches. Vs_{30} values are calibrated to that of the station by removing lower velocities related to surficial sediments not present at the station. Extension and extrapolation of the base Vs is applied at stations where the resolution depth into the rock is less than 30 m to predict Vs_{30}. We track both the optimal Vs_{30} as well as its probability distribution. We determine Vs_{30} site classification at 16 out of 23 stations (70%). One station was confidently classified as site class B while five stations were classified as site class A. The standard deviation of the site classes between stations varied (i.e. having A/B, B/A, and B/C) with 8 stations are site class A/B, one station is each site class B/A, and 1 B/C. A multi-method site characterization metric was developed to combine the outcomes of all methods and obtain a single quantitative measure to compare stations. 17 of the 25 stations (68%) have a MM site metric less than 0.5 indicating harder rock conditions, as expected. Five out of 25 stations (20%) were above 0.5 of the normalized MM site metric indicating softer rock, and 3 stations have an intermediate MM site metric and does not distinguish between softer or harder rock conditions. Vs_{30} is the classification scheme used by the NBCC, but other metrics are also useful in understanding the site conditions. Combining them all works effectively in understanding the station's subsurface ground conditions.

Chapter 2 and 3's methods for characterizing and classifying Eastern Canada seismograph stations had a mixed success rate where rock velocity was not measured at all stations. Some stations had rock velocity measured from their dispersion estimates. A multi-method approach was successful in gathering various data at the stations though some methods and stations were more successful than others. Instead, more methods with different equipment, if available, is encouraged in gathering multiple types of information at the station and to constrain the rock velocities with greater confidence. Other authors have had success in generating Love wave dispersion curves through MAS_LW testing which requires horizontal geophones and a shear source (Martin et al., 2017; Poggi et al., 2017). Love wave dispersion curves can be jointly inverted with Rayleigh wave dispersion curves to have a constrained model. Vs refraction is a successful method used by other researchers calculating the rock Vs directly where similar equipment is used as MAS_LW. Varying the source energy is also a method in other studies to penetrate surface and shear waves into the subsurface deeper to ensure 30 m is reached (e.g. Catchings et al., 2019).

Chapter 4 presents contributions made to the Metro Vancouver microzonation project where sites are glaciated and relatively stiff ground conditions. A multi-method site characterization approach is applied to classify 10 sites. The layering ratio method was used to have a robust way to invert sites by multiple operators to avoid user biases when performing dispersion curve inversions. The multi-method testing and Vs profiling procedure is successful at 8 sites (80%) and is effective at characterizing sites in Vancouver. The two sites that did not have successful AVA measurements did not meet the required 30 m depth resolution to calculate Vs_{30} and determine site class. These two sites need to be revisited or have measurements accomplished at a nearby location. To meet the resolution depth, a greater energy source (compared to a sledgehammer) can be used to penetrate deeper into the subsurface by generating longer wavelength surface waves. Increased receiver spacing also assists in penetrating deeper into the subsurface if enough space is feasible at the measurement site.

5.1 Future Work

It is recommended to revisit 17 of the 25 (68%) Eastern Canada seismograph stations with horizontal geophones and a seismic shear source with varying source energies to acquire a robust, more constrained Vs profile to characterize the sites more confidently. Visiting sites again where microtremor measurements were saturated with noise and/or not accessible to have an estimate of the site amplification would be beneficial. Stations A11 and A21 on higher elevation outcropping rock may never be adequately characterized by seismic array methods that require an area upon which to perform the surveys. Drilling a borehole(s) and performing downhole or crosshole Vs measurements is more appropriate to these space-limited station sites but is not feasible due to cost. Taking an abundance of rock samples from the stations would also be helpful in performing Vs and Vp lab measurements to compare with *in situ* velocities. Lastly, using more frequent smaller magnitude earthquakes (< M 3.5) in the calculated EHVSRs would be beneficial to compare the site response from microtremors and from different magnitude earthquakes.

A multi-method seismic testing approach at glaciated sites across Vancouver, British Columbia, was also largely successful to obtain Vs_{30} site classification. Interpretation of the dispersion and MHVSR measurements is relatively challenging for these stiffer ground condition sites. Redundancy in data collection is recommended, e.g., overlapping array radii and/or a minimum

of three MHVSR measurements. A growing geodatabase for the region will also help with interpretation amongst all sites. Adding seismic refraction (ideally Vs but also Vp) testing would help increase velocity measurements and aid in constraining inversion model limits. The use of stronger energy sources (weight drop) is also recommended to penetrate or excite these stiffer ground conditions. Implementation of these recommendations will help gather more velocity data at sites that have been unsuccessful and provides redundancy if one methodology fails. Having a much more detailed site amplification map in the region with the highest earthquake risk in Canada is important especially for emergency planners. Insurance companies also use this information for calculating risk in a region where a major earthquake can occur and cause significant loss.

5.2   References

Catchings, Rufus D., et al. (2019) "Two-Dimensional Seismic Velocities and Structural Variations at Three British Columbia Hydro and Power Authority (BC Hydro) Dam Sites, Vancouver Island, British Columbia, Canada." *USGS Open-File Report*, 2019, doi:10.3133/ofr20191015.

Martin, A., Yong, A. Stephenson, W. Boatwright,. J, Diehl,. J. (2017). Geophysical Characterization of Seismograph Station Sites in the United States – Importance of a Flexible Multi-Method Approach. In *Proc. from the 16th World Conf. on Earthquake Engineering*.

Monahan, P. A., & Levson, V. M. (2001). Development of a Shear Wave Velocity Model of the Near-Surface Deposits of Southwestern British Columbia, Canada.

Poggi, V., Burjanek, J., Michel, C., & Fäh, D. (2017). Seismic site-response characterization of high-velocity sites using advanced geophysical techniques: application to the NAGRA-Net. *Geophysical Journal International*, *210*(2), 645-659.

Wathelet, M. (2008). An improved neighborhood algorithm: parameter conditions and dynamic scaling. *Geophysical Research Letters*, *35*(9).

Appendices

Appendix A

Maps depicting locations of seismic surveys performed at each seismograph station (station code in upper left). Station locations are shown by a yellow pin and blue pin indicate coordinates provided by NRCAN. Red lines indicate passive AVA testing, green lines indicate active MASW and Vp refraction testing. MASW surveys with Tromino sensors are outlined with a blue line. Images were generated by Samantha Palmer.
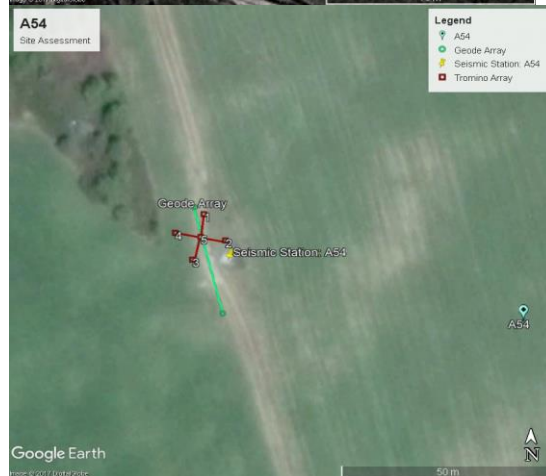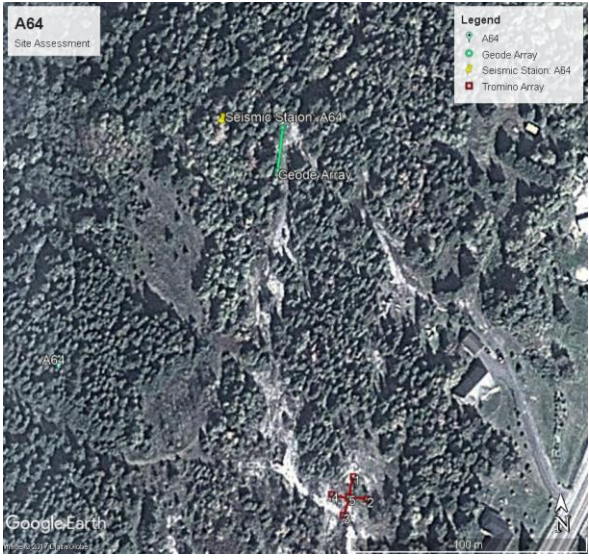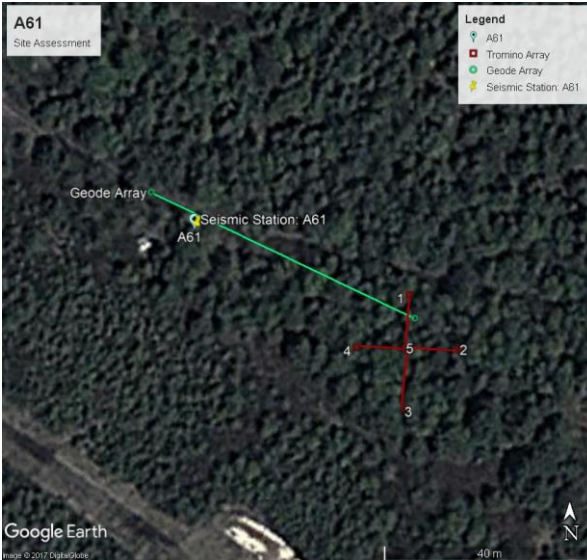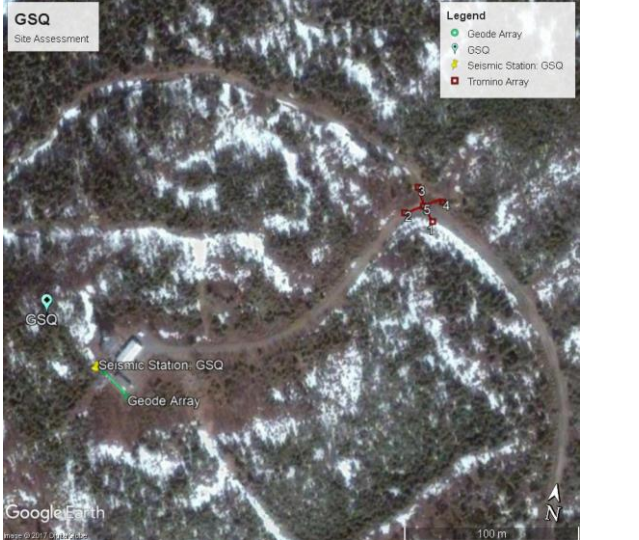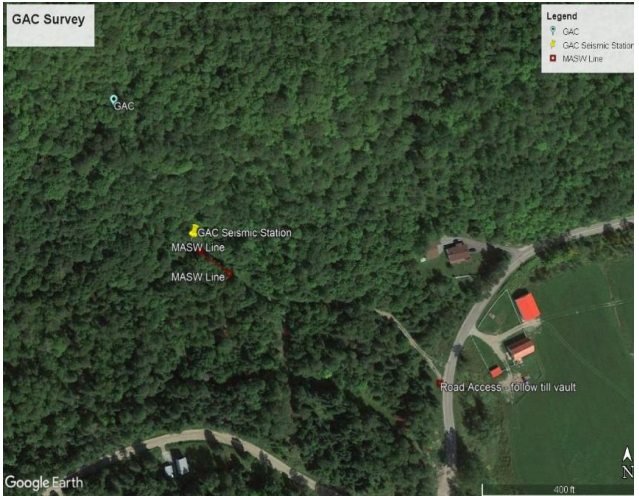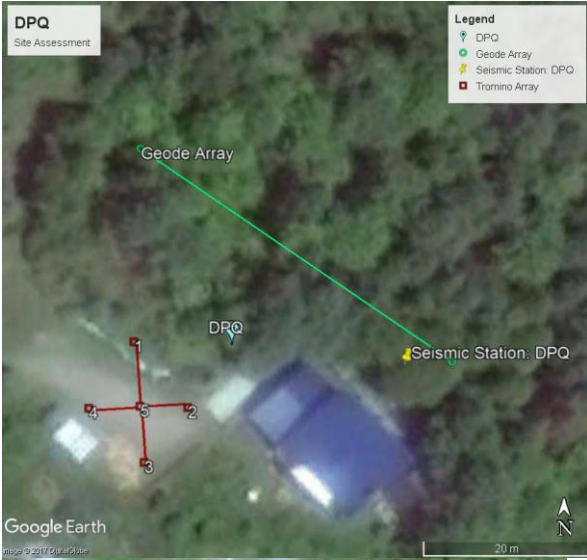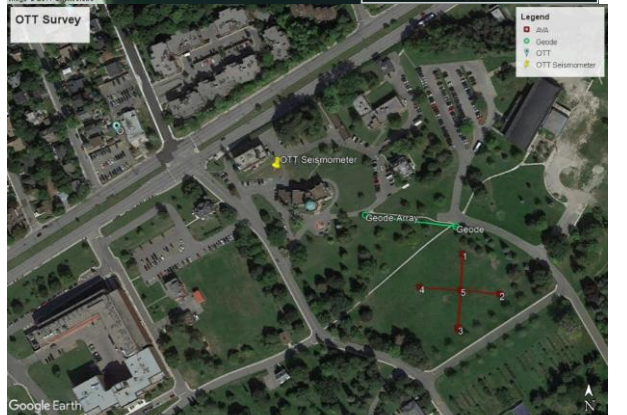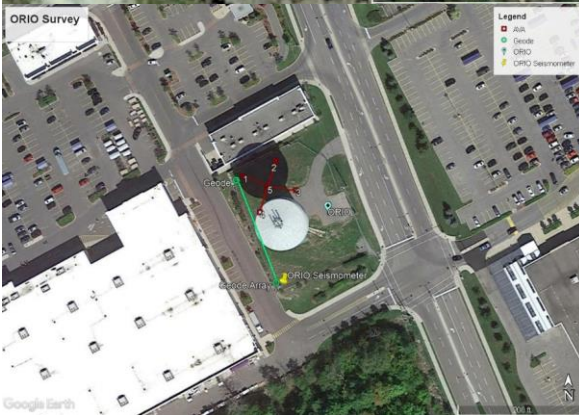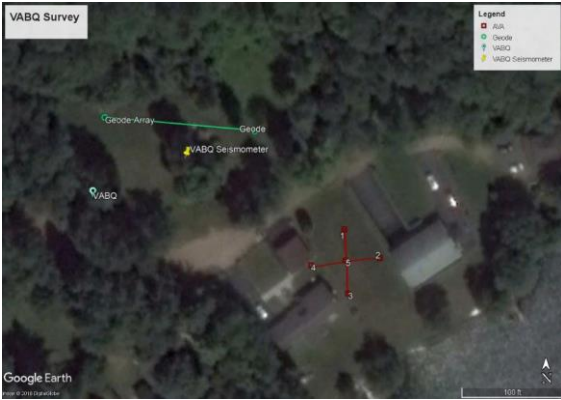
Appendix B

Supplementary histogram plots and velocity profiles for measurements made nearby each station (not the surface the stations reside on) in Chapters 2 and 3. MASW histogram plots with darker shades indicate high count and lighter with low count. Passive AVA measurements are shown similarly with darker and lighter shades to indicate high and low counts, respectively. Station and measurement location site conditions are compared in looking at both locations' MHVSR.
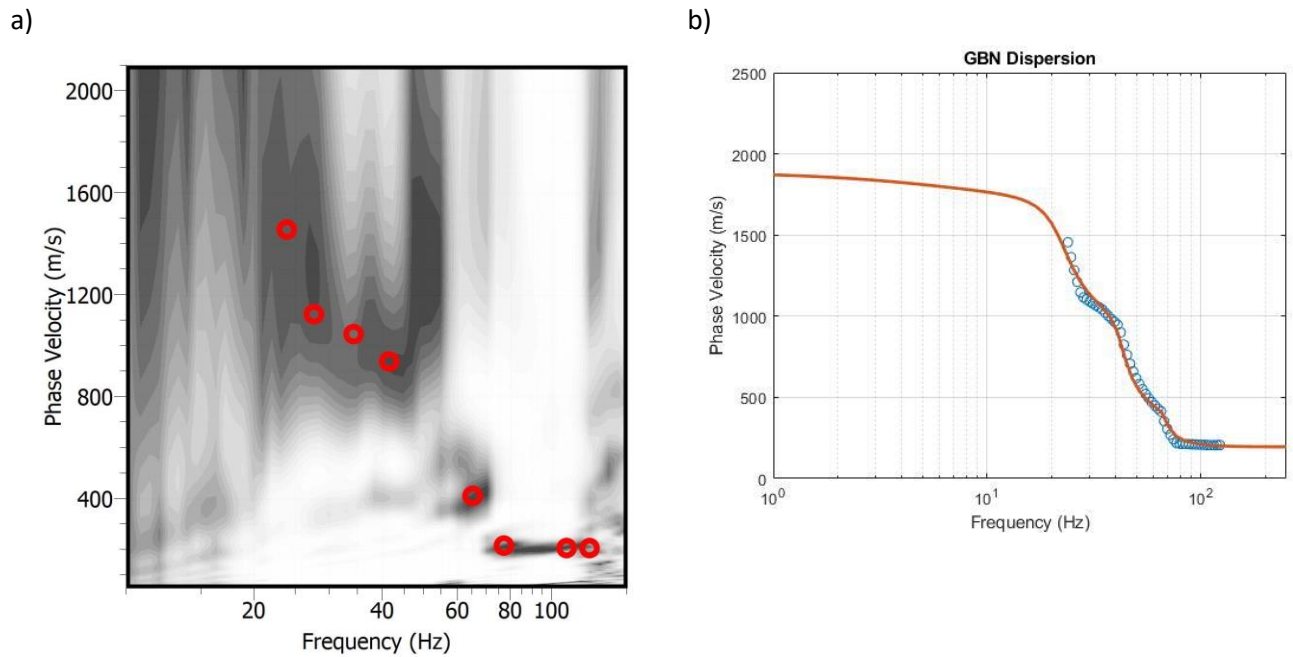
a)

b)
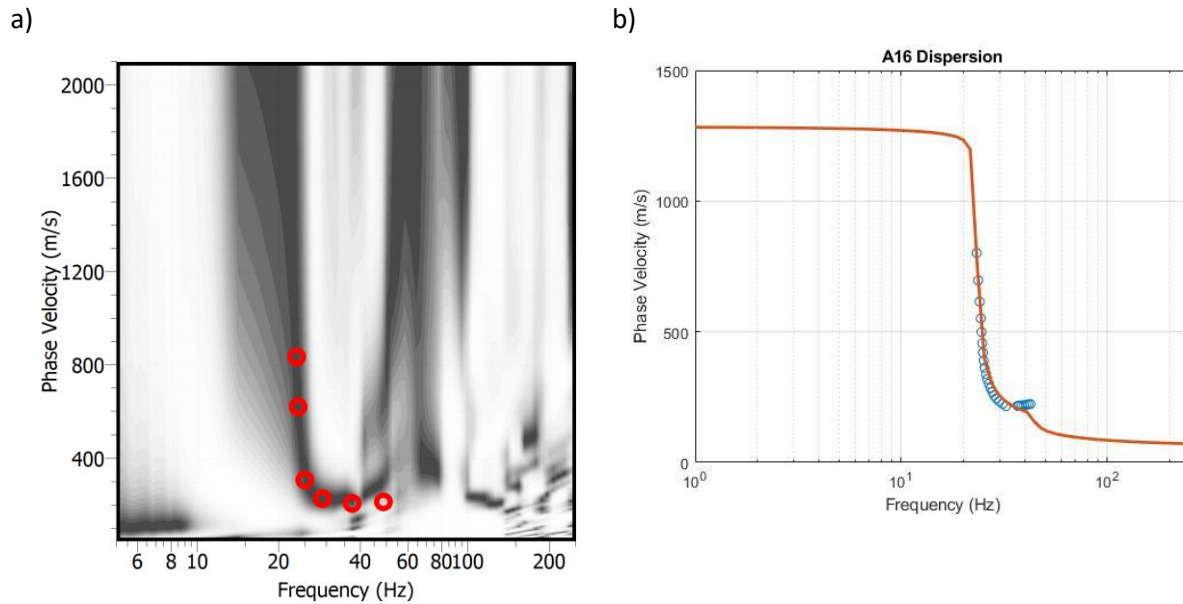
Figure A1: Station A16's a) MASW dispersion histogram with picks in red open circles and b) lowest misfit forward model plotted (orange) with data points (blue).

a)
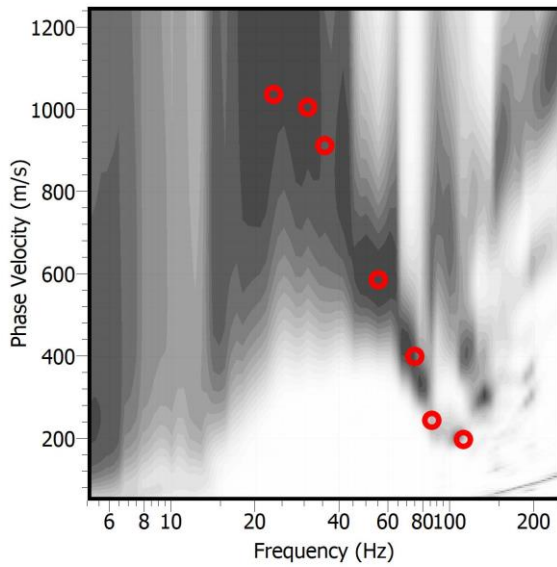
b)
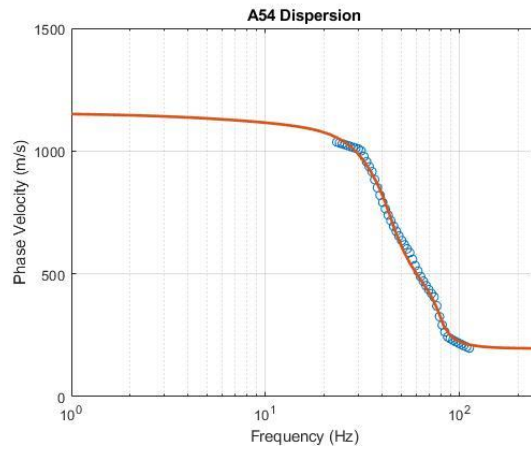
c)
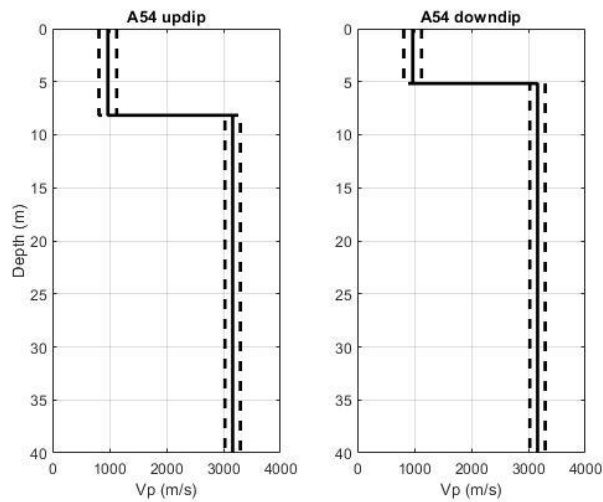
Figure A2: Station A54's : a) MASW dispersion histogram with picks in red open circles and b) lowest misfit forward model plotted (orange) with data points (blue), and c) the average dipping refraction velocity model (solid black line) with the standard deviation (dashed black lines). A dipping interface was identified at the measurement location and is shown in the updip and downdip measurements.

a)
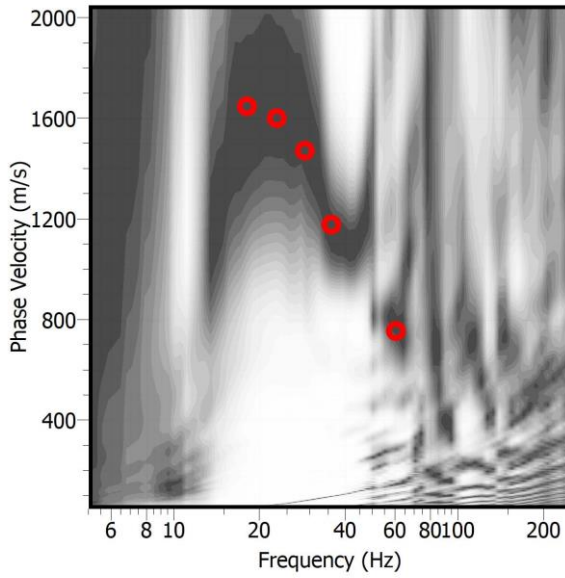
b)
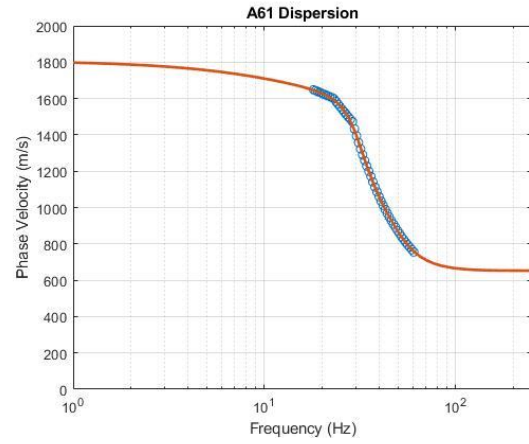
c)
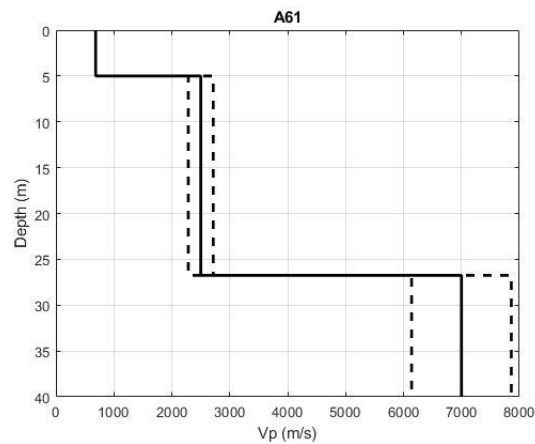
Figure A3: Station A61's : a) MASW dispersion histogram with picks in red open circles and b) lowest misfit forward model plotted (orange) with data points (blue), and c) Station A61's average dipping refraction velocity model (solid black line) with the standard deviation (dashed black lines).
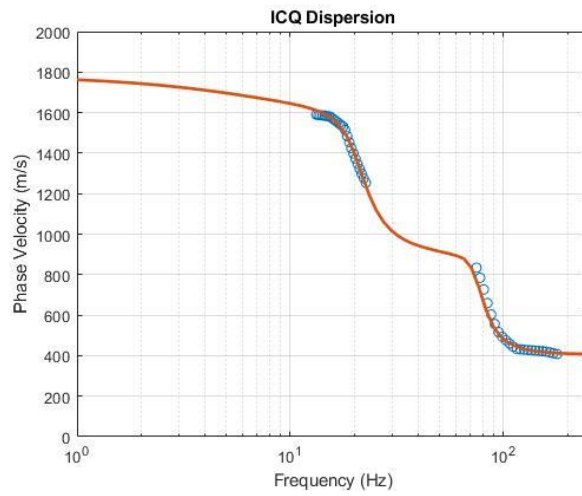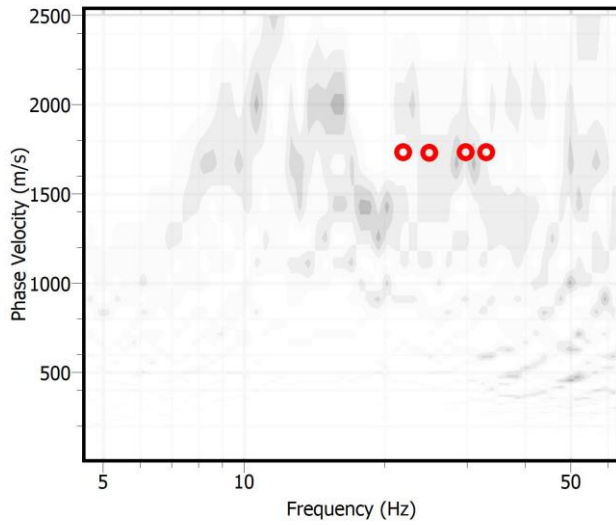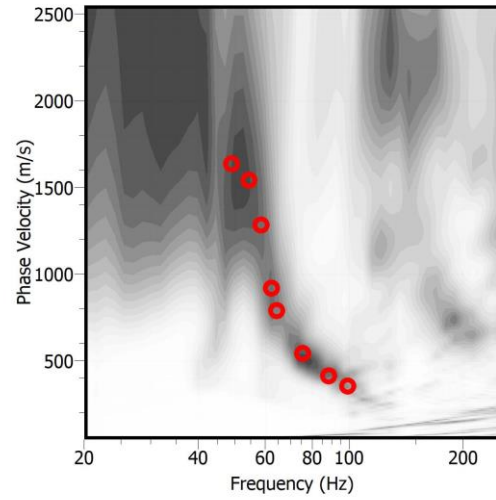
a)

b)

c)
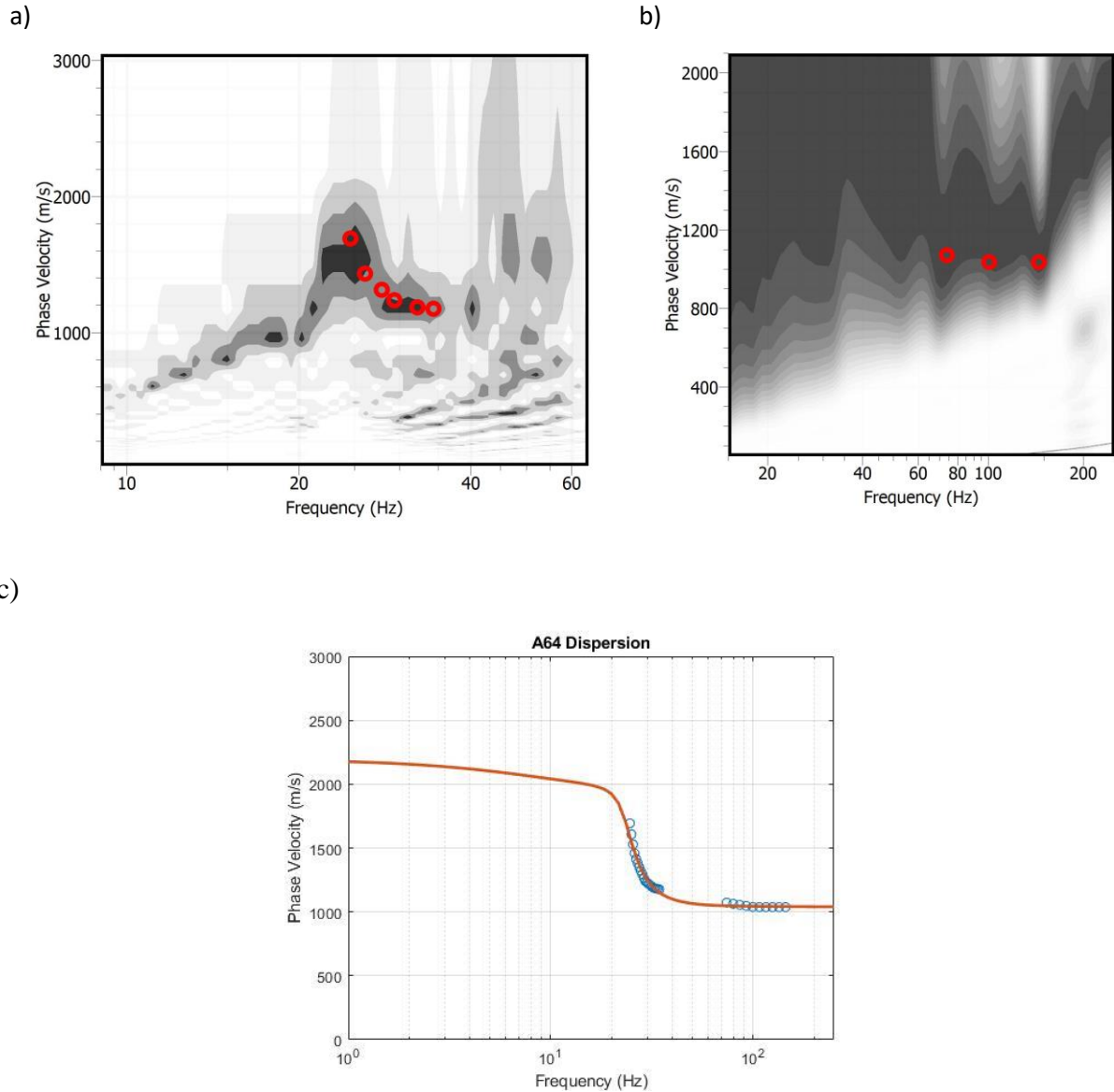
Figure A4 Station A64's a) AVA dispersion histogram with dispersion estimates made in open red circles and b) MASW dispersion histogram with picks in red open circles and b) lowest misfit forward model plotted (orange) with data points (blue) c) Lowest misfit forward model plotted (orange) with data points (blue).

a)
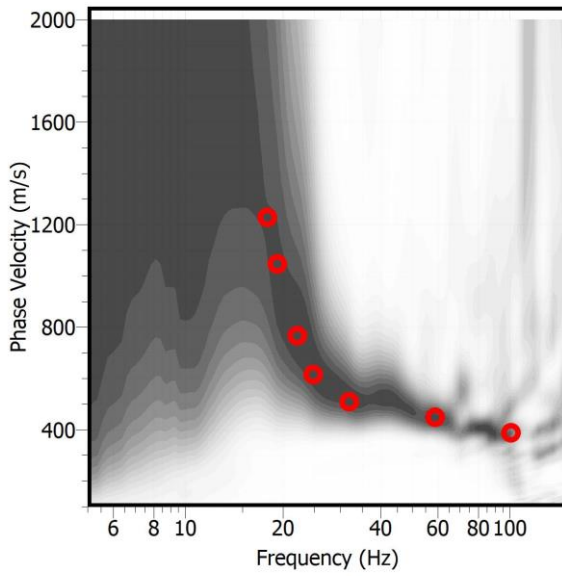
b)
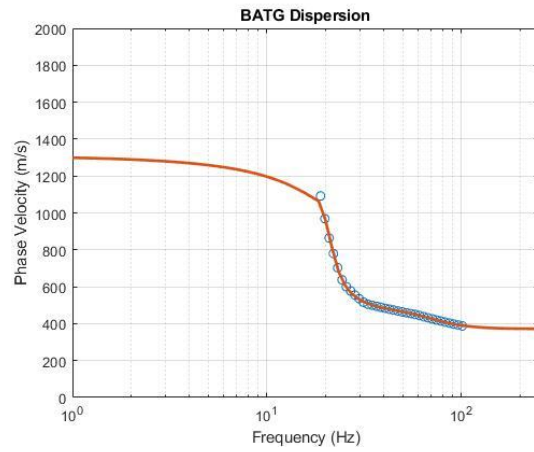
c)
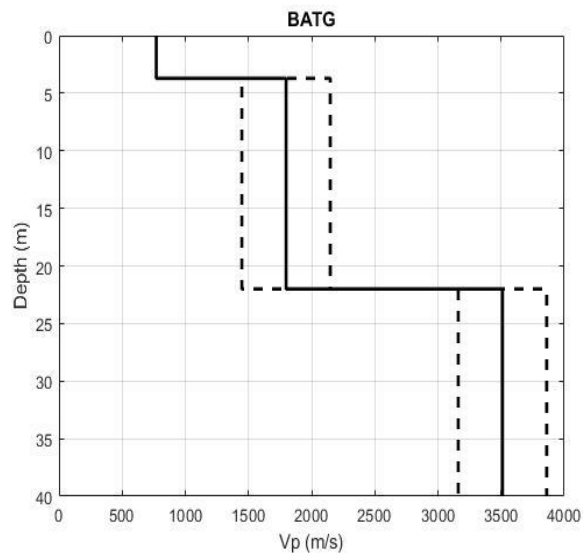
Figure A5: Station BATG's a) MASW dispersion histogram with dispersion estimates made in open red circles and b) lowest misfit forwar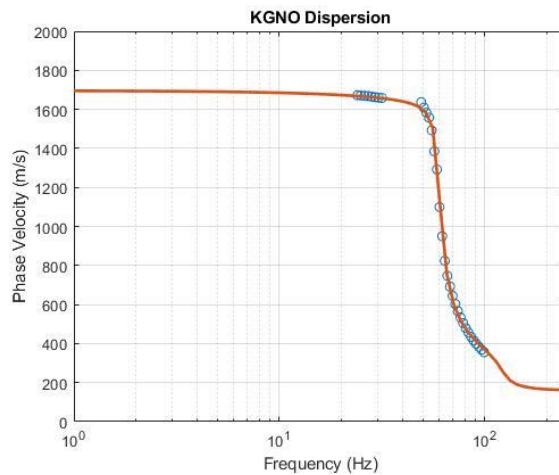d model plotted (orange) with dispersion estimates (blue), and d) the average refraction velocity model (solid black line) with the standard deviation (dashed black lines).

a)
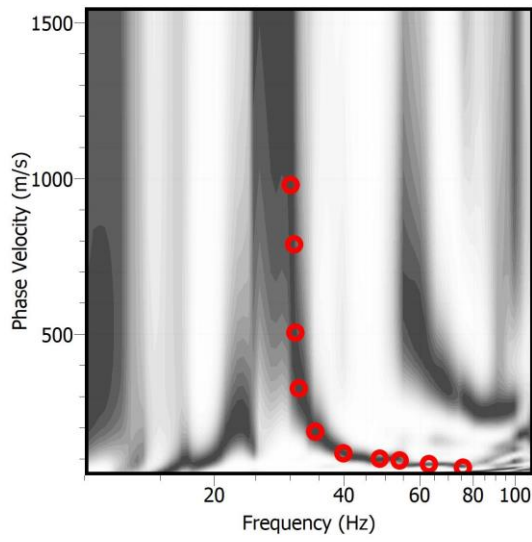
b)
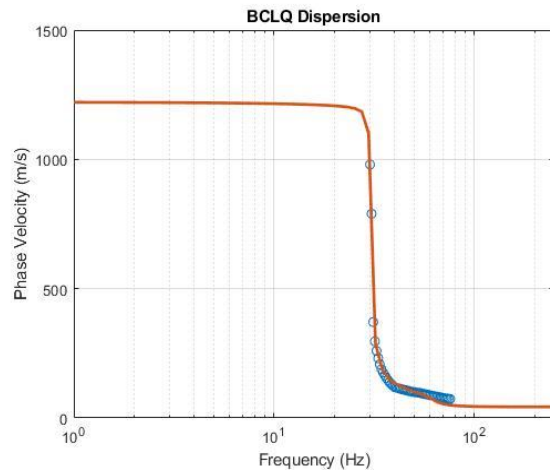
c)
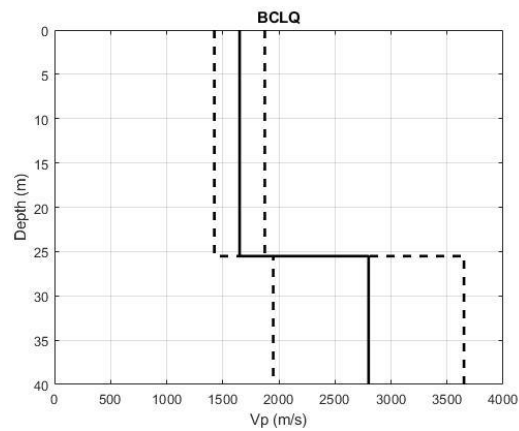
Figure A6: Station BCLQ's a) MASW dispersion histogram with dispersion estimates made in open red circles and b) lowest misfit for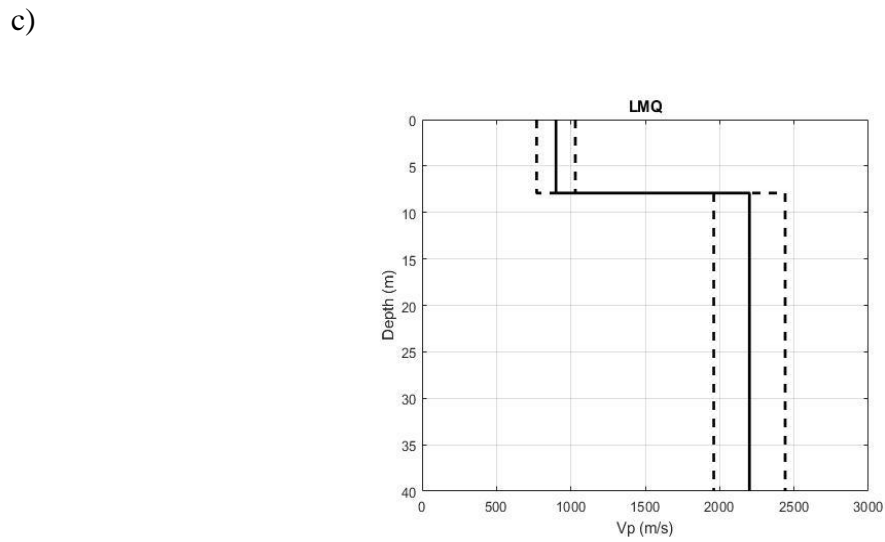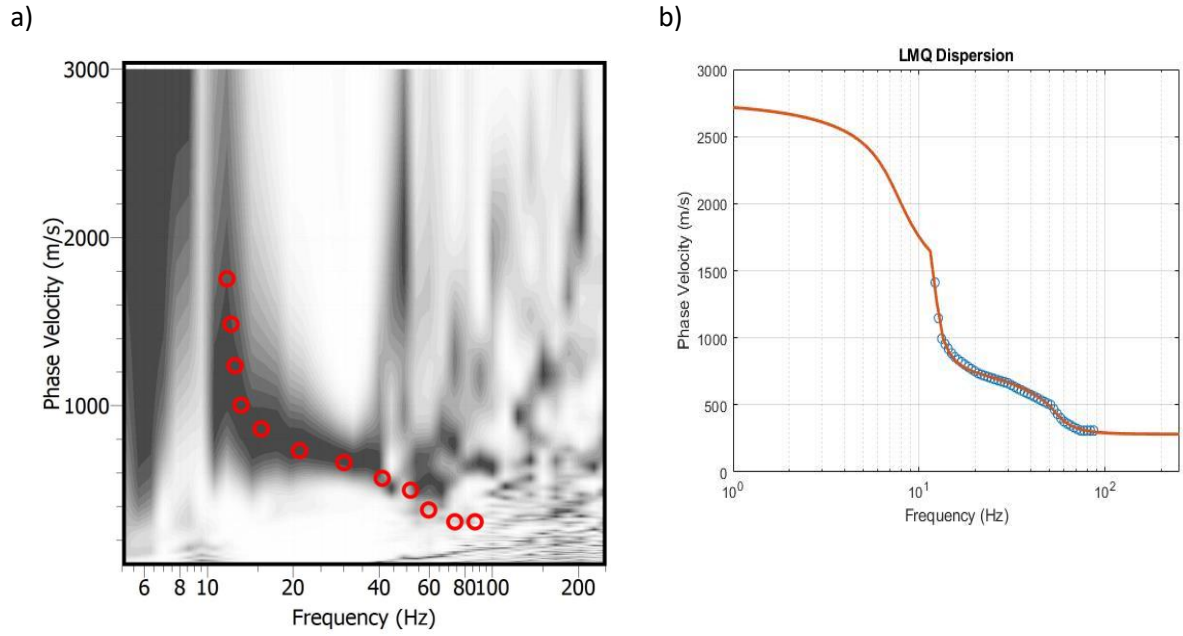ward model plotted (orange) with dispersion estimates (blue), and c) the average refraction velocity model (solid black line) with the standard deviation (dashed black lines).

a)
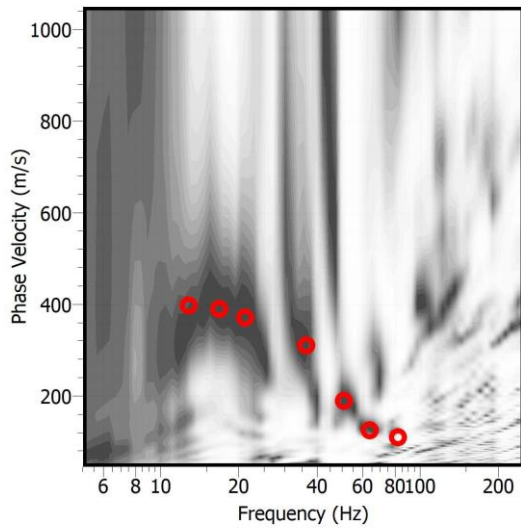
b)
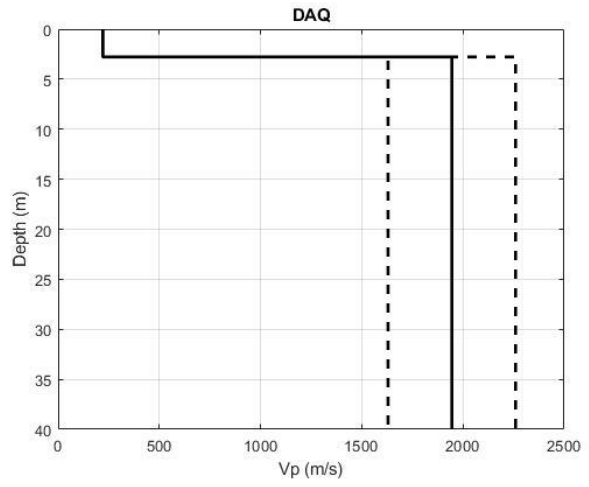
Figure A7: Station DAQ's a) MASW dispersion histogram with dispersion estimates made in open red circles indicating only surficial sediments measured b) the average refraction velocity model (solid black line) with the standard deviation (dashed black lines).
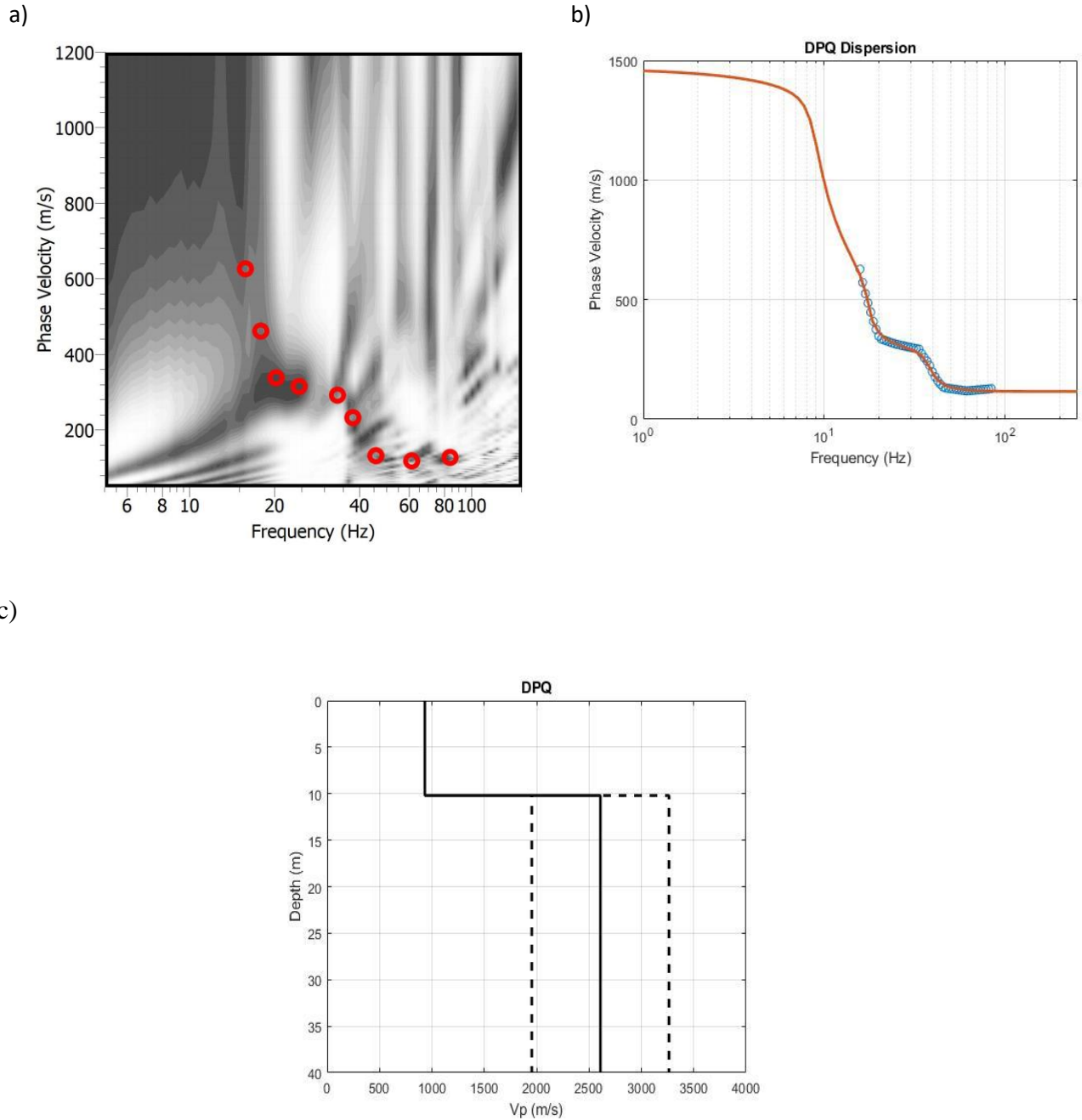
Figure A8: Station DPQ's a) MASW dispersion histogram with dispersion estimates made in open red circles and b) lowest misfit forward model plotted (orange) with dispersion estimates (blue), and c) the average refraction velocity model (solid black line) with the standard deviation (dashed black lines).
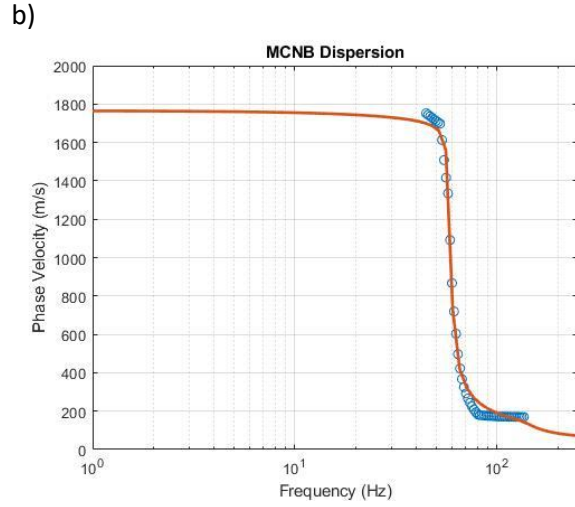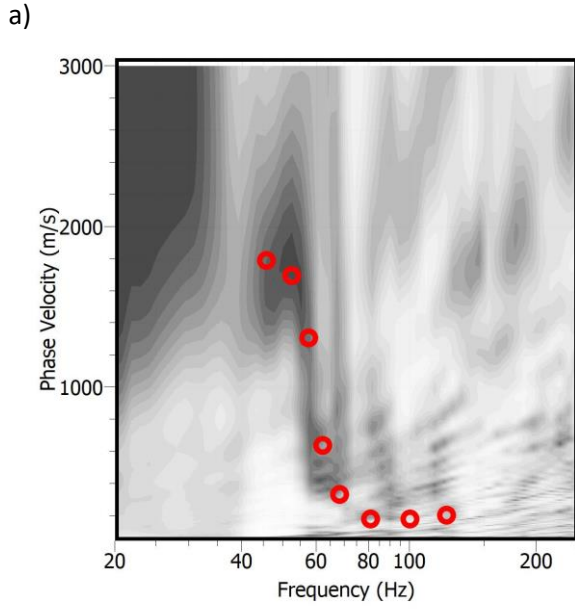
a)

b)
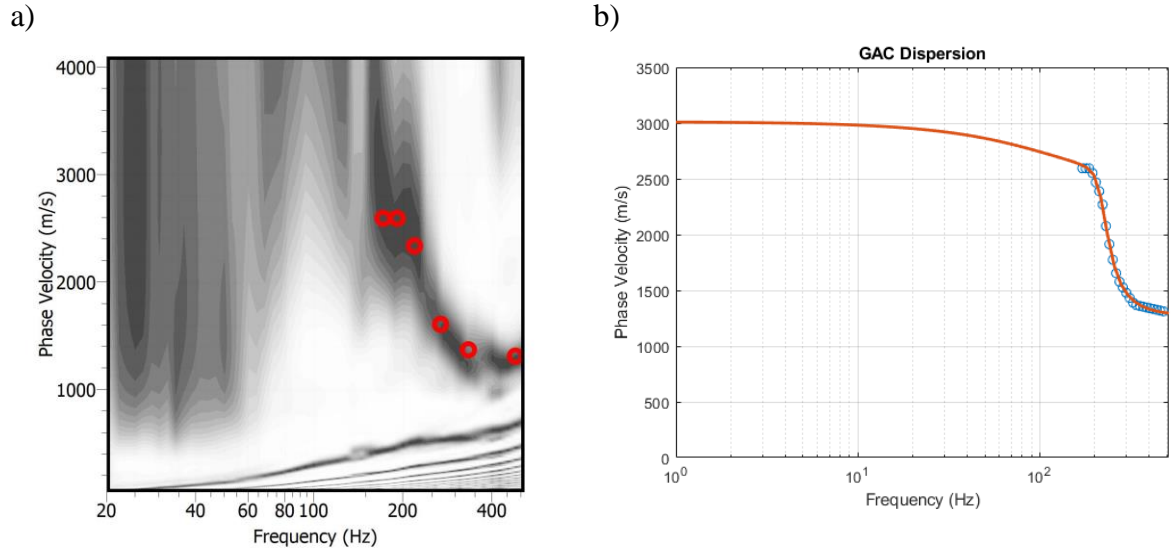
Figure A9: Station GAC's MASW dispersion histogram with dispersion estimates made in open red circles and b) lowest misfit forward model plotted (orange) with data points (blue).

a)

b)

Figure A10 :Station GBN's: a) MASW dispersion histogram with picks in red open circles and b) lowest misfit forward model plotted (orange) with data points (blue).
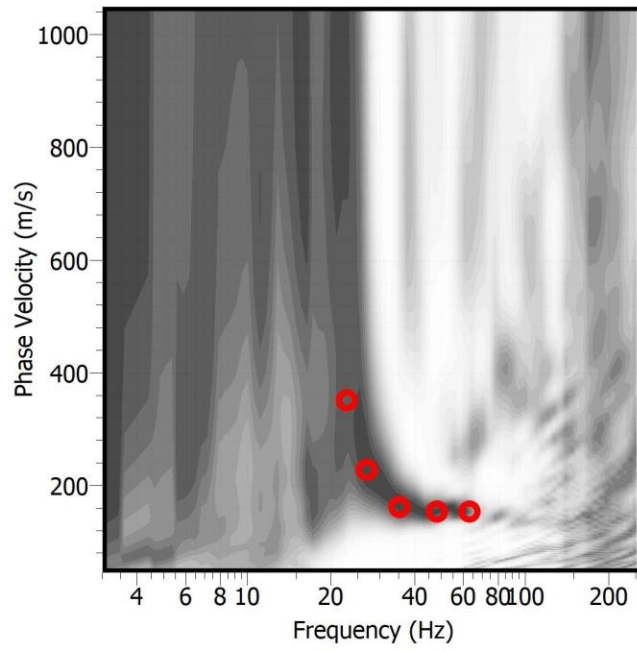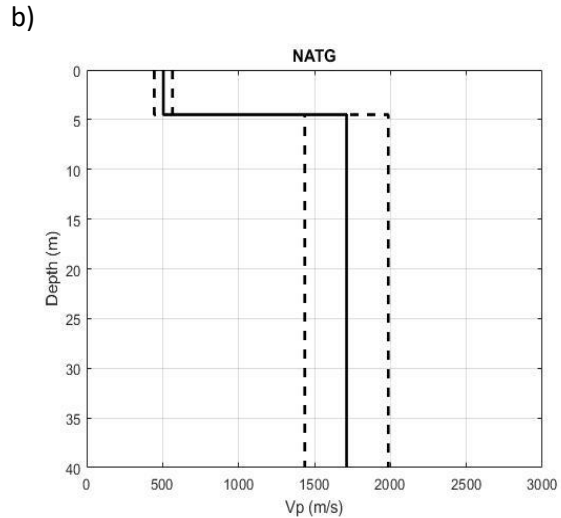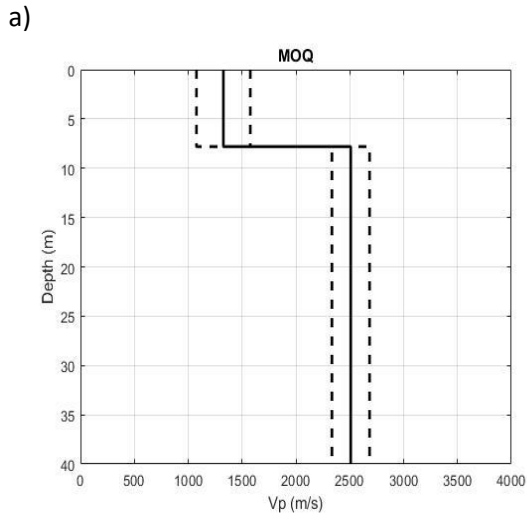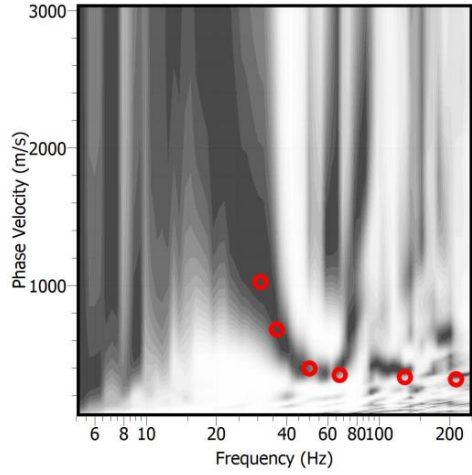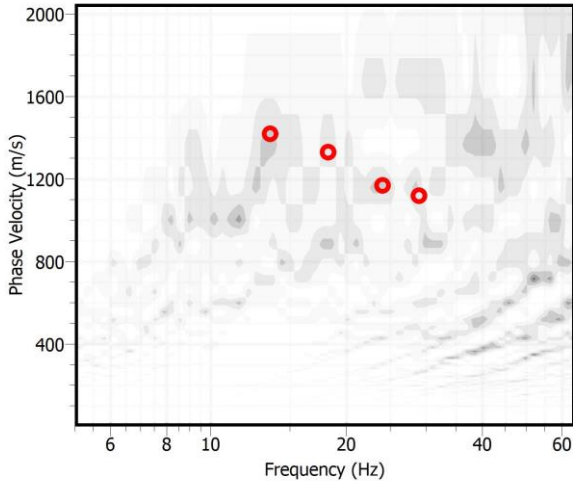
Figure A11: Station GSQ's MASW dispersion histogram with dispersion estimates made in open red circles.

137

a)
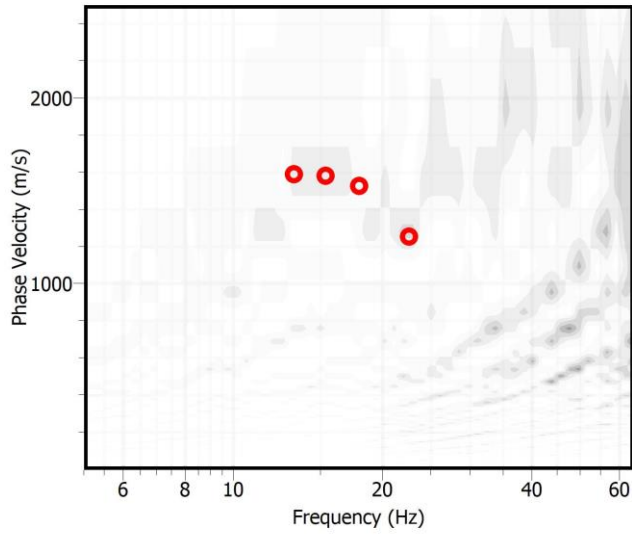
b)
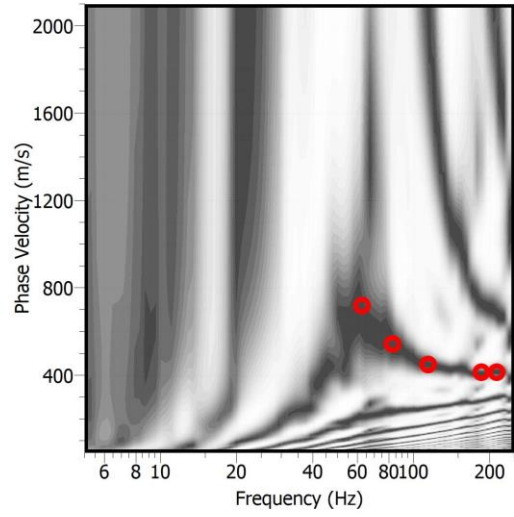
c)

Figure A12: Station ICQ's a) AVA dispersion histogram with dispersion estimates made in open red circles, b) MASW dispersion histogram with dispersion estimates made in open red circles, and c) lowest misfit forward model plotted (orange) with dispersion estimates (blue)

a)

b)

c)

Figure A13: Station KGNO's a) AVA dispersion histogram with dispersion estimates made in open red circles, b) MASW dispersion histogram with dispersion estimates made in open red circles, and c) lowest misfit forward model plotted (orange) with dispersion estimates (blue).

a)

b)

c)

Figure A14: Station LMQ's a) MASW dispersion histogram with dispersion estimates made in open red circles and b) lowest misfi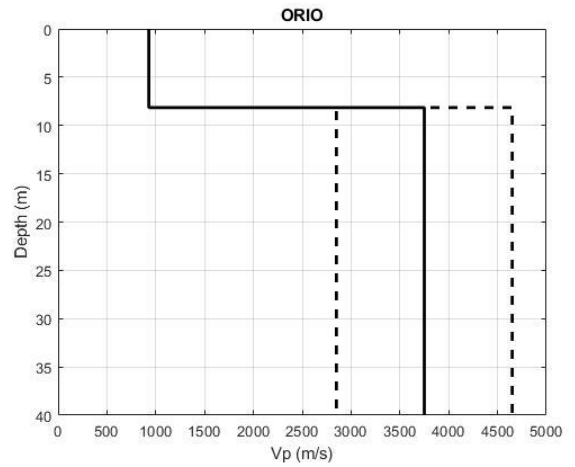t forward model plotted (orange) with dispersion estimates (blue), and c) the average refraction velocity model (solid black line) with the standard deviation (dashed black lines).
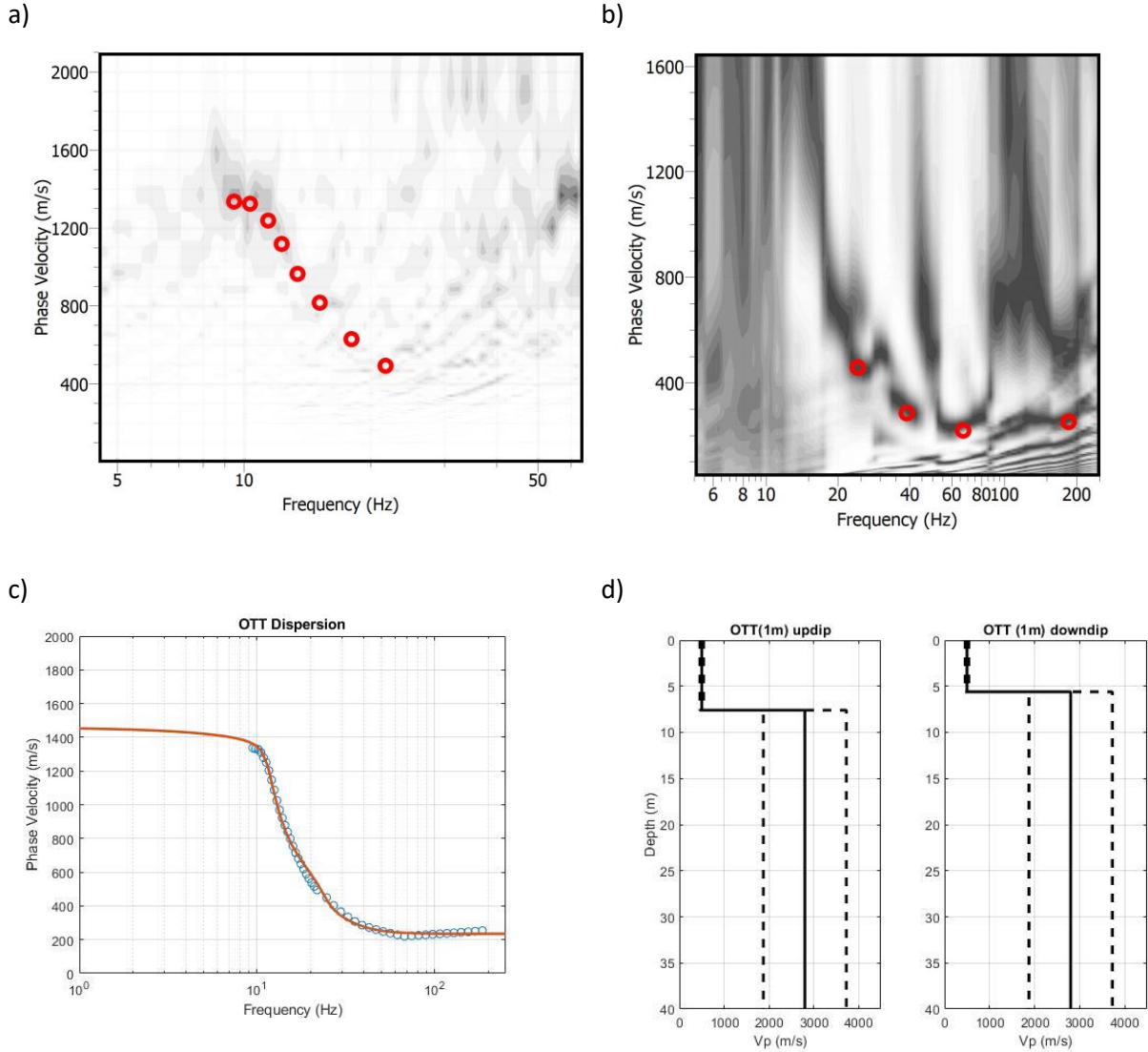
Figure A15: Station MCNB's : a) MASW dispersion histogram with picks in red open circles and b) lowest misfit forward model plotted (orange) with data points (blue).

Figure A16: the average refraction velocity model (solid black line) with the standard deviation (dashed black lines) for stations a) MOQ and b) NATG.

a)   b)
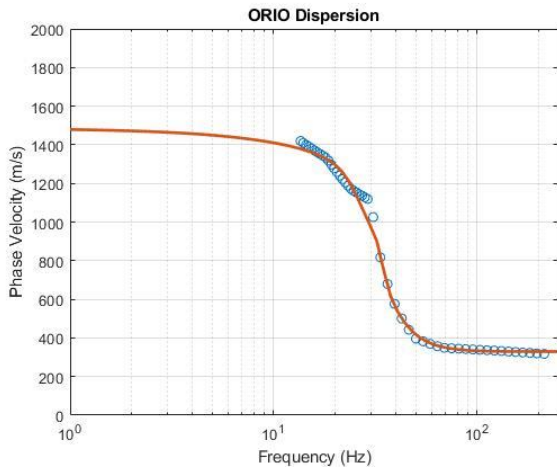
Figure A17: Station ORIO's a) AVA dispersion histogram with dispersion estimates made in open red circles, b) MASW dispersion histogram with dispersion estimates made in open red circles, c) lowest misfit forward model plotted (orange) with dispersion estimates (blue), and d) the average refraction velocity model (solid black line) with the standard deviation (dashed black lines).

a)

b)

c)

d)

Figure A18: Station OTT's a) AVA dispersion histogram with dispersion estimates made in open red circles, b) MASW dispersion histogram with dispersion estimates made in open red circles, c) lowest misfit forward model plotted (orange) with dispersion estimates (blue), and d) the average dipping refraction velocity model (solid black line) with the standard deviation (dashed black lines). A dipping interface was identified at the measurement location and is shown in the updip and downdip measurements.
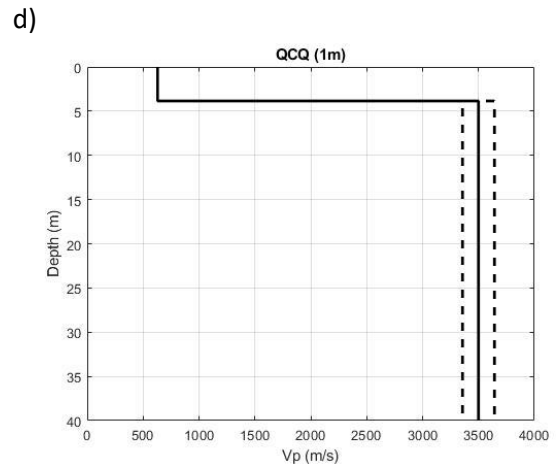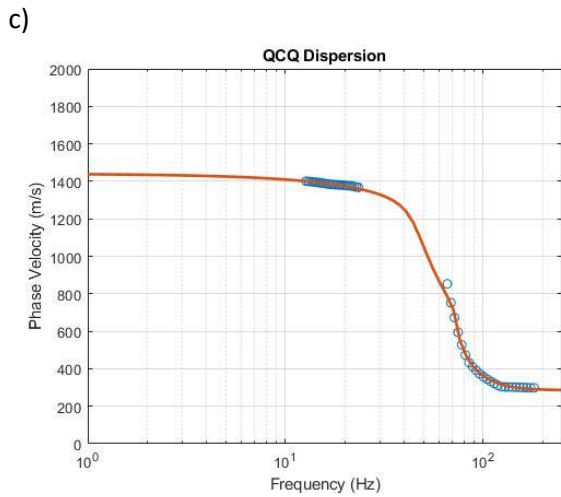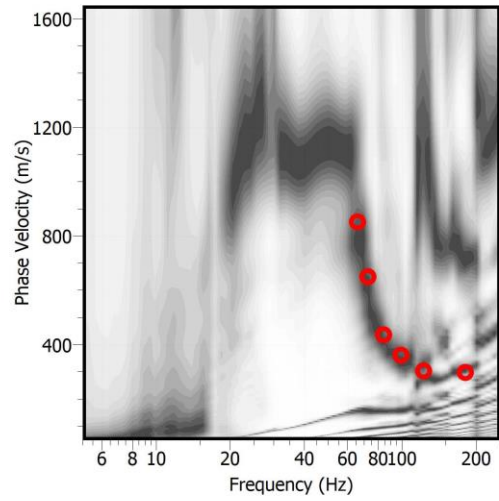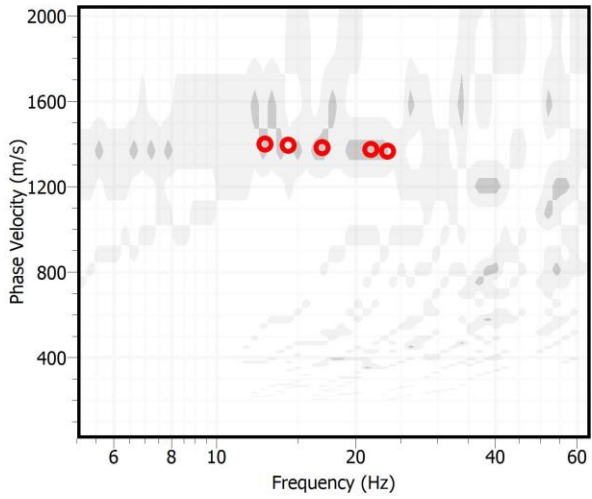
a)

b)

143

Figure A19 :Station QCQ's a) AVA dispersion histogram with dispersion estimates made in open red circles, b) MASW dispersion histogram with dispersion estimates made in open red circles, c) lowest misfit forward model plotted (orange) with dispersion estimates (blue), and d) the average refraction velocity model (solid black line) with the standard deviation (dashed black lines).
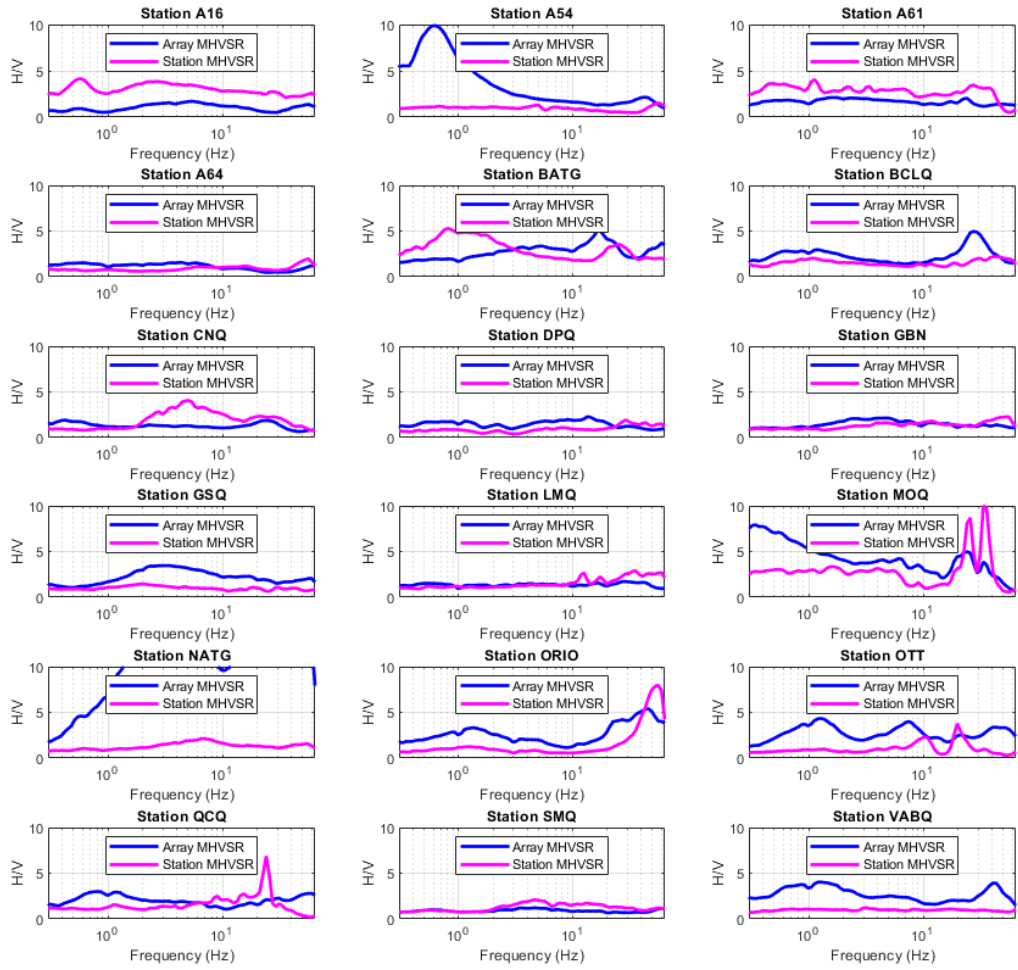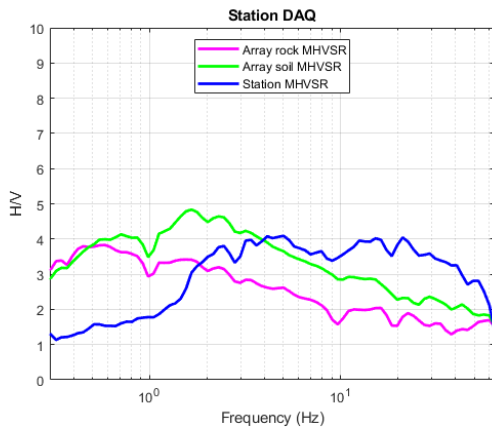
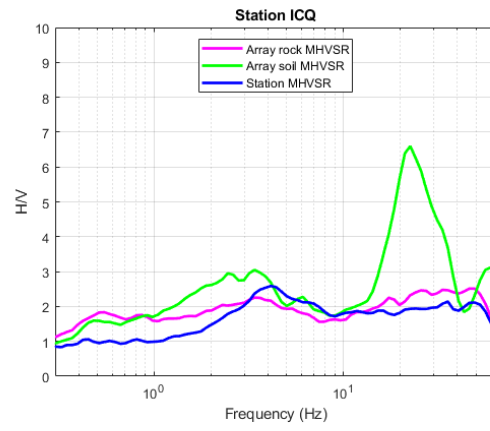**Figure A20: Comparison of single station and array-average MHVSR for each station.**

a)

b)

Figure A21: Single station and array-average MHVSRs on soil and rock surfaces compared for station a) DAQ and b) ICQ.

Curriculum Vitae

Name:	Sameer Ladak
Post-Secondary Education:	University of Alberta, Edmonton, Alberta, Canada
	2012-2016 B.Sc. Specialization, Geophysics
	The University of Western Ontario (UWO), London, Ontario, Canada
	2018-2020 M.Sc. Geophysics
Honours and Awards:	Jason Lang Scholarship, fulfilled by the University of Alberta
	September, 2012
Related Work Experience	Graduate Research Assistant, UWO
	December 2017-April 2020
	Graduate Teaching Assistant, UWO
	December 2017-December 2019
	Undergraduate Thesis co-supervisor
	January– April 2019
	Geophysical Field Assistant, Charlevoix seismic mapping project
	August 2019
	Participant, COSMOS "Blind Trial Interpreting Passive-source Data from Sparse Arrays". Phase II (July 2018), Phase 3 (August 2018), and Phase 4 (November 2018).

Conference Paper Publications:

Ladak, S., Molnar, S., Palmer, S., & Atkinson, G. M. (2019) Application of active and passive seismic methods for determining the shear wave velocity profile at hard rock sites in Eastern Canada: Canadian Conference on Earthquake Engineering (CCEE) 2019, Quebec City, Quebec, Canada, June 17-20, 2019, Paper 192-bN89-149.

Technical Reports:

Ladak, S., Molnar, S., Jackson, F. (2019). Report on Site Characterization of Eastern Canada CNSN Seismograph Stations, University of Western Ontario, GVE Report 19-01, 120 p.

Ladak, S and Molnar, S. (2020). Site Characterization at Stiff Ground Sites in Vancouver, Metro Vancouver Seismic Zonation Mapping Project, Univ. Western Ontario with ICLR and EMBC, Report 20-01, 15 pg.

Conference Presentations with Published Abstract:

Ladak, S., Molnar, S., Atkinson, G. M., Palmer, S. (2018). Application of Active and Passive – Seismic Array Techniques at Hard Rock Sites in Eastern Canada., Seismological Society of America (SSA) Annual Meeting, Miami, Florida, United States of America, May 2018, Poster Presentation.

Ladak, S., Molnar, S., Atkinson, G. M., Palmer, S. (2018). Non-invasive methods for determining the shear wave velocity profile at hard rock sites in Eastern Canada., Canadian Geophysical Union (CGU) 2018 Joint Annual Meeting, Niagara Falls, Ontario, Canada, June 2018, Poster Presentation.

Ladak, S., Molnar, S., Atkinson, G. M., Palmer, S. (2018). Application of non-invasive active and passive methods for determining the shear wave velocity profile at hard rock sites in Eastern Canada., The European Seismological Commission (ESC) 36th General Assembly, Valletta, Malta, September 2018, Oral Presentation by Dr. Sheri Molnar.

Ladak, S., Molnar, S., Atkinson, G. M., Palmer, S. (2019). Earthquake Site Characterization at Seismograph Stations in Eastern Canada., 12th Canadian Conference on Earthquake Engineering (CCEE), Quebec City, Quebec, Canada, June 2019, Oral Presentation.